

Optimal Transport Strategies

by

Wonjung Kim

Submitted to the Department of Mechanical Engineering
in partial fulfillment of the requirements for the degree of

Doctor of Philosophy in Mechanical Engineering

at the

MASSACHUSETTS INSTITUTE OF TECHNOLOGY

February 2013

© Massachusetts Institute of Technology 2013. All rights reserved.

Author
Department of Mechanical Engineering
January 11, 2013

Certified by
John W. M. Bush
Professor
Thesis Supervisor

Certified by
Anette (Peko) Hosoi
Professor
Chairman, Thesis Committee

Accepted by
David Hardt
Chairman, Department Committee on Graduate Theses

Optimal Transport Strategies

by

Wonjung Kim

Submitted to the Department of Mechanical Engineering
on January 11, 2013, in partial fulfillment of the
requirements for the degree of
Doctor of Philosophy in Mechanical Engineering

Abstract

It is generally presupposed that the shapes and mechanisms encountered in nature have evolved in such a way as to maximize the robustness of a species. However, most such optimization problems arising in biology are sufficiently complex that it is neither clear what is being optimized, nor what are the relevant constraints. We here consider a number of natural fluid transport systems that may be framed in terms of constrained optimization problems.

We first examine natural drinking strategies. We classify the drinking strategies of a broad range of creatures according to the principal forces involved, and present physical pictures for each style. Simple scaling arguments are developed and tested against existing data. While suction is the most common drinking strategy, various alternative styles have evolved among creatures whose morphological, physiological and environmental constraints preclude it. Many small creatures rely on relatively subtle capillary effects for fluid uptake.

Particular attention is given to nectar drinking strategies. Nectar drinkers must feed quickly and efficiently due to the threat of predation. While the sweetest nectar offers the greatest energetic rewards, the sharp increase of viscosity with sugar concentration makes it the most difficult to transport. An optimal sugar concentration is thus expected for which the energy intake rate is maximized. An extensive data set indicates that the sugar concentration that optimizes energy transport depends exclusively on the drinking technique employed. We identify three nectar drinking techniques: active suction, capillary suction, and viscous dipping and rationalize the reported optimal concentrations for each through consideration of the appropriate constrained optimization problem.

Blood flow in vertebrates and phloem flow in plants are known to be optimized for efficient transport of oxygen and sugar, respectively. Efficient transport of material is similarly advantageous in engineered transport systems such as traffic and wireless networks. We thus develop a general framework for determining the concentration that maximizes the material flow in a number of transport systems.

Thesis Supervisor: John W. M. Bush
Title: Professor

Acknowledgments

I would like to acknowledge my advisor, Professor John Bush, for his support and guidance throughout my graduate career, and for serving as a role model. Working with him has been my great pleasure and made me a better scientist.

I thank Professor Ho-Young Kim for his advice on my academic career. Special thanks also go to my thesis committee, Professors Peko Hosoi and Gareth McKinley.

This thesis would not have been possible without the help of many people. I gratefully acknowledge Tristan Gilet for many valuable discussions about optimal concentrations in nectar feeding and Kaare Jensen for the development of a general framework for a number of transport systems. I thank Francois Peudecerf and Maude Baldwin for their contributions to the understanding of the hummingbird's drinking technique and Wade Sherbrooke for his contributions to the understanding of the Texas horned lizard's drinking technique.

I thank M. Prakash, A. Biewener, P. Ramirez, and I. Ros for assistance with experimental work and M. Zwieniecki, R. Rosales, J. Savage, N. Carroll, K. Ho, and D. Weitz for valuable discussions about general framework for transport systems. I thank the New York and Missouri Botanical Gardens for use of online images and the Gray Herbarium (Harvard University Herbaria) for assistance and use of specimens.

Finally, I acknowledge the National Science Foundation and STX Scholarship Foundation for their financial support.

Contents

1	Introduction	19
1.1	Dynamic classification of drinking strategies	21
1.2	Optimal concentrations in nectar feeding	21
1.3	The tongue of the hummingbird	22
1.4	Optimal concentration in transport networks	23
2	Natural Drinking Strategies	25
2.1	Dynamic classification	26
2.2	Suction	30
2.2.1	Inertial suction ($Re(d/h) \gg 1$)	31
2.2.2	Viscous suction ($Re(d/h) \ll 1$)	32
2.2.3	Capillary suction	34
2.3	Capillary and viscous entrainment	36
2.3.1	Viscous dipping	36
2.3.2	Licking	38
2.4	Inertial entrainment: lapping and ladling	38
2.5	Contact angle hysteresis	41
3	Optimal Concentrations in Nectar Feeding	45
3.1	Optimal sugar concentrations	46
3.2	Coevolution between flowers and pollinators	53
3.3	Methods	53

4	The hummingbird’s tongue: a self-assembling capillary syphon	55
4.1	<i>In vivo</i> observations	57
4.2	Tongue deformation	60
4.3	Elastocapillary suction	61
4.4	Capillary suction vs. Fluid trapping	64
4.5	Discussion	66
4.6	Methods	67
4.6.1	<i>In vivo</i> high-speed imaging	67
4.6.2	Tension stress experiment	68
4.6.3	Finite Element Method	68
5	Optimal Concentrations in Transport Networks	71
5.1	General formulation	72
5.2	Biological transport networks	74
5.2.1	Nectar drinking from a tube	74
5.2.2	Blood flow in vertebrates	76
5.2.3	Sugar transport in plants	79
5.2.4	Drinking by viscous dipping	80
5.3	Applications to engineered transport systems: Traffic flow	81
5.4	Universal properties of transport networks	84
5.5	Discussion	87
5.6	Methods	87
5.6.1	Viscosity and density of nectar and phloem sap	87
5.6.2	Viscosity of blood	88
6	Conclusions	89
A	Supplementary Tables	93
B	Supplementary Figures	97

List of Figures

2-1 Various drinking techniques. Schematic illustration of (a) viscous suction, as employed by a moth, (b) capillary suction, as employed by a hummingbird, (c) viscous dipping, as employed by a bee [62], (d) licking, as employed by a lizard, (e) lapping, as employed by a cat [105], and (f) laddling, as employed by a dog. Images courtesy of (a) Small Wildlife Films, (b) Richard Houde, (e) Pedro Reis, and (f) Discovery Networks (<http://dsc.discovery.com/videos/time-warp-dog-drinking-water.html>). . . . 27

2-2 Drinking styles as a function of $\widetilde{Re} = \rho u L / \mu \cdot (L/H)$ and $\widetilde{Bo} = \rho g H L / \sigma$. For tube feeders, L and H are the tube diameter and height, respectively; for others, $L = H$ is the characteristic mouth size. Data is compiled from various sources: elephants [147, 144], cows [2], camels [124], lions [105], dogs [1], donkeys [124], jaguars [105], humans [89], sheep [16], cats [105], monkeys [76], chickens [48], wild ducks [68], snakes [25, 8], rats [143, 81], pigeons [151], finches [49], phalaropes [99], turtles [28, 7, 4], lizards [140], Texas horned lizards [127], bats [148, 113], sunbirds [123], hummingbirds [133, 65], orchid bees [14, 15], bees [46], mosquitoes [115, 73], moths [57], butterflies [98], ants [95], and *Rhodnius* [6]. 29

2-3 $Re = \rho u d / \mu$ and $Bo = \rho g d^2 / \sigma$ for creatures employing inertial suction. We note that since inertial suction does not depend on surface tension, Bo is here simply a proxy for body size. 32

2-4 (a) A schematic illustration of the proboscis. (b) The dependence of $Re = \rho u d / \mu$ on Bo^* as defined in (2.7) for viscous suction feeders: mosquitoes [115, 73], butterflies [78, 98, 12], bees [14], hawkmoths [57] and ants [95]. 33

2-5	(a) A schematic illustration of the hummingbird’s tongue. (b) The dependence of Q on μ for hummingbirds [44, 133, 111] and honeyeaters [85]. The line represents $Q \sim \mu^{-1/2}$, as anticipated from our scaling.	34
2-6	(a) A bumblebee drinking. Inset: a schematic illustration of the bee’s tongue. (b) Scanning Electron Microscope (SEM) image of the bumblebee’s tongue. (c) The dependence of Q on μ for bats [113], bees [116, 46] and ants [95], all of which employ viscous dipping. The line corresponds to the scaling suggested by (2.11), specifically, $Q \sim \mu^{-1/6}$	36
2-7	A schematic illustration of licking, the drinking strategy common to lizards and rats. Fluid imbibition into the papillae plays a critical role in increasing the volume entrained.	37
2-8	A schematic illustration of ladling by (a) cats, (b) dogs, and (c) zebra finches [49].	39
2-9	The dependence of $Re = \rho u R / \mu$ on $Bo = \rho g R^2 / \sigma$ for lapping cats. Data of u and R [105] were estimated from f and M with the assumption of body shape isometry in <i>Felidae</i>	40
2-10	Schematic illustrations of the drinking strategies of (a) the Namib desert beetle (Image courtesy of Roberto Osti Illustrations), (b) the Phalarope, and (c) the Texas horned lizard, all of which rely critically on contact angle hysteresis.	42
3-1	Optimal sugar concentrations for various nectar feeders [91]. The optimal concentration is that for which the energy intake rate is highest based on drinking rates measured at various nectar concentrations in a laboratory setting.[95, 13, 78, 12, 98, 45, 57, 131, 111, 133, 85, 46, 116, 113, 67] . . .	47

3-2 The dependence of scaled volumetric flow rate $Q/\langle X \rangle$ on nectar viscosity μ . The red points represent data for active suction, the blue points for capillary suction, and the green points for viscous dipping. The slopes of the expected lines for suction and viscous dipping are $-1/2$ and $-1/6$ respectively. Inset: optimal concentrations of 33% and 52% are evident for, respectively, suction feeding and viscous dipping from the dependence of relative energy intake rate on nectar viscosity. Characteristic error bars are shown. [78, 98, 12, 14, 57, 95, 85, 44, 133, 111, 116, 46, 113] 50

3-3 Bees uptake nectar via viscous dipping. A schematic illustration of the experiment that allows us to visualize the viscous dipping of a honeybee (*Apis*) with a long-distance microscope and a high-speed camera operating at 250 frames per second. Here, the bee's tongue is dipped into a 40% sucrose solution, then withdrawn. 52

4-1 A hummingbird (*Archilochus colubris*) drinking from a transparent feeder. (a) A photograph of the drinking bird. Inset: schematic illustration of the hummingbird's tongue and feeder. The feeder is made of glass plates, and wrapped with red paper in order to attract the bird. (b) High-speed images of the hummingbird drinking from a feeder. Owing to the transparency of the tongue, the meniscus of the rising nectar (arrows) is observable. As the tongue tip touches the surface, interfacial forces drive the liquid along the tongue at speeds of approximately 20 cm/s. 58

- 4-2 Capillary suction through a hummingbird's tongue (*Archilochus colubris*).
 (a) A dorsal view of the tongue of a hummingbird drinking sucrose solution of 20% concentration by mass. The arrows indicate the two menisci of the rising nectar. The tongue width becomes smaller after the inner surface is wetted by the nectar. (b) The position of the tongue tip (open circles) and meniscus (closed circles) during two consecutive licks. The measurement is interrupted when the meniscus moves beyond the field of view. The nectar rise speed is approximately 20 cm/s. The capillary rise of the nectar clearly precedes the tongue retraction. 59
- 4-3 A schematic illustration of nectar rise along the flexible tongue of the hummingbird, which closes in response to the surface tension. For the sake of clarity, only one of the tongue's two grooves is illustrated. 61
- 4-4 The dependence of the energy intake rates on the opening angle 2α for different $\Gamma = \sigma a^2/B$, where a is the undeformed radius and B is the bending stiffness per unit length. Here the energy intake rate is scaled by that for the tongue of $\alpha = 0$, $\Gamma = 0$, and $a = 150 \mu\text{m}$. The closed circles represent α_c , a limit below which the two lateral edges come into contact after bending. The tongue perimeter is the same for all cases. The optimal opening angles 2α that maximize energy intake rates are indicated by the dashed line and lie between 140° and 170° 63
- 4-5 The dependence of the tongue length loaded by capillary suction, h_c , on sucrose concentrations c for a range of biologically relevant loading times τ . We represent three different nectar reservoir depths of $H_1 = 1 \text{ mm}$, $H_2 = 5 \text{ mm}$, and $H_3 = 10 \text{ mm}$ by dotted lines. Provided that the tongue immersion depth $h_i \sim H$, curved and dotted lines allow for a comparison between nectar volumes loaded via capillary suction and fluid trapping. . . 66

5-1 Optimal concentrations in biological transport networks. (a) Drinking from a tube. Histogram showing distribution of observed sugar concentrations that maximizes nectar uptake for 16 bird and insect species that use muscular contractions or surface tension to feed through cylindrical tubes [62, 91]. Normalized sugar mass flow $J_s/J_{s,max}$ (solid line, Eqns. (5.6) and (5.7)) and nectar viscosity μ/μ_0 (dashed line, data from [47]) are plotted as a function of nectar sugar concentration \bar{c} . Mass flow is predicted to be maximum when $\bar{c}_{opt} = 35\%$, in good agreement with the observed average nectar concentration (37%). (b) Blood flow. Histogram showing distribution of observed red blood cell concentrations (hematocrit) from 57 vertebrate species [130]. Normalized oxygen flow $J_r/J_{r,max}$ (solid line, Eq. (5.8)) and blood viscosity μ/μ_0 (dashed line, see § 5.6.2) are plotted as a function of hematocrit \tilde{c} . Flow is predicted to be maximum when $\tilde{c}_{opt} = 40\%$, in good agreement with the observed average hematocrit (40%). (c) Sugar transport in plants. Histogram showing distribution of observed sugar concentrations from 28 plant species that use active sugar loading [56]. Normalized sugar flow $J_p/J_{p,max}$ (solid line, Eq. (5.9)) and sap viscosity μ/μ_0 (dashed line, data from [47]) are plotted as a function of nectar sugar concentration \bar{c} . Mass flow is predicted to be at a maximum when $\bar{c}_{opt} = 24\%$, in good agreement with the observed average sugar concentration (22%). 75

5-1 (d) Nectar drinking by viscous dipping. Histogram showing distribution of observed sugar concentrations that maximizes nectar uptake for 6 insect species that use viscous dipping [62, 91]. Normalized sugar mass flow $J_v/J_{v,max}$ (solid line) and nectar viscosity μ/μ_0 (dashed line, data from [47]) are plotted as a function of nectar sugar concentration \bar{c} . Mass flow is predicted to be at a maximum when $\bar{c}_{opt} = 57\%$, in good agreement with the observed average nectar concentration (55%). In (a)-(d), the numbers given above the bins indicate the percentage of species in the bin. 76

5-2 Optimal vehicle concentration for maximizing traffic flow. Grey dots show measured vehicle flow rate J_v plotted as a function of vehicle concentration $c = \rho/\rho_{\text{opt}}$ where $\rho_{\text{opt}} = 133$ vehicles/km. The flow rate is normalized by 1483 vehicles/hour which corresponds to $J_v(\rho_{\text{opt}}) = J_{v,\text{max}}$ in Bando & Hasebe's model [3]. Histograms show the states occupied by the system in the morning (green, 6-8AM) and evening (blue, 4-6PM) rush-hour traffic. The data were collected by the Minnesota Department of Transportation from a sensor on the westbound direction of I-94 (Minneapolis, MN, USA) on Fridays (7, 14, 21, 28) in September 2012 [84]. The predicted vehicle transport rate $J_v/J_{v,\text{max}}$ (thick solid black line: Bando & Hasebe's model; thin solid red line: Greenberg's model) and traffic impedance μ/μ_0 (dashed line: Bando & Hasebe's model) are plotted as a function of vehicle concentration c 83

5-3 Universal properties of biological and engineered flows. (a) Normalized flow rate $J^* = J(c)/J(c_{\text{opt}})$ plotted as a function of normalized concentration $c^* = c/c_{\text{opt}}$. The solid thick black line shows the prediction of Eq. (5.3). (b) Normalized impedance $\mu^* = \mu(c)/\mu(c_{\text{opt}})$ plotted as a function of normalized concentration c^* . The solid and dashed thick black lines show the predictions of Eq. (5.4). The inset indicates the dependence of $(\mu^*)^{1-\gamma}$ on c^* 86

B-1 *Campsis radicans*. The arrows indicate the basal corolla diameters used in our estimation of nectar height. (<http://www.tropicos.org/Image/100002820>) 98

B-2 *Ipomoea coccinea*. The arrows indicate the inferred basal corolla diameters. (<http://www.tropicos.org/Image/100004180>) 99

B-3 *Ipomopsis rubra*. The arrows indicate the inferred basal corolla diameters. (Gray Herbarium, Harvard University Herbaria, *Ipomopsis rubra* J.M. Tracy No.8311) 100

B-4 *Lobelia cardinalis*. The arrows indicate the inferred basal corolla diameters. (<http://www.tropicos.org/Image/100015764>) 101

B-5 *Aquilegia canadensis*. The arrows indicate the inferred basal corolla diameters. (<http://www.tropicos.org/Image/100105516>) 102

List of Tables

5.1	Parameters describing the material flow $J = Qc = Xfc/\mu$ (see Eq. (5.2)) for each of the systems considered. See Appendices 5.6.1 and 5.6.2 for details on the viscosity η of blood, nectar and phloem sap.	77
5.2	Comparison between theoretical predictions (T) and experimental observations (E) of the optimum concentration c_{opt} , the optimum viscosity μ_{opt} and the exponent α . Concentration units are % wt/wt for nectar drinking and sugar transport in plants, % vol/vol for blood flow, and % vehicle density/max vehicle density for traffic flow.	84
A.1	. Estimation of the nectar depth for six flowers visited by <i>A. colubris</i>	94
A.2	. Corolla measurement (diameter at base of corolla tube).	95

Chapter 1

Introduction

“If one way be better than another, that, you may be sure, is nature’s way.”

Aristotle thus stated the basic premise of optimization in biology. It is generally presupposed that the shapes and mechanisms encountered in nature have evolved in such a way as to maximize the robustness of a species. However, most such optimization problems arising in biology are sufficiently complex that it is neither clear what is being optimized, nor what are the relevant constraints. We here consider a number of natural fluid transport systems that may be framed in terms of constrained optimization problems.

Biocapillarity is a relatively unexplored field at the boundary of interfacial science, fluid mechanics and organismic biology. The nascent field of microfluidics may exploit a variety of nature’s designs thanks to the diversity of life and the associated variety of mechanisms for fluid transport on a small scale [132, 129]. For example, the water-repellent integument of plants and insects has provided inspiration for the rapid recent developments in the design of superhydrophobic, self-cleaning surfaces [33, 34]. Zhai *et al.* [150] demonstrated that ‘Super Plastic,’ the manufactured surface that mimics the Namib beetle’s back, can be applied to water harvesting in the developing world, and Garrod *et al.* [37] investigated the optimal surface topology for maximizing the water harvesting rate. It is thus our hope that elucidating poorly understood fluid transport mechanisms exploited by the earth’s smallest creatures may inform microfluidics research.

Drinking is a critical behavior in the animal kingdom because water is essential in the

sustenance of all life forms [20]. While water uptake is typically associated with drinking, some creatures also do so in order to capture suspended prey [152, 38]. Moreover, many insects and birds ingest fluid primarily in the form of nectar, which serves as their principle source of energy [64, 65, 98, 66, 46, 78, 91]. Efficient strategies for fluid uptake have thus been evolving for millions of years within the animal kingdom.

The styles of water uptake in nature are myriad, depending largely on the size of the drinker. Drinking is generally facilitated by some combination of muscular and capillary pressure and resisted by some combination of fluid inertia, gravity and viscosity. On a small scale, viscous effects typically dominate inertia, and surface tension effects dominate gravity; consequently, drinking strategies are strongly scale-dependent. For example, inertial entrainment is exploited by lapping dogs and cats [105], while viscous entrainment is exploited by some insects, small licking lizards [140] and birds [48]. Categorizing and rationalizing all natural drinking strategies is one of the principal contributions of this thesis.

Nectar feeding is one of the few natural mechanisms that can be rationalized by consideration of a clean constrained optimization problem [65, 66]. Nectar drinkers must feed quickly and efficiently due to the threat of predation. While the sweetest nectar offers the greatest energetic rewards, the sharp increase of viscosity with sugar concentration makes it the most difficult to transport. An optimal sugar concentration is thus expected for which the energy intake rate is maximized. Another contribution of this thesis is the formulation of the various nectar drinking strategies in terms of constrained optimization problems.

There are many transport networks in natural and engineering systems. Whether biological such as the vascular systems of plants and animals, or engineered such as roads and wireless networks, they serve to move material from one place to another. There are many instances where it is advantageous for these systems to transport matter efficiently. Blood flow of invertebrates [90, 130] and phloem flow in plants [54] are known to be optimized for efficient transport of oxygen and sugar, respectively. Efficient transport of matter is similarly advantageous in engineered transport systems. The final contribution of this thesis is the development of a general framework for understanding concentration-impeded natural and engineered transport networks.

In this thesis, we consider the fluid mechanics of natural drinking strategies with a view

to informing optimal transport strategies. In Chapter 2, we categorize the drinking styles of a broad range of terrestrial creatures by identifying the principal force balances involved in the fluid transport. In Chapter 3, we focus on nectar drinking strategies, that we frame in terms of constrained optimization problems. In Chapter 4, we consider the particular case of nectar drinking by the hummingbird, a natural example of capillary origami. In Chapter 5, we develop a general framework for optimizing concentration-impeded transport systems.

1.1 Dynamic classification of drinking strategies

In Chapter 2, we examine the fluid mechanics of drinking in nature. We classify the drinking strategies of a broad range of creatures according to the principal forces involved, and present physical pictures for each style. Simple scaling arguments are developed and tested against existing data. While suction is the most common drinking strategy, various alternative styles have evolved among creatures whose morphological, physiological, and environmental constraints preclude it. Particular attention is given in our study to the drinking styles employed by creatures small relative to the capillary length that rely on relatively subtle interfacial effects. The later represent an interesting class of biocapillarity problems.

Chapter 2 appears as published in Kim, W. and Bush, J. W. M. 2012, Natural drinking strategies. *Journal of Fluid Mechanics* vol. 705, pp 7-25.

1.2 Optimal concentrations in nectar feeding

Many insects and birds feed primarily on floral nectar. Most butterflies and moths suck nectar through their probosci, along which a pressure gradient is generated by cibarial muscles [64, 98]. Nectar-feeding birds such as hummingbirds and sunbirds rely on capillary pressure, which drives flow along the tongue once its tip touches the nectar [65]. Most bees and some ants ingest nectar by dipping their tongue into, then extracting it from, the viscous nectar [66, 95]. It is advantageous for creatures to ingest energy rapidly due to the threat of predation during feeding. While the sweetest nectar offers the greatest energetic rewards,

the exponential increase of viscosity with sugar concentration [98] also makes it the most difficult to transport. Optimal conditions may thus be sought to maximize their energy intake rate. In Chapter 3, we rationalize the different optimal concentrations reported for the different nectar drinking strategies by developing dynamic models for these strategies, which indicate the dependence of flux on nectar concentration.

Chapter 3 appears as published in Kim, W., Gilet, T. and Bush, J. W. M. 2011, Optimal concentrations in nectar feeding. *Proceedings of the National Academy of Sciences*, vol. 108, pp 16618-16621.

1.3 The tongue of the hummingbird

The hummingbird's tongue is forked and flexible, with characteristic length 2 cm and width of 0.5 mm, effectively a sliced cylinder. It is passive, with no enervation or muscular control in its outer 1 cm [44]. The elastocapillary length, specifically, the length beyond which capillary forces can cause the flexure of solid sheets, is comparable to the perimeter of the tongue $\pi d \sim 500 \mu\text{m}$, thus raising the possibility of a dynamic role for tongue flexibility. Indeed, when the tongue makes contact with floral nectar, it zips shut in response to capillary forces, and fluid rises along its length by capillary action. The hummingbird tongue thus has the form of a self-assembling syphon, the dynamics of which raises a number of novel and fundamental fluid mechanics questions. As the fluid rises, some of the surface energy is diverted to elastic energy of tongue flexure. How does the rise speed depend on the flexibility of the tongue? For what range of material properties and shapes can a sliced flexible tube serve as a self-assembling syphon? In Chapter 4, these questions are addressed through a combined experimental and theoretical investigation.

Chapter 4 appears as published in Kim, W., Peaudecerf, F., Baldwin, M. W. and Bush, J. W. M. 2012, The hummingbirds tongue: a self-assembling capillary syphon. *Proceedings of the Royal Society B*, vol. 279, pp 4990-4996.

1.4 Optimal concentration in transport networks

Given the widespread use of bio-inspired design in the development of engineered systems, it seems likely that man-made transport networks such as roads or the electrical grid may benefit from an improved understanding of natural transport systems. In Chapter 5, we draw on a number of biological examples in order to develop a general framework for understanding the efficiency of concentration-impeded transport networks. Predictions of our theoretical model are compared with experimental data on transport in over 100 animal and plant species collected from the literature, and shed light on an often less than optimized man-made transport system, traffic flow.

Chapter 2

Natural Drinking Strategies

Sir James Lighthill coined the word ‘biofluidynamics’ to describe fluid mechanics problems arising in biology [74], a theme that has been pursued with great success by the honouree of this edition. Substantial effort has been devoted to elucidating natural locomotion strategies, including those of fish [138], flying insects [141], birds [149] and microorganisms [97, 71]. Flow through elastic tubes has been examined in order to elucidate the dynamics of flows in the respiratory, pulmonary [96] and nervous systems [21]. ‘Biocapillarity’ might likewise be used to describe the subset of biofluidynamics problems dominated by interfacial effects. One well explored such problem is that of natural strategies for water-repellency employed by plants and insects [18], which have served as a source of inspiration in the design of superhydrophobic surfaces [22]. Another is the role of surfactants in the respiratory system, a problem of critical importance in the treatment of premature infants [43]. More recently, natural strategies for propulsion at the water surface have been explored [17]. We here examine natural strategies for fluid transport, wherein a number of novel biocapillary problems arise.

Although water can be ingested with food, drinking is the principal route for water intake, critical in the sustenance of most animals. We loosely define drinking as fluid uptake required for the sustenance of life. Some creatures uptake water in order to capture suspended prey; for example, flamingoes feed on algae suspended in water [152], and tiger salamanders capture aquatic prey by drawing in water [38]. Finally, we note that drinking need not involve water; for example, many insects and birds ingest fluid primarily in the

form of nectar, which serves also as their principle source of energy. Nectar drinking will be one subject of focus in our study.

Most creatures ingest fluid either by suction through an orifice (e.g. lips or a beak) or a tube (e.g. a proboscis or a trunk) or by entrainment onto the tongue. However, drinking styles in nature are myriad, depending on the creature's size, the morphology of its mouth parts, and its environment. Some creatures have developed ingenious drinking techniques in response to harsh environmental constraints. In most previous studies of drinking strategies, emphasis was given to reporting observations of particular drinking styles. Only in very few such studies have the fluid mechanics of drinking been highlighted. Dynamic models for nectar drinking in hummingbirds and butterflies were established by Kingsolver *et al.* [65, 98]. In an attempt to rationalize observed drinking rates for butterflies, Kingsolver & Daniel [64] were the first to pose nectar drinking through a tube as a constrained optimization problem, an approach that has been recently advanced [62]. Prakash *et al.* demonstrated that a class of shorebirds relies on contact angle hysteresis for the mouthward transport of prey-bearing droplets [99]. Recently, Reis *et al.* [105] and Crompton & Musinsky [23] rationalized the drinking strategies of cats and dogs, respectively, demonstrating that they use inertial forces generated by their lapping tongues to overcome gravity.

In the current study, we focus on terrestrial creatures, excluding from consideration underwater creatures, such as fish and amphibians, that drink primarily via osmosis. In § 2.1, we categorize the drinking styles of a broad range of terrestrial creatures by identifying the principal force balances involved in the fluid transport. We suggest consistent physical pictures and present simple scalings that describe the dynamics of each drinking style, specifically, suction (§ 2.2), dipping, licking (§ 2.3), lapping, and ladling (§ 2.4). Finally, several novel drinking techniques that rely on contact angle hysteresis are highlighted in § 2.5.

2.1 Dynamic classification

The drinking styles of terrestrial creatures, as shown in Figure 2-1, can be classified according to the dominant driving and resistive forces. Drinking is generally accomplished

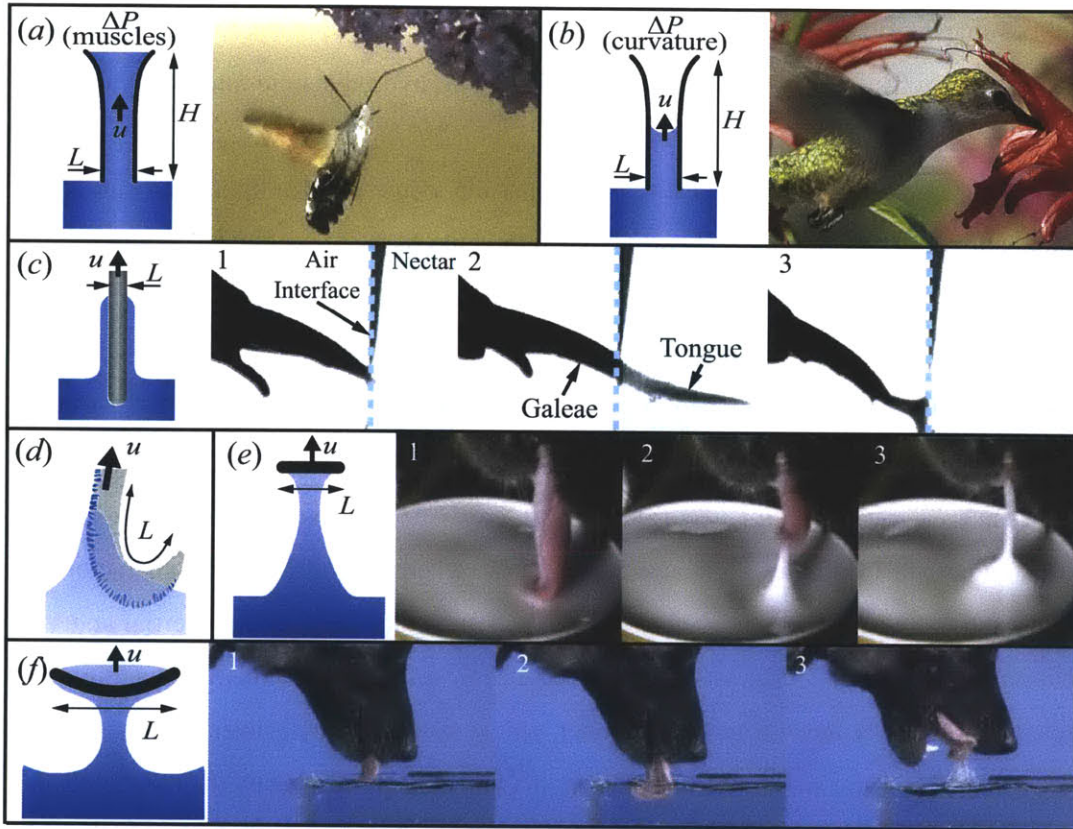


Figure 2-1: Various drinking techniques. Schematic illustration of (a) viscous suction, as employed by a moth, (b) capillary suction, as employed by a hummingbird, (c) viscous dipping, as employed by a bee [62], (d) licking, as employed by a lizard, (e) lapping, as employed by a cat [105], and (f) ladling, as employed by a dog. Images courtesy of (a) Small Wildlife Films, (b) Richard Houde, (e) Pedro Reis, and (f) Discovery Networks (<http://dsc.discovery.com/videos/time-warp-dog-drinking-water.html>).

by virtue of a driving pressure generated by some combination of muscular contraction and capillarity, and resisted by some combination of fluid inertia, gravity, and viscosity. The dominant driving and resisting forces depend on the size and morphology of drinkers as well as the properties of the fluid.

Consider a fluid of density ρ and viscosity μ being driven with velocity u through a domain of characteristic scale L by a pressure difference ΔP in the presence of a gravitational acceleration g . Characteristic magnitudes of the various hydrodynamic forces may be written as $F_{inertia} \sim \rho u^2 L^2$, $F_{viscous} \sim \mu u L$, $F_{pressure} \sim \Delta P L^2$, and $F_{gravitational} \sim \rho g L^3$. In drinking, ΔP is typically produced by either muscular contraction or interfacial curvature. In the latter case, it scales as $\Delta P \sim \sigma/L$ where σ is the surface tension. The relative magnitudes of the various force components can be written in terms of standard dimensionless groups, specifically, the Reynolds number, $Re = \rho u L / \mu$, denotes the ratio of inertial to viscous forces, the Bond number, $Bo = \rho g L^2 / \sigma$, the ratio of hydrostatic to capillary forces, and the Capillary number, $Ca = \mu u / \sigma$, the ratio of viscous to capillary forces.

Many creatures, including nectar-feeding or blood-sucking insects, use tubes (e.g. probosci, snouts, or trunks) of high aspect ratio H/L , where H and L are the characteristic length and diameter of the tube, respectively. For such tube feeders, the inertial and viscous forces scale as $F_{inertia} \sim \rho u^2 L^2$ and $F_{viscous} \sim \mu u H$, so their relative magnitude is prescribed by the reduced Reynolds number, $\widetilde{Re} = Re(L/H)$. Moreover, $F_{gravitational} \sim \rho g H L^2$ and $F_{curvature} \sim \sigma L$, so their relative magnitude is prescribed by the reduced Bond number, $\widetilde{Bo} = Bo(H/L)$, where $Bo = \rho g L^2 / \sigma$. Assessment of the magnitudes of these dimensionless groups indicates the dominant forces at play. The \widetilde{Re} and \widetilde{Bo} for various creatures are compiled in Figure 2-2, where the different drinking styles are represented by different colors. For creatures that do not rely on tubes for drinking, $H \sim L$, so $\widetilde{Re} = Re$ and $\widetilde{Bo} = Bo$. We first discuss general characteristics of the drinking styles represented on the plot; later, we present a more technical examination.

For large creatures, including most mammals, $\widetilde{Bo} \gg 1$, so capillary pressures are negligible. Fluid transport is thus typically generated by pressure induced by muscular contraction, except in the case of a few creatures such as cats and dogs, which have morphological constraints that preclude suction [105]. Reptiles, amphibians, and birds, for which $\widetilde{Bo} \sim 1$,

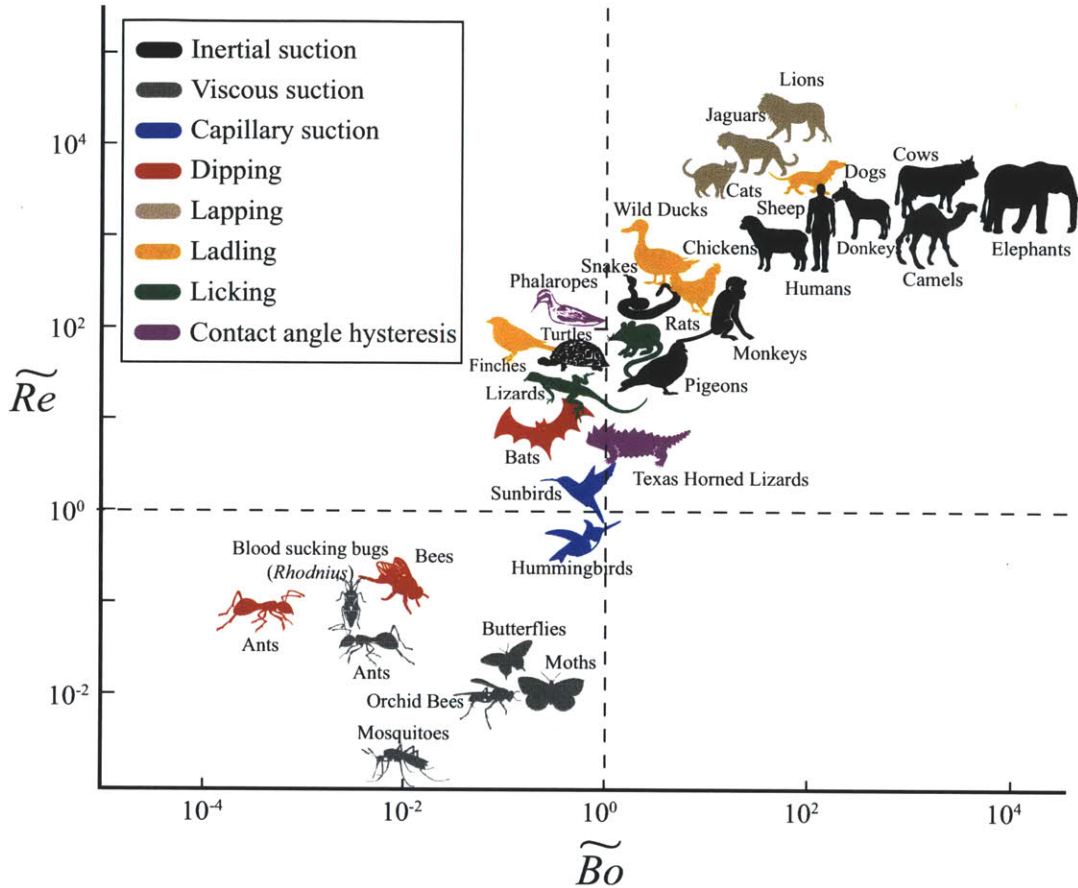


Figure 2-2: Drinking styles as a function of $\widetilde{Re} = \rho uL/\mu \cdot (L/H)$ and $\widetilde{Bo} = \rho gHL/\sigma$. For tube feeders, L and H are the tube diameter and height, respectively; for others, $L = H$ is the characteristic mouth size. Data is compiled from various sources: elephants [147, 144], cows [2], camels [124], lions [105], dogs [1], donkeys [124], jaguars [105], humans [89], sheep [16], cats [105], monkeys [76], chickens [48], wild ducks [68], snakes [25, 8], rats [143, 81], pigeons [151], finches [49], phalaropes [99], turtles [28, 7, 4], lizards [140], Texas horned lizards [127], bats [148, 113], sunbirds [123], hummingbirds [133, 65], orchid bees [14, 15], bees [46], mosquitoes [115, 73], moths [57], butterflies [98], ants [95], and *Rhodnius* [6].

can exploit capillary forces and so exhibit a relatively diverse variety of drinking styles. Small creatures such as insects, for which $\widetilde{Bo} \ll 1$ and $\widetilde{Re} \ll 1$, rely principally on some combination of capillary suction and viscous entrainment.

2.2 Suction

Suction is the most common drinking strategy in nature. We classify suction drinking styles according to what produces the driving pressure and whether the flow is resisted principally by fluid inertia or viscosity. The pressure-driven flow with mean speed u of a fluid of density ρ and viscosity μ along a tube of diameter d and height h is described by Newton's second law:

$$(m + m_a)\dot{u} = \frac{\pi}{4}d^2\Delta P - mg - \frac{\pi}{8}\rho u^2 d^2 - \pi h d \tau, \quad (2.1)$$

where m is the mass of the fluid in the tube, m_a the added mass of the fluid preceding the inlet of the tube, ΔP the pressure difference applied at the height h of the fluid, and τ the shear stress along the outer wall. One can estimate m , m_a , and τ as

$$m = \frac{\pi}{4}\rho d^2 h, \quad m_a = k_1 \frac{\pi}{4}\rho d^3, \quad \tau = k_2 \mu \frac{u}{d}, \quad (2.2)$$

where k_1 and k_2 are order 1 constants. After dividing by $\pi d^2/4$, rearrangement of (2.1) yields:

$$\Delta P = \rho \left(1 + k_1 \frac{d}{h}\right) h \dot{u} + \frac{1}{2} \left(1 + \frac{8k_2}{Re(d/h)}\right) \rho u^2 + \rho g h, \quad (2.3)$$

where $Re = \rho u d / \mu$. When fluid is accelerating, the characteristic acceleration time is of order h/u , so that $\dot{u} \sim u^2/h$. We further note that, while the shape of the mouth parts varies widely, commonly $d/h \leq 1$, particularly for tube feeders.

For active suction, ΔP is generated by muscular contraction, while for capillary suction, $\Delta P \sim \sigma/d$ is the Laplace or capillary pressure. A cornerstone of biomechanics is that the force that a creature of characteristic size l can generate $F \sim l^2$ [82]; thus, one expects the suction pressure generated by muscles, $\Delta P \sim F/l^2 \sim l^0$, to be independent

of scale and so to be of comparable magnitude for all creatures. For example, $\Delta P \sim 10$ kPa for mosquitoes [73], humans [89], and elephants [144]; the highest ΔP appears to be 80 kPa for bed bugs [26]. We can thus infer the tube diameter $d \sim \sigma/\Delta P \sim 10 \mu\text{m}$ below which capillary pressure dominates the applied suction pressure. For most creatures, the tube or mouth diameter d is significantly larger than $10 \mu\text{m}$, so the capillary pressure is negligible. Nevertheless, capillary suction is employed by certain creatures for which applied suction is precluded by virtue of geometrical and physiological constraints such as the open, passive tongue of the hummingbird (Chapter 4) [63], and the open beak of the zebra finch.

We can also use the near constancy of the suction pressure ΔP across species to assess the tube height $h \sim \Delta P/\rho g \sim 1$ m below which the applied suction pressure dominates hydrostatic pressure. For virtually all creatures using active suction (except the elephant), $h \ll 1$ m, indicating the relatively minor effect of gravity on the dynamics. Also, most capillary suction feeders have tubes of characteristic length $h \sim 1$ cm; consequently, $\rho g h d/\sigma \sim 0.1$, and the effect of gravity is negligible. In this limit, (2.3) may be expressed

$$\Delta P \sim \left(\frac{3}{2} + \frac{4k_2}{Re(d/h)} \right) \rho u^2. \quad (2.4)$$

The applied suction pressure must overcome inertial and viscous resistance, the relative magnitudes of which are prescribed by $Re(d/h)$.

2.2.1 Inertial suction ($Re(d/h) \gg 1$)

For many large creatures including human, monkeys, sheep and pigeons, $Re(d/h) \gg 1$, and the fluid speed in (2.4) scales as $u \sim (\Delta P/\rho)^{1/2}$. Therefore, Re may be expressed

$$Re = \frac{\rho u d}{\mu} \sim \left(Bo \frac{\sigma \Delta P}{\mu^2 g} \right)^{1/2}, \quad (2.5)$$

where $Bo = \rho g d^2/\sigma$. Assuming ΔP to be comparable for all suction drinkers, one expects a slope of 1/2 in the plot of Re and Bo , as evident in Figure 2-3. Scatter in the data presumably results from morphological variation between species. Specifically, $h \sim 3$

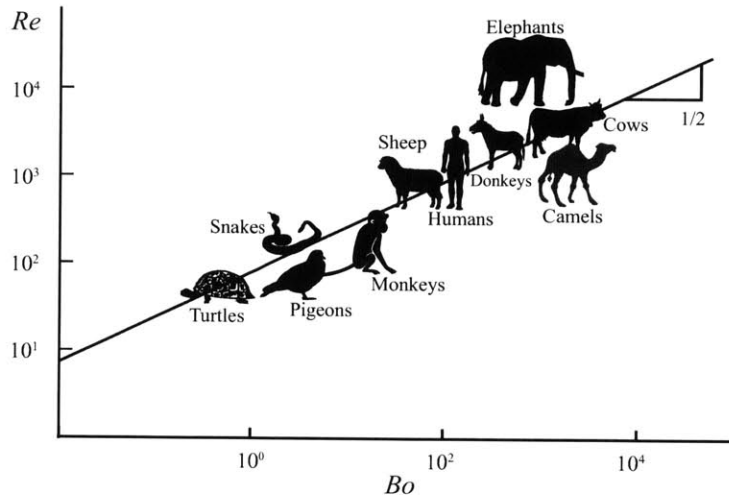


Figure 2-3: $Re = \rho u d / \mu$ and $Bo = \rho g d^2 / \sigma$ for creatures employing inertial suction. We note that since inertial suction does not depend on surface tension, Bo is here simply a proxy for body size.

m for elephants, which must thus generate relatively large pressures in order to counter gravitational forces negligible to other creatures.

2.2.2 Viscous suction ($Re(d/h) \ll 1$)

Many insects such as butterflies and mosquitoes feed on nectar or blood with their probosci. For such creatures, typically, $h \sim 1$ cm, $0.001 < \mu < 0.1$ Pa·s, $u \sim 1$ cm/s, $\rho \sim 1000$ kg/m³ and $d \sim 100$ μ m [64, 98, 73], so that $Re(d/h) \ll 1$, indicating that inertial effects are negligible. Thus, the fluid motion is described by Poiseuille flow, for which $k_2 = 8$ in (2.2), and the flow speed is given by $u \sim d^2 \Delta P / (32 \mu h)$. The viscosity of nectar increases exponentially with sugar concentration; specifically, $\mu = 0.0013$ Pa·s for a 10% sugar solution and 0.06 Pa·s for a 60% solution [142]. By measuring the dependence of flow rate on sugar concentration, Pivnick & McNeil inferred that butterflies apply constant suction power in drinking, regardless of nectar concentration [98]. The work per unit time required to overcome the viscous friction on the wall, or equivalently the power output \dot{W} of the pump, is given by $\dot{W} = Q \Delta P$, where Q is the volumetric flow rate. Expressing ΔP in terms of Q then yields:

$$Re = \frac{\rho u d}{\mu} \sim \frac{\rho d^3 \dot{W}}{32 \mu^2 h Q}, \quad (2.6)$$

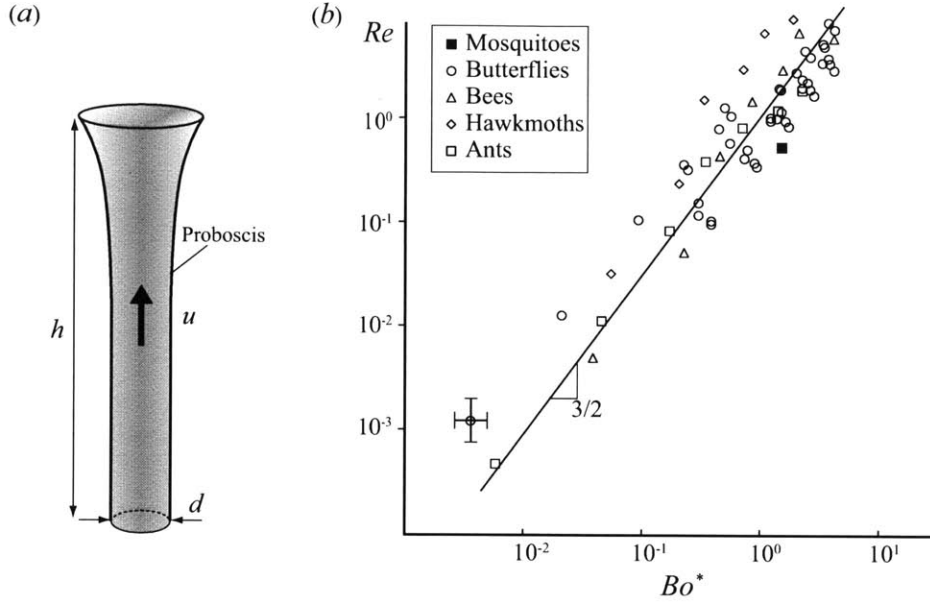


Figure 2-4: (a) A schematic illustration of the proboscis. (b) The dependence of $Re = \rho u d / \mu$ on Bo^* as defined in (2.7) for viscous suction feeders: mosquitoes [115, 73], butterflies [78, 98, 12], bees [14], hawkmoths [57] and ants [95].

where \dot{W} depends in general on both species and individual.

The dependence of flux Q on sugar concentration s has been reported for many insects [78, 98, 12, 14, 57, 95]. Kim *et al.* compiled the data, which indicate that $dQ(s)/ds < 0$: flux decreases with increasing sugar concentration s [62]. Using our upper bound on applied suction pressure, $\Delta P_{max} \sim 10$ kPa, we can assess $\dot{W} \sim Q \Delta P_{max}$ for each individual creature. Eliminating d in (2.6) with $Bo = \rho g d^2 / \sigma$ yields:

$$\log Re \sim \frac{3}{2} \left(\log Bo + \frac{2}{3} \log \frac{\sigma^{3/2} \dot{W}}{32 \mu^2 h \rho^{1/2} g^{3/2} Q} \right) \equiv \frac{3}{2} \log Bo^*. \quad (2.7)$$

We thus expect a slope of $3/2$ in the plot of Re versus Bo^* , as is evident in Figure 2-4. Nectar drinkers have an incentive to feed quickly, specifically the threat of predation. While the sweetest nectar offers the greatest energetic rewards, it is also the most viscous and so the most difficult to transport. Kingsolver & Daniel pointed out that one might thus anticipate an optimal sugar concentration for which the energy intake rate is maximized [64]. Since $Q \sim u$, (2.6) indicates that $Q \sim \mu^{-1/2}$ for a particular creature, provided \dot{W} is

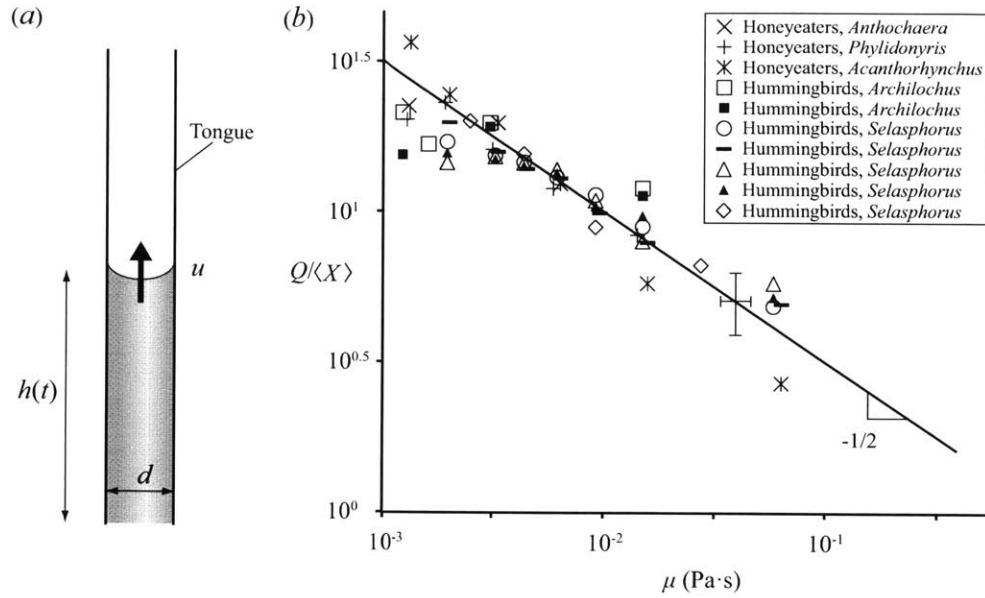


Figure 2-5: (a) A schematic illustration of the hummingbird's tongue. (b) The dependence of Q on μ for hummingbirds [44, 133, 111] and honeyeaters [85]. The line represents $Q \sim \mu^{-1/2}$, as anticipated from our scaling.

constant. The energy intake rate \dot{E} is proportional to both s and Q , so $\dot{E} \sim sQ \sim s\mu^{-1/2}$. Considering the dependence of nectar viscosity $\mu(s)$ on s [142], Kim *et al.* demonstrated that \dot{E} is maximized with respect to s subject to the constraint of constant work rate for $s \sim 33\%$, which represents the optimal sugar concentration for viscous suction feeders [62].

2.2.3 Capillary suction

Hummingbirds, honeyeaters, and sunbirds use their long tongues to collect floral nectar from the tubular corollas of flowers. The distal portion of the bird's tongue has a C-shape groove consisting of a thin keratinized membrane, from which vascular and nervous tissues recede [44, 145]. Consequently, the bird has no muscular control over the shape of its tongue, and active suction is impossible; instead, these birds rely on capillarity. When the tongue is extended out of the bill and touches the nectar, capillary pressure drives the nectar into the grooves. The tongue, once loaded with nectar, is then retracted into the bill [108]. While extending the tongue again in the next cycle, the hummingbird keeps the gap between its upper and lower bills smaller than the width of the tongue, thereby squeezing

the nectar out of the tongue [32].

For creatures employing capillary suction, specifically hummingbirds and honeyeaters, typically $h \sim 1$ cm, $0.001 < \mu < 0.1$ Pa·s, $u \sim hf \sim 10$ cm/s, where $f \sim 10$ Hz is the tongue insertion frequency, $\rho \sim 1000$ kg/m³, and $d \sim 100$ μ m [65]. Therefore, $Re(d/h) < 1$, indicating negligible inertial effects, and (2.4) again reduces to Poiseuille flow:

$$\Delta P \sim \left(\frac{32}{Re(d/h)} \right) \rho u^2, \quad (2.8)$$

where now $\Delta P \sim 4\sigma/d$, and the height of the nectar is time-dependent: $h = h(t)$ and $u = h'(t)$. The solution of the force balance, $\sigma d = 8\mu h h'$, with initial condition $h(0) = 0$, is given by Washburn's Law: $h(t) = (\sigma d t / 4\mu)^{1/2}$. Capillary suction consists of repeated cycles of tongue insertion and retraction. Over the nectar loading time in a single cycle, T , the average flow speed is given by

$$\bar{u} \sim h(T)/T \sim (\sigma d f / (2\mu))^{1/2}. \quad (2.9)$$

The average volumetric flow rate is thus given by

$$Q \sim \frac{\pi d^2}{4} \bar{u} \sim \left(\frac{\pi^2 d^5 f}{32\mu} \right)^{1/2}, \quad (2.10)$$

where the f depends only weakly on viscosity [111], so $Q \sim \mu^{-1/2}$. To test this proposed scaling against experimental data, we introduce a relation between Q and μ : $Q = X\mu^n$, where X is a geometry-dependent prefactor that we expect to be different for each individual. If we plot Q as a function of μ on a log scale, n and X represent the slope and the offset on the y-axis respectively. For each individual creature, we calculate an average value $\langle X \rangle = \langle Q\mu^{-n} \rangle$ based on the measured dependence of flow rate on viscosity. Figure 2-5b indicates the dependence of $Q/\langle X \rangle$ on μ , and that the observed dependence, $Q \sim \mu^{-1/2}$, is consistent with our expectation. We note that the dependence of Q on μ for capillary suction is the same as that for active viscous suction, so $Q \sim \mu^{-1/2}$. The optimal sugar concentration, specifically that which maximizes energy flux $\dot{E} \sim sQ$, is thus 33% for both active viscous and capillary suction [62].

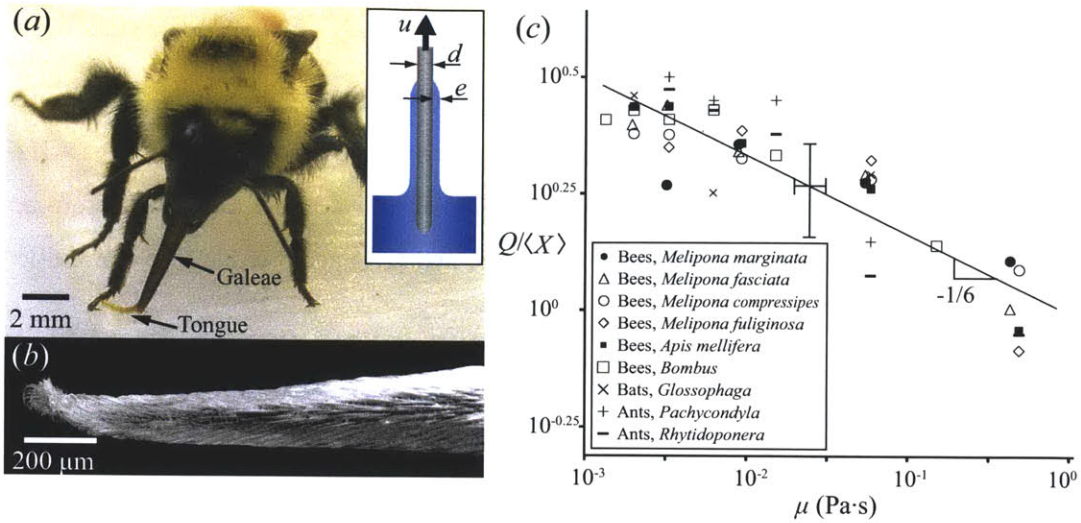


Figure 2-6: (a) A bumblebee drinking. Inset: a schematic illustration of the bee's tongue. (b) Scanning Electron Microscope (SEM) image of the bumblebee's tongue. (c) The dependence of Q on μ for bats [113], bees [116, 46] and ants [95], all of which employ viscous dipping. The line corresponds to the scaling suggested by (2.11), specifically, $Q \sim \mu^{-1/6}$.

2.3 Capillary and viscous entrainment

2.3.1 Viscous dipping

We present a simple model for a nectar drinking strategy in which the fluid is entrained by the outer surface of the tongue through the combined action of viscosity and capillarity. This drinking style, henceforth 'viscous dipping' [62], is used by most bees, some ants, and nectar feeding bats, whose tongues are solid rather than hollow (see Figure 2-6). Dipping is generally characterized by an extensible tongue being immersed into nectar, coated, then extracted in a cyclic fashion. For bees, the tongue diameter d and length h are typically of order $200 \mu\text{m}$ and 2 mm , respectively, and the tongue extraction speed $u \sim 2 \text{ cm/s}$. We expect the volume entrained to be proportional to the area of the immersed tongue surface and the thickness e of the nectar layer. The average volumetric flow rate must thus scale as $Q \sim \pi d e u$, where u is tongue speed. For steady flows, Landau-Levich-Derjaguin theory predicts $e \sim d Ca^{2/3}$ in the limit of $Ca < 0.1$, $We \ll 1$, and $Bo \ll 1$, where $We = \rho u^2 d / \sigma$ is the Weber number, $Ca = \mu u / \sigma$, and $Bo = \rho g d^2 / \sigma$ [103]. We introduce the assumption that the work rate applied in dipping is independent of μ for a given creature. The retraction

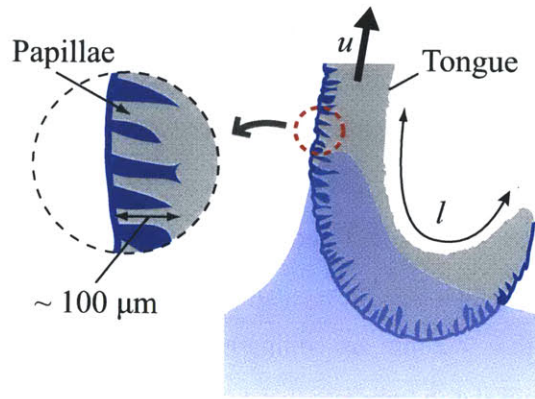


Figure 2-7: A schematic illustration of licking, the drinking strategy common to lizards and rats. Fluid imbibition into the papillae plays a critical role in increasing the volume entrained.

of the tongue through the viscous nectar requires the power $\dot{W} \sim \mu h u^2$ to overcome the viscous drag. Expressing the volume intake rate in terms of \dot{W} yields:

$$Q \sim \pi d e u \sim \frac{\pi d^2 \dot{W}^{5/6}}{\sigma^{2/3} h^{5/6} \mu^{1/6}}, \quad (2.11)$$

so $Q \sim \mu^{-1/6}$ for each individual creature. For the relation between Q and μ , $Q = X \mu^n$, as introduced in §2.2.3, we estimate an average value $\langle X \rangle = \langle Q \mu^{-n} \rangle$ based on the measured dependence of flow rate on viscosity [113, 116, 46, 95]. Figure 2-6 indicates the dependence of $Q/\langle X \rangle$ on μ , and the observed dependence of Q on μ , specifically $Q \sim \mu^{-1/6}$, is consistent with our prediction (2.11). Using this scaling $Q \sim \mu^{-1/6}$, Kim *et al.* inferred that energy intake rate $\dot{E} \sim sQ \sim s\mu^{-1/6}$ is maximized subject to the constraint of constant work rate for $s \sim 52\%$, which roughly corresponds to the measured optimal sugar concentrations for creatures that drink via viscous dipping [62]. The model provides new rationale for why the measured optimal concentrations are higher for creatures that use viscous dipping (50-60%) than for creatures that use suction (30-40%).

2.3.2 Licking

Lizards and rats lick water, a process relying on multiple cycles of tongue immersion and retraction. While licking resembles dipping in nectar feeders such as bees and ants in some regards, the licking mechanism is qualitatively different. We note that for dipping in nectar feeders, the high viscosity of nectar results in a thick layer of nectar on the tongue, and a relatively large volume of nectar transported to the mouth. For the lizard, the tongue speed for licking $u \sim 1$ cm/s, so $Ca = u\mu/\sigma \sim 10^{-4}$ while the tongue width $w \sim 4$ mm and extrusion length $l \sim 2$ mm are comparable to the capillary length l_c [140]. Thus Landau-Levich-Derjaguin theory predicts that the film thickness of the water layer on the tongue is given by $e \sim l_c Ca^{2/3} \sim 10 \mu\text{m}$ [103]. The water intake rate should thus be given by $Q \sim el^2 f \sim 0.5 \mu\text{l/s}$, where $f \sim 3$ Hz is the observed licking frequency. However, measurements of volume uptake in rats $Q \sim 10 \mu\text{l/s}$ suggest the importance of a physiological adaptation, specifically, the papillae on the tongue. It was reported that the tongue of the chameleon has papillae whose depth is of order $100 \mu\text{m}$ [104]. Since this depth is significantly greater than the coating thickness of water on the tongue, the efficiency of this licking mechanism is evidently greatly enhanced by the capillary imbibition of water into the papillae (see Figure 2-7). Fluid is expelled from the papillae during the final phase of licking, when the tongue is straightened and contracted. Based on the similar tongue sizes and drinking behaviour of rats, we suspect that they employ a similar drinking strategy.

2.4 Inertial entrainment: lapping and ladling

Owing to the open geometry of their cheeks, many creatures in the biological family *Felidae* (e.g. house cats and lions) and *Canis* (e.g. dogs and wolves) cannot seal their mouths in order to generate suction; consequently, they drink by moving their tongue in a lapping motion. These creatures extend their tongues to the water, curled ventrally into a ladle shape. After contacting the water, the tongue is retracted, transporting entrained water with it. When the tongue is retracted to a height H , the creatures catch the entrained water by closing their jaws at some intermediate height (see Figure 2-8a,b). With the characteristic half-width of the tongue tip $R \sim 1$ cm and tongue speed $u > 10$ cm/s, $Re = \rho u R / \mu > 1000$

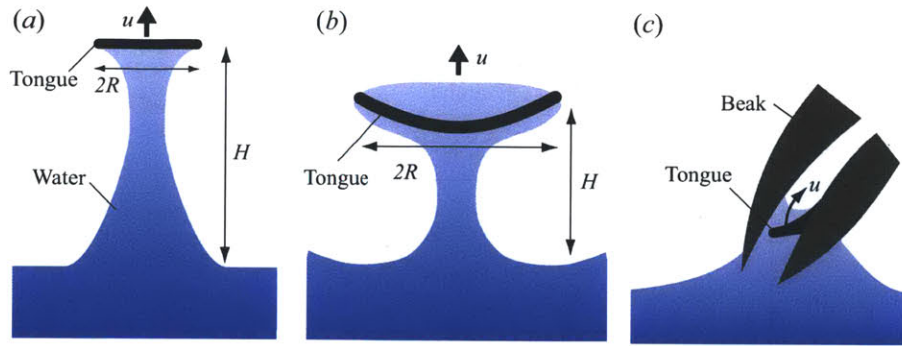


Figure 2-8: A schematic illustration of lading by (a) cats, (b) dogs, and (c) zebra finches [49].

and $Bo = \rho g R^2 / \sigma \sim 10$, indicating negligible viscous effects and capillary pressures. For this class of creatures, the water is thus raised mouthwards through inertial entrainment.

Reis *et al.* elucidated the drinking technique of cats, using high-speed videography, which indicates that cats do not immerse the tongue in water, so water is entrained only below the tongue [105]. From analog lab experiments, they demonstrated that the entrained water volume, specifically, that displaced above the initially horizontal interface, increases up to order R^3 shortly before pinch-off and then sharply decreases. They observed that the cat catches the raised water just before pinch-off and thus ingests a water volume of order R^3 . The study further demonstrates that the lapping frequency f is that which maximizes the volume flux of water; $f \sim (gH)^{1/2} / R$. The assumption of isometry suggests that H and R will be proportional to body size, so that the lapping frequency $f \sim \ell^{-1/2}$, where ℓ is the characteristic body size. Therefore, the tongue velocity $u \sim Rf \sim \ell^{1/2}$, and $Re = \rho u R / \mu \sim \ell^{3/2}$. Since $Bo = \rho g R^2 / \sigma \sim \ell^2$, we expect $Re \sim Bo^{3/4}$. Isometry of *Felidae* would indicate that the tongue width scales as $R \sim M^{1/3}$ [82], where M is the body weight, and that the tongue speed scales as $u \sim fR \sim fM^{1/3}$. From the data on M and f for various felines [105], we plot the dependence of Re on Bo in Figure 2-9. Here, the slope is consistent with our expectation, specifically $Re \sim Bo^{3/4}$.

Using X-ray videography, Crompton & Musinsky recently examined the drinking technique of dogs [23]. They demonstrated that, as for the cat, fluid is entrained onto the base on the tongue; however, it is also entrained above the tongue. Their high-speed videos indicate that the dog immerses its tongue into the water before extracting it, thereby en-

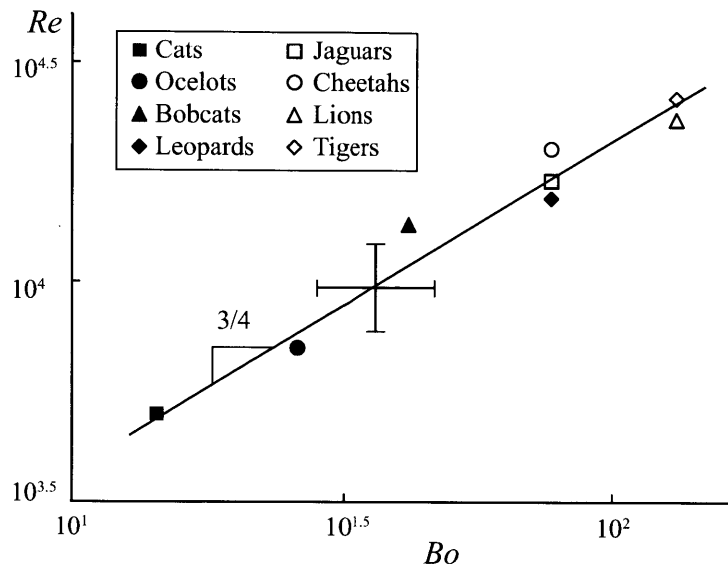


Figure 2-9: The dependence of $Re = \rho u R / \mu$ on $Bo = \rho g R^2 / \sigma$ for lapping cats. Data of u and R [105] were estimated from f and M with the assumption of body shape isometry in *Felidae*.

training fluid both above and below the tongue. Since the dog also closes its jaws before the entrained water column pinches off, the volume entrained below the tongue is of order R^3 , as for the cat. The ladling tongue may be roughly described as a bowl of radius R , so the dog can ingest volumes of order R^3 entrained both above and below the tongue.

The delineation between the various drinking strategies is never entirely clear. Zebra finches use a variant of ladling that depends explicitly on capillary pressure, as one might anticipate since the tongue size $R \sim 1$ mm and $Bo \sim 1$. The zebra finch immerses its beak into the water surface with a slight opening angle, causing water to rise by capillary action into the resulting gap (see Figure 2-8c). It then ladles water with its tongue in order to transport water to the esophagus. This drinking style is markedly different from that of many other birds such as pigeons, which suck water into their mouths by closing their beaks and applying suction across the resulting thin gap. We note that birds, for which characteristic tongue and beak sizes are often comparable to the capillary length $l_c = (\sigma / \rho g)^{1/2} \sim 2$ mm, may generally use either suction or capillary pressure. Indeed, drinking strategies in birds often depend on the interplay of these two forces.

2.5 Contact angle hysteresis

The equilibrium contact angle θ_e of a drop on a solid is prescribed by Young's Law: $\sigma \cos \theta_e = \gamma_{SG} - \gamma_{SL}$, where γ_{SG} and γ_{SL} are the interfacial energies per unit area between solid-gas and solid-liquid, respectively. In reality, for a given solid-fluid combination, a range of static contact angles may arise [30]. Consider a drop of fluid emplaced on a solid. If the drop is filled, it will grow, and its contact angle increase progressively until reaching a critical value, θ_a , at which the contact line begins to advance. If conversely, fluid is withdrawn from the drop, its contact angle will decrease progressively until reaching a critical value, θ_r , at which the contact line begins to recede. Observed static contact angles θ may thus lie anywhere within the range $\theta_r < \theta < \theta_a$, bounded below and above by the receding and advancing contact angles. While contact angle hysteresis normally impedes drop motion along surfaces, several creatures have evolved unique drinking strategies that exploit it.

The Namib beetle resides in a desert where it rarely rains; nevertheless, it is able to condense water from micron-scale fog droplets that sweep in daily from the coast. Their surface is composed of hydrophilic bumps on hydrophobic valleys. The fog droplets thus stick to the peaks, remaining pinned there by contact angle hysteresis, then grow through accretion until becoming large enough to be blown by the wind onto the hydrophobic valleys, across which they roll with little resistance (see Figure 2-10a). By guiding these rolling droplets towards their mouths, the beetles reap the rewards of the refrigeration-free condenser on their backs [92].

Phalaropes are small birds that inhabit the American and Russian coastlines of the arctic seas, and prey on small aquatic organisms such as miniature shrimp and phytoplankton. By swimming in a tight circle on the surface of shallow bodies of water, they generate a vortex that sweeps their prey upwards, like tea leaves in a swirling cup [117]. By pecking the free surface, they capture a prey-bearing droplet in the tip of their beak. Then, by successively opening and closing their beaks in a tweezing motion, they draw the droplet mouthwards. Prakash *et al.* demonstrated that this capillary ratchet mechanism relies critically on contact angle hysteresis. During the closing phase of the tweezing motion, both contact lines of

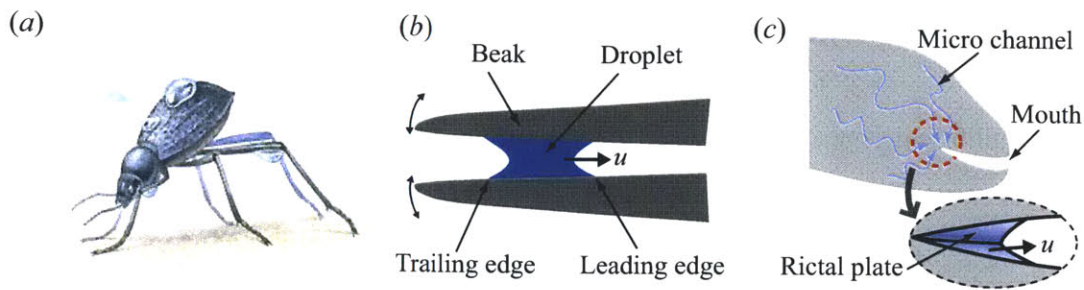


Figure 2-10: Schematic illustrations of the drinking strategies of (a) the Namib desert beetle (Image courtesy of Roberto Osti Illustrations), (b) the Phalarope, and (c) the Texas horned lizard, all of which rely critically on contact angle hysteresis.

the droplet have the tendency to progress outward, but the leading edge always does so first while the trailing edge is pinned due to the contact angle hysteresis (see Figure 2-10b) [99]. Conversely, during the opening phase, both contact lines tend to retreat inward, but the trailing edge does so first. The drop thus advances through a ratcheting motion. In each cycle, both leading and trailing edges of the contact lines advance and retreat; however, due to the asymmetry in the wedge geometry, net mouthward drop motion is achieved. This drinking strategy illustrates how contact angle hysteresis may, when coupled to dynamic boundary motion, enhance rather than impede drop transport.

Some lizards such as Australian thorny devils and Texas horned lizards live in environments where water is rarely encountered in the form of extended bodies of water such as puddles or ponds. The lizards have thus evolved a novel rain harvesting technique that relies on their integumental morphology. The skin of the lizard consists of multiple layers whose warped shape forms micro-channels that uptake water from any source, from raindrops to wet soils, via capillary action [128]. The water is transported through the skin to the base of the mouth through the microchannels; however, it has not yet been clearly elucidated how the lizard uptakes the water from the microchannels. Specifically, once the capillary network of its skin is filled with water, capillarity suction can no longer play a role; therefore, the lizard requires a pumping system [127]. The lizard has a rictal plate, a fold of skin at the corner of the mouth whose geometry is controlled by the jaw movement (see Figure 2-10c). Sherbrooke proposed that the jaw movement may draw water into the mouth through contact angle hysteresis, in a manner reminiscent of the phalarope [127].

Further study is underway to elucidate this subtle drinking mechanism.

Chapter 3

Optimal Concentrations in Nectar Feeding

Many insects and birds feed primarily or opportunistically on floral nectar. There are three principal techniques employed by nectar feeders: active suction, capillary suction, and viscous dipping. Lepidopterans (e.g. butterflies and moths) employ the former, sucking nectar through their probosci, along which a pressure gradient is generated by cibarial muscles [64, 98]. Nectar-feeding birds (e.g. hummingbirds and sunbirds) employ capillary suction, in which capillary pressure drives flow along the tongue once its tip touches the nectar [65]. Most bees (except orchid bees) and some ants ingest nectar by dipping their tongue into, then extracting it from, the viscous nectar [66, 95]. It is advantageous for creatures to ingest energy rapidly due to the threat of predation during feeding. Optimal conditions might thus be sought to maximize their energy intake rate. While the sweetest nectar offers the greatest energetic rewards, the exponential increase of viscosity with sugar concentration [98] also makes it the most difficult to transport. We here rationalize the different optimal concentrations reported for the different drinking strategies by developing a dynamic model for viscous dipping and comparing it to existing models of suction feeding. Our new viscous dipping model indicates an optimal sugar concentration of 52%, which is higher than that for suction feeding, 33%. This result suggests a rationale for the fact that the nectar concentration of flowers pollinated by viscous dippers such as bees (35%) is typically higher than that of those pollinated by suction feeders such as hummingbirds or butterflies

(20-25%) [102].

The sugar concentration that maximizes energy intake rate has been evaluated for a variety of nectar feeders in previous experimental studies (Figure 3-1). Careful consideration of all of these results indicates that this so-called ‘optimal concentration’ depends exclusively on feeding mechanism but not on body size, quantity of intake, or species. Roughly speaking, the optimal concentration for active or capillary suction feeders is 30-40% while that for creatures using viscous dipping is 50-60%. Optimal sugar concentrations for suction feeders have been previously rationalized by Kingsolver & Daniel, who established dynamic models for both active [64] and capillary [65] suction. Pivnick & McNeil [98] advanced the active suction model by introducing the assumption of constant power output for the suction pump, and so predicted an optimal concentration of approximately 35%, consistent with that observed. Daniel *et al.* further demonstrated how the optimal concentration of 35% emerges for active suction when muscular mechanics is considered [27]. Kingsolver & Daniel [66] also suggested a dynamic model for bees that relies on capillary imbibition into the hairs of the tongue, a physical picture expected to be valid only in the limit of small nectar uptake rates. Owing to its reliance on capillary suction, their model implies an optimal concentration of 30-40%, identical to that for suction feeders. However, for larger uptake volumes (Figure 3-1), this suction model is no longer expected to be valid, and fails to rationalize the higher optimal concentrations of 50-60% reported, for example, for bees [46, 116]. We proceed by briefly reviewing the active suction model developed by Pivnick & McNeil [98] and the capillary suction model of Kingsolver & Daniel [65], then developing a new dynamic model for viscous dipping. The result is a global physical picture that describes all nectar feeders, and indicates that the optimal concentration depends exclusively on drinking style.

3.1 Optimal sugar concentrations

Suction feeding may be simply described mathematically. The pressure-driven flow of a fluid of density ρ and viscosity μ along a tube of radius a , with mean speed u , is described

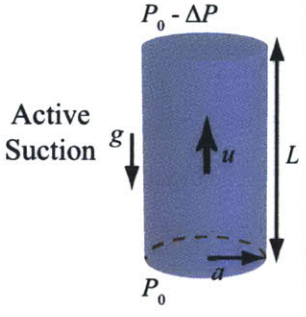
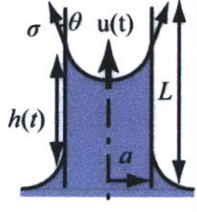
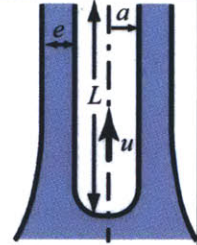
Mechanism	Name	Genus	Optimal (%)
 <p>Active Suction</p>	Ants	<i>Atta</i> <i>Camponotus</i>	30 40
	Bees	<i>Euglossa</i>	35
	Butterflies	<i>Agraulis</i>	40
		<i>Phoebis</i>	35
		<i>Speryeria</i>	35
		<i>Thymelicus</i>	40
	Moths	<i>Vanessa</i>	40
<i>Pseudaletia</i>		40	
<i>Macroglossum</i> <i>Manduca</i>		35 30	
 <p>Capillary Suction</p>	Humming-birds	<i>Selasphorus</i> <i>Selasphorus</i>	35-45
	Honey-eaters	<i>Anthochaera</i>	50
		<i>Phylidonyris</i>	40
		<i>Acanthorhynchus</i>	30
	Sunbirds	<i>Cinnyris</i>	30
 <p>Viscous Dipping</p>	Ants	<i>Pachycondyla</i>	50
		<i>Rhytidoponera</i>	50
	Bees	<i>Bombus</i>	55
		<i>Apis</i>	55
		<i>Melipona</i>	60
	Bats	<i>Glossophaga</i>	60

Figure 3-1: Optimal sugar concentrations for various nectar feeders [91]. The optimal concentration is that for which the energy intake rate is highest based on drinking rates measured at various nectar concentrations in a laboratory setting.[95, 13, 78, 12, 98, 45, 57, 131, 111, 133, 85, 46, 116, 113, 67]

by Newton's second law:

$$h \frac{du}{dt} = \frac{\Delta P}{\rho} - \frac{8\mu hu}{\rho a^2} - gh, \quad (3.1)$$

where g is the gravitational acceleration and ΔP the pressure difference applied at the height h of the nectar. For active suction, ΔP is mainly generated by cibarial muscles [64, 98], while for capillary suction, $\Delta P \sim \sigma/a$ results from curvature pressure, where σ is the surface tension [65]. A cornerstone of biomechanics is that the force that a creature of characteristic size l can generate [82] $F \sim l^2$; thus, one expects the suction pressure generated by muscles, $\Delta P \sim F/l^2 \sim l^0$, to be independent of scale and to be of comparable magnitude for all creatures (e.g. $\Delta P \sim 10$ kPa for both mosquitoes [66] and humans [89]). One can thus assess the tube scale $a \sim \sigma/\Delta P \sim 10 \mu\text{m}$ below which curvature pressure dominates the applied suction pressure ΔP . For most suction feeders, the radius a of the proboscis is of order $100 \mu\text{m}$ [78, 44], so the curvature pressure is less than the pressure applied in active suction. Nevertheless, capillary suction is employed by certain creatures (Figure 3-1) for which active suction is precluded by virtue of geometrical and physiological constraints such as the open, passive tongue of the hummingbird [44]. We further note that most suction feeders have tubes of characteristic length $L \sim 1$ cm [78, 44]; consequently, $\rho g L / \Delta P < 0.1$, and the effect of gravity on the flows is negligible. Finally, the ratio of inertial to viscous terms scales as $\rho a^2 f / \mu < 0.1$, where $f \sim 10$ Hz is the typical suction frequency [73, 32], indicating negligible inertial effects. Neglecting the gravitational and inertial terms in (3.1) yields $8\mu hu = a^2 \Delta P$.

In active suction, the nectar motion is described by Poiseuille flow, for which the volumetric flow rate is given by $Q = \pi a^2 u = \pi a^4 \Delta P / 8\mu L$. By measuring the dependence of flow rate on sugar concentration, Pivnick [98] inferred that butterflies apply constant suction power in drinking, regardless of nectar concentration. The work per unit time required to overcome the viscous friction on the wall or power output \dot{W} of the pump is given by $\dot{W} = Q \Delta P$. Expressing ΔP in terms of Q then yields the dependence of volume flux on viscosity: $Q = (\pi a^4 \dot{W} / 8\mu L)^{1/2} \propto \mu^{-1/2}$. In capillary suction, $\Delta P = 2\sigma \cos \theta / a$, where θ denotes the contact angle, and the height of the nectar is time-dependent: $h = h(t)$ and $u = h'(t)$ (Figure 3-1). The solution of the force balance, $4\mu h h' = a \sigma \cos \theta$, with initial

condition $h(0) = 0$ is given by $h(t) = (a\sigma t \cos \theta / 2\mu)^{1/2}$. Capillary suction consists of repeated cycles of tongue insertion and retraction. The whole time for a cycle is thus the sum of the time to absorb the nectar, T , and the time to unload it, T_0 . The average volumetric flow rate per cycle, \bar{Q} , is given by $\bar{Q} = \pi a^2 h(T) / (T + T_0) \propto (T/\mu)^{1/2} / (T + T_0)$, where $T^{1/2} / (T + T_0)$ depends weakly on viscosity [111], and so $\bar{Q} \propto \mu^{-1/2}$. Thus, for all suction mechanisms, we anticipate $Q \propto \mu^{-1/2}$.

To test these proposed scalings against experimental data, we introduce a general relation between Q and μ : $Q = X\mu^n$, where X is a geometry-dependent prefactor that we expect to be different for each species. If we plot Q as a function of μ on a log scale, n and X represent the slope and the offset on the y-axis respectively. For each species, we calculate an average value $\langle X \rangle = \langle Q\mu^{-n} \rangle$ based on the measured dependence of flow rate on viscosity. In Figure 3-2, red and blue points, respectively, indicate the dependence of $Q/\langle X \rangle$ on μ for active and capillary suction. The convincing collapse of the data, plus the fact that, for each species, the slopes are close to $-1/2$, together support the proposed scalings.

The energy intake rate \dot{E} is given by the product of the energy content per unit mass of sugar c , the sucrose concentration s , and the volumetric flow rate Q : $\dot{E} = Q\rho cs \propto s \cdot \mu(s)^{-1/2}$. For the sake of simplicity, density is treated as constant since its variation with sugar concentration is much less than that of viscosity. Considering the known dependence of nectar viscosity $\mu(s)$ on s [98], the dependence of \dot{E} on s can be computed as shown in the inset of Figure 3-2 and reveals an optimal concentration of 33% as inferred by Pivnick & McNeil for butterflies [98] and Kingsolver & Daniel for hummingbirds [65]. These predicted optimal concentrations are consistent with the results from the experimental studies reported in Figure 3-1.

We proceed by presenting a new model for feeding in which the nectar intake relies on viscous entrainment by the outer surface of the tongue (Figure 3-3). Viscous dipping is generally characterized by an extendible tongue being immersed into nectar, coated, then extracted as shown in Figure 3-3, where a honeybee (*Apis*) drinks nectar from a reservoir. One expects the volume entrained to be proportional to the area of the immersed tongue surface and the thickness e of the nectar layer. As in capillary suction, the feeding by

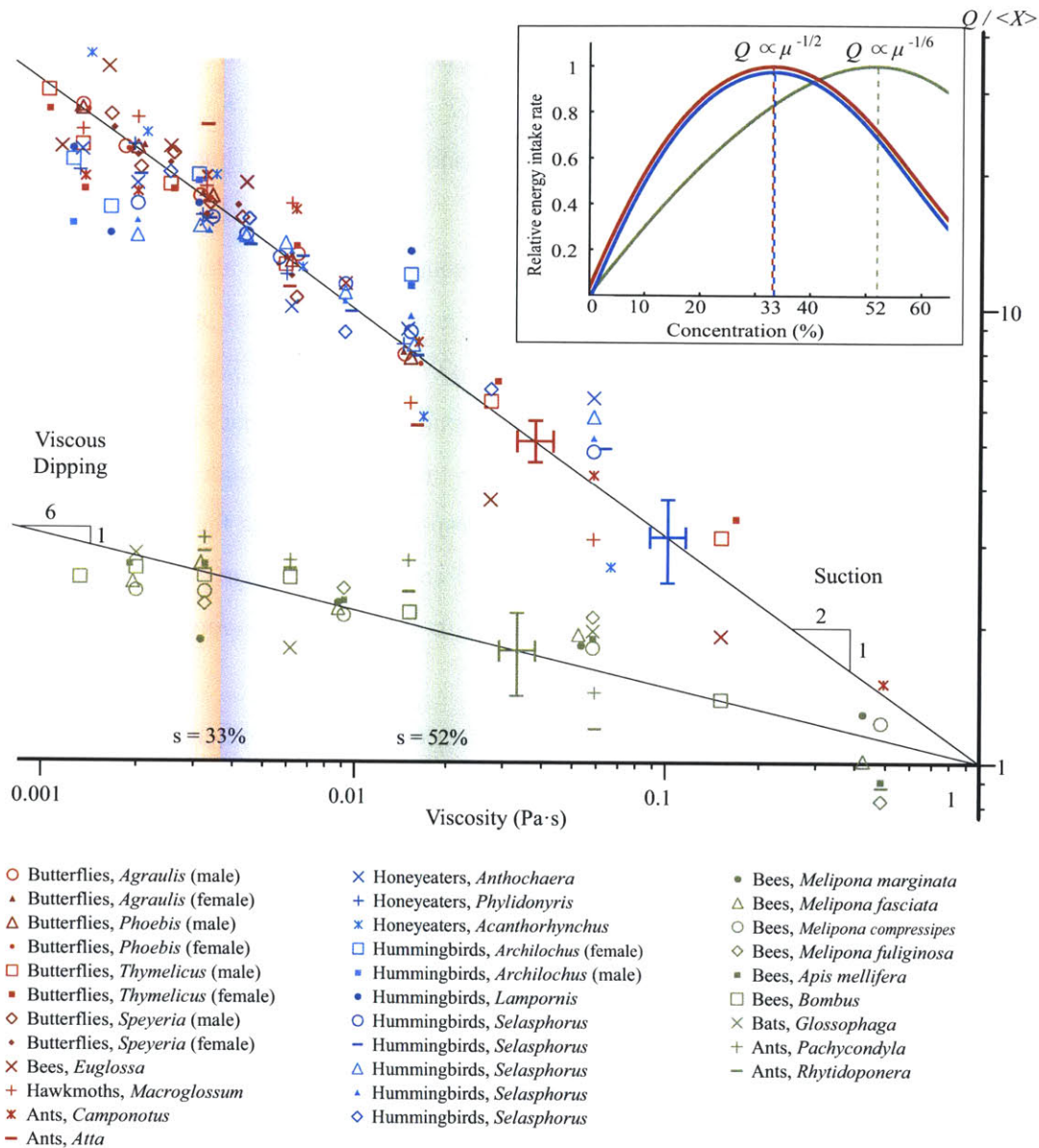


Figure 3-2: The dependence of scaled volumetric flow rate $Q/\langle X \rangle$ on nectar viscosity μ . The red points represent data for active suction, the blue points for capillary suction, and the green points for viscous dipping. The slopes of the expected lines for suction and viscous dipping are $-1/2$ and $-1/6$ respectively. Inset: optimal concentrations of 33% and 52% are evident for, respectively, suction feeding and viscous dipping from the dependence of relative energy intake rate on nectar viscosity. Characteristic error bars are shown. [78, 98, 12, 14, 57, 95, 85, 44, 133, 111, 116, 46, 113]

viscous dipping consists of repeated cycles. If T and T_0 represent, respectively, the time needed for tongue retraction and the interval between each cycle, then the volumetric flow rate is given by $\bar{Q} = 2\pi a e u T / (2T + T_0)$, where u represents the average tongue retraction speed.

Encouraged by its success in the modeling of suction feeding, we introduce the assumption that the work rate applied in viscous dipping remains constant with respect to nectar concentration. The movement of the tongue in the fluid requires the power $P_v \sim \mu L u^2$ to overcome the viscous drag, where L is the tongue length (Figure 3-3). The power required for tongue acceleration $P_t \sim m u' u \sim \rho a^2 u^3$, where $m \sim \rho a^2 L$ is the tongue mass. The ratio $P_t / P_v \sim \rho u a^2 / \mu L \ll 1$, so the effect of P_t is negligible. Assuming constant applied power P_v thus suggests that $u \propto \mu^{-1/2}$. One does not expect $T / (2T + T_0)$ to depend strongly on viscosity since if T is shorter in less viscous nectar due to a faster retraction, the unloading time T_0 would also be shorter, so that $T \propto T_0$. Thus, the average volumetric flow rate may be expressed as $\bar{Q} = 2\pi a e u T / (2T + T_0) \propto e \mu^{-1/2}$.

The thickness of the fluid layer entrained by a cylinder of radius a depends explicitly on three dimensionless groups: the Bond number $\text{Bo} = \rho g a^2 / \sigma$ (the ratio of hydrostatic to capillary pressures), the Weber number $\text{We} = \rho u^2 a / \sigma$ (the ratio of inertial to curvature pressures), and the Capillary number $\text{Ca} = \mu u / \sigma$ (the ratio of viscous stresses to curvature pressures). For bees, $\text{We} \sim 10^{-3} \ll 1$, $\text{Bo} \sim 10^{-3} \ll 1$, and $\text{Ca} < 0.1$ for $s < 65\%$, so the thickness of the liquid layer on a tongue is prescribed by the Landau-Levich-Derjaguin theory [103] that predicts $e \sim \text{Ca}^{2/3} a$. We thus anticipate that $\bar{Q} \propto e \mu^{-1/2} \propto \mu^{-1/6}$. In Figure 3-2, this proposed scaling is validated by the data for all creatures that employ viscous dipping. The energy intake rate, $\dot{E} = Q \rho c s$, thus scales as $\dot{E} \propto s \cdot \mu(s)^{-1/6}$. In the inset of Figure 3-2, the energy intake rate is plotted as a function of the sucrose concentration, and peaks at a concentration of 52%, which is consistent with the data presented in Figure 3-1. Our analysis thus provides the first rationale for the different optimal concentrations reported for creatures using suction and viscous dipping. For example, we can now rationalize the observation that orchid bees that employ active suction have optimal concentrations of 35%, while honeybees and bumblebees that use viscous dipping, 50-60% [13].

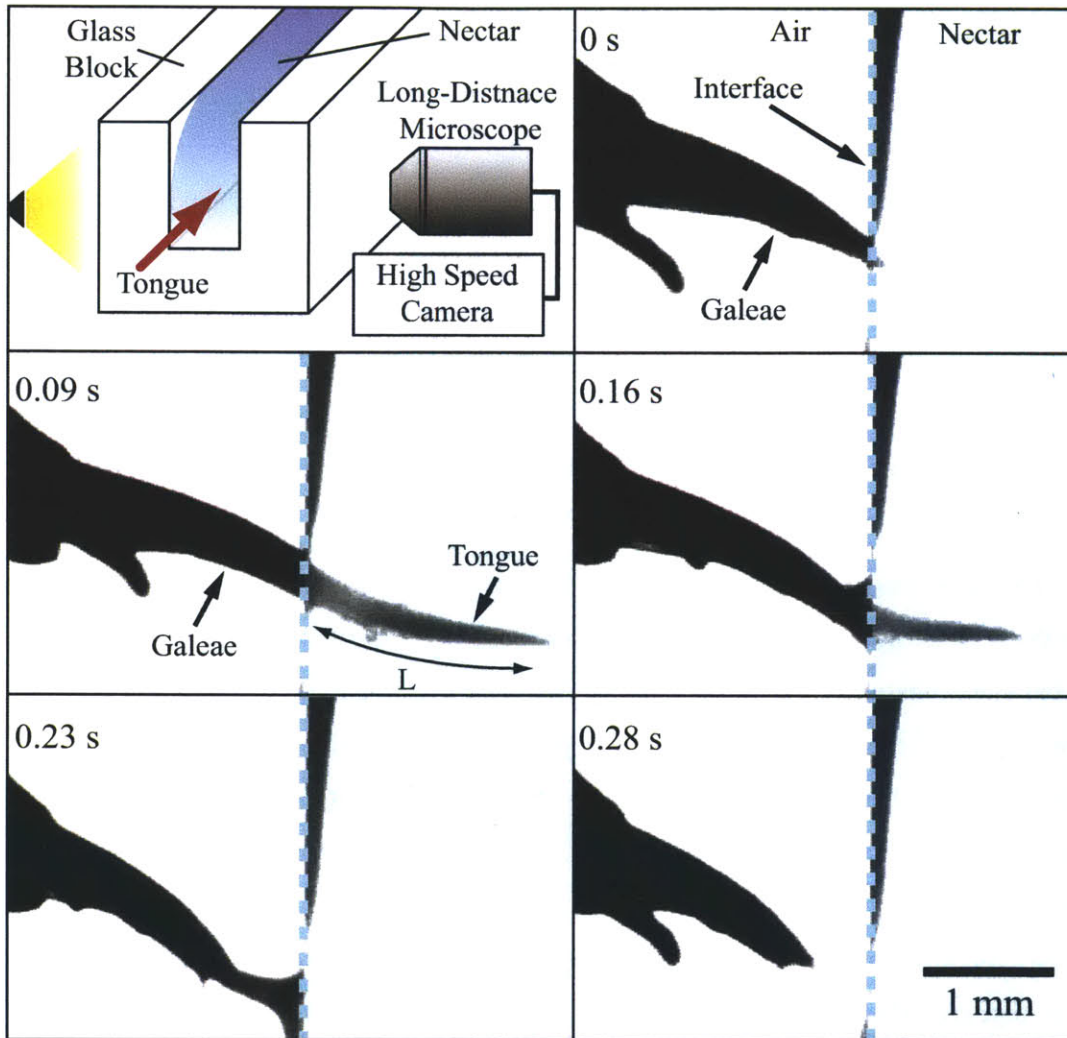


Figure 3-3: Bees uptake nectar via viscous dipping. A schematic illustration of the experiment that allows us to visualize the viscous dipping of a honeybee (*Apis*) with a long-distance microscope and a high-speed camera operating at 250 frames per second. Here, the bee's tongue is dipped into a 40% sucrose solution, then withdrawn.

3.2 Coevolution between flowers and pollinators

A relatively complete physical picture of the fluid dynamics of nectar feeding has emerged. First and foremost, the optimal nectar concentration for a given creature depends only on its drinking style, being higher for viscous dippers than suction feeders. When considered in light of the coevolution between flowers and pollinators, this deduction provides rationale for the observation that the nectar concentration of flowers pollinated by bees (35%) is generally higher than that of those pollinated by butterflies and hummingbirds (20-25%) [102]. Several caveats are in order, however. The optimal concentration in the laboratory might differ from that preferred in nature due to the limited availability of nectar in the wild. Specifically, in addition to energy intake rate, nectar feeders in the wild presumably consider competition between other individuals or colonies [116], and travel costs [52]. Moreover, the nectar concentration proffered by flowers need not correspond to the optimal value owing to the pollination strategy of flowers [50]. Indeed, it has been suggested that flowers try to keep their pollinators hungry and faithful [146] because too great an energy reward would decrease the inter-flower movement of pollinators, and too small a reward would bring about desertion of the pollinators. Hence, the optimal concentrations suggested by dynamic models still need to be carefully scrutinized in attempts to understand the cues of coevolution between flowers and nectar feeders.

3.3 Methods

Live honeybees were purchased from a merchant in Paju, South Korea in June, 2010. One of the bees was confined to a cylindrical cage of inner diameter 15 mm. One end of the cylindrical cage had a window through which the bee could extrude its head. A feeder made with glass blocks was filled with a 40% (by mass) sucrose solution and placed sufficiently close to the window that the bee could drink from it. We filmed the drinking process with a high speed camera (Photron APX-RS) operating at 250 frames per second with a zoom lens (Navitar 12X Zoom) (Figure 3-3).

Chapter 4

The hummingbird's tongue: a self-assembling capillary syphon

Capillary action was one of several mechanisms proposed to account for hummingbird nectar uptake in the 19th century [77, 36]. The question received renewed attention in the 1930s, and despite disagreements regarding the relative importance of capillarity [121, 120] and a mechanism relying on the combined action of the bill and the tongue [86, 88], a consensus emerged that capillarity plays at least a partial role [87]. According to this hypothesis, once the tongue tip touches a nectar reservoir, surface tension drives the nectar flow through the tongue's grooves, loading the tongue before its subsequent withdrawal and unloading.

The distal portion of the hummingbird's tongue forms two parallel C-shaped grooves that split in a bifurcated end [44] (Figure 4-1*a*). These grooves consist of keratinized membranes on the order of 25 μm in thickness, which curl around a relatively rigid, keratinized rod [145]. The free edge of the groove ends in fine fringes or lamellae that are generally attributed to wear [75, 108]. Since vascular and nervous tissues recede at the tip of the tongue [145, 44], no active change of shape of these grooves is possible: tongue groove deformation can only be driven by hydrodynamic forces arising from interaction with the nectar.

Flexible solids in the presence of liquids can be deformed by interfacial forces [114]. Py *et al* [101] presented the first example of capillary origami, demonstrating that thin sheets

with bending stiffness B can be folded up by the surface tension σ of a water droplet placed on them, provided that the largest sheet dimension exceeds the elastocapillary length $l_E = (B/\sigma)^{1/2}$. Recently, Rico-Guevara and Rubega [108] demonstrated that a hummingbird tongue closes around nectar, thus representing a natural example of capillary origami [105]. Their high-speed videography indicates that when the tongue is withdrawn from the nectar, the formerly immersed portion of the tongue changes shape, so that the thin membrane curls inwards and traps liquid inside its grooves. They thus described the drinking mechanism as a fluid trap: surface tension causes the trap to close, after which the fluid is transported mouthward by tongue retraction.

An open question remains concerning how the nectar fills the entire tubular grooves, each of which is on the order of 1 cm in length and 150 μm in radius [44]. Specifically, what is the relative importance of fluid trapping and capillary suction in the loading of the tongue? We note that the former does not preclude the latter, and so expect both to be significant. Since the nectar reservoirs of many of the hummingbirds' target flowers are shorter than the tongue groove length, the entire groove can not always be immersed in the reservoir [67], in which case fluid trapping without capillary suction would not optimally load the tongue.

Kingsolver and Daniel [65] proposed the first dynamic model for capillary suction in a solid tube. By demonstrating that this model successfully predicts the dependence of nectar intake rate on nectar concentration, Kim *et al.* [62] recently provided a rationale for the optimal concentrations [52] for the fastest energy uptake, 33% for suction feeders, as measured in a laboratory setting. Here we present *in vivo* observations of capillary suction in a hummingbird tongue using high-speed videography [109, 61]. We also report direct observations of elastocapillary behavior [101, 59, 114, 10], as the tongue is deformed by capillary forces during nectar uptake. We then develop a theoretical model for the hummingbird's drinking process, thereby elucidating how the elastic deformation of the tongue affects the nectar dynamics.

4.1 *In vivo* observations

We filmed captive ruby-throated hummingbirds (*Archilochus colubris*) drinking a sucrose solution (10% by mass) from a feeder (see Figure 4-1). A 1.6 mm diameter hole on the top of the feeder allows the bird to insert only the distal portion of its beak into the feeder. We adjusted the level of the sucrose solution so that the bird had to extend its tongue tip approximately 13 mm out of its bill to reach the reservoir. Figure 4-1B indicates that as soon as the tongue tip touches the free surface of the reservoir, the liquid begins to rise along the tongue groove, thus clearly demonstrating capillary suction of the sucrose solution along the hummingbird's tongue. The rise continues until the tongue is extracted from the liquid, and the tongue is retracted into the beak.

For quantitative analysis of the capillary suction and tongue deformation, the tongue is observed at a higher magnification (see Figure 4-2). Before entering the liquid, the tongue tips adhere to each other due to surface tension, indicating that the tongue is prewetted with either nectar or saliva. Upon contact with the fluid, the immersed tips separate, and the sucrose solution starts to climb up along the tongue, as indicated by the rising menisci in Figure 4-2a. The menisci advance at a speed $u \sim 20$ cm/s in response to capillary action, and the tongue is moving at a speed less than 7 cm/s while the tongue tip is immersed in the nectar. After being loaded by capillary suction, the tongue retracts with peak speeds of 33 cm/s. The tongue protrusion and retraction are repeated at a frequency of approximately 6 Hz.

Examining dorsal views of the tongue during capillary suction indicates the deformation of the tongue since the tongue's lateral extent becomes smaller after its inner surface is wetted by the nectar (Figure 4-1a). Our measurements reveal that the outer tongue diameter decreases by approximately 10% near the advancing meniscus, but we observe that surface tension does not cause the complete closure of the groove. A schematic illustration of the deformation of one of the two tongue tubes is presented in Figure 4-3.

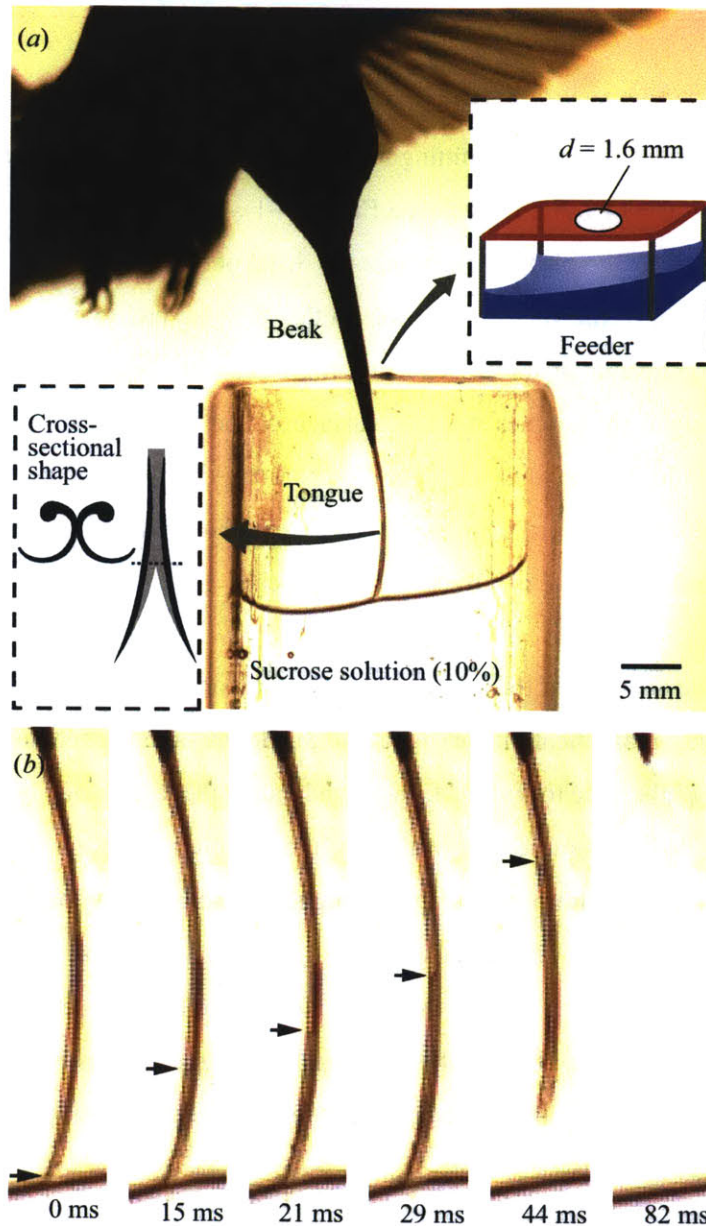


Figure 4-1: A hummingbird (*Archilochus colubris*) drinking from a transparent feeder. (a) A photograph of the drinking bird. Inset: schematic illustration of the hummingbird's tongue and feeder. The feeder is made of glass plates, and wrapped with red paper in order to attract the bird. (b) High-speed images of the hummingbird drinking from a feeder. Owing to the transparency of the tongue, the meniscus of the rising nectar (arrows) is observable. As the tongue tip touches the surface, interfacial forces drive the liquid along the tongue at speeds of approximately 20 cm/s.

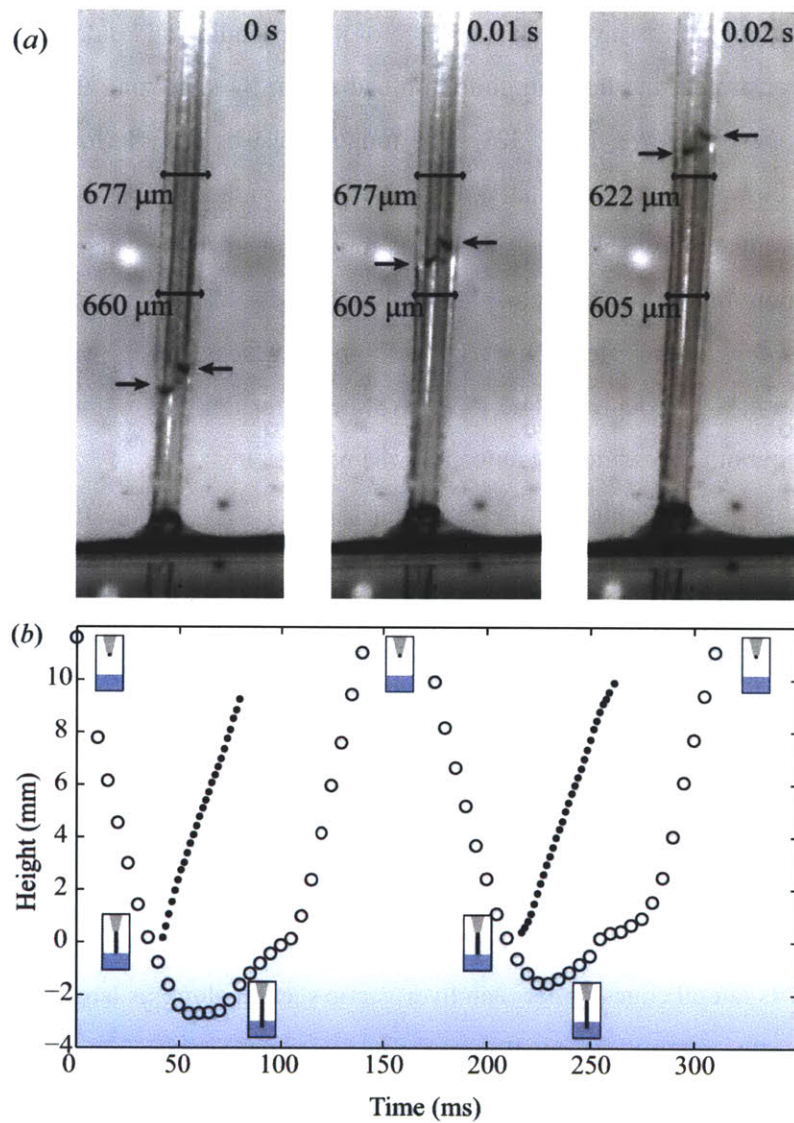


Figure 4-2: Capillary suction through a hummingbird's tongue (*Archilochus colubris*). (a) A dorsal view of the tongue of a hummingbird drinking sucrose solution of 20% concentration by mass. The arrows indicate the two menisci of the rising nectar. The tongue width becomes smaller after the inner surface is wetted by the nectar. (b) The position of the tongue tip (open circles) and meniscus (closed circles) during two consecutive licks. The measurement is interrupted when the meniscus moves beyond the field of view. The nectar rise speed is approximately 20 cm/s. The capillary rise of the nectar clearly precedes the tongue retraction.

4.2 Tongue deformation

Drinking in hummingbirds involves a sequence of nectar loading and unloading events. It has been demonstrated that hummingbirds unload nectar by squeezing their tongues between their upper and lower bills [32]. The tongue must be flexible for this unloading process. In addition, when only small quantities of nectar are available in the target flowers, a flexible tongue may make it easier for the tongue lamellae to sweep the corolla tube [94, 108]. Hummingbirds feed from plants with a variety of floral morphologies: Jewelweed (*Impatiens capensis*) even have forward-pointing nectar spurs which require the tongue to bend at a 180 degree angle [53]. We thus infer that the tongue's flexibility is advantageous in both accessing and unloading the nectar.

We proceed by examining its role in nectar transport. We model the tongue as an open circular groove without longitudinal variation (see Figure 4-3), with radius $a \sim 150 \mu\text{m}$, thickness $e \sim 25 \mu\text{m}$, length $l \sim 1 \text{ cm}$, and opening angle 2α ranging from 0 to π [145, 44]. The ratio of hydrostatic to capillary pressures is prescribed by the Bond number $Bo = \rho g a l / \sigma$, where ρ is the density of the nectar, g the gravitational acceleration and σ the surface tension. Owing to the weak dependence of σ and ρ on sucrose concentration [65], we treat $\sigma \sim 0.07 \text{ N/m}$ and $\rho \sim 1000 \text{ kg/m}^3$ as constants with respect to sucrose concentration. Since Bo attains a maximum value of 0.2 for the worst-case scenario of a vertical tongue, we infer that tongue deformation is caused principally by surface tension applied along its lateral edges rather than hydrostatic suction along its length.

To estimate the tongue deformation, we consider a lateral segment of the groove of length βa , as shown in Figure 4-3, where the angle β is measured clockwise from the edge. Balancing moments about the point C yields the bending moment $M(\beta)$ per unit length at the cross section, $a\beta$ away from the edge: $M(\beta) = \sigma a [\cos \alpha - \cos(\alpha + \beta)]$, where a clockwise moment is defined as positive. Then, applying Castigliano's theorem [137] yields the maximum tongue displacement δ at the edge:

$$\delta = \int_0^{\pi-\alpha} \frac{M}{B} \frac{\partial M}{\partial \sigma} a d\beta = \frac{\sigma a^3}{B} \Omega, \quad (4.1)$$

where $B \sim Y e^3$ is the bending stiffness per unit length, Y the tongue's Young's modulus,

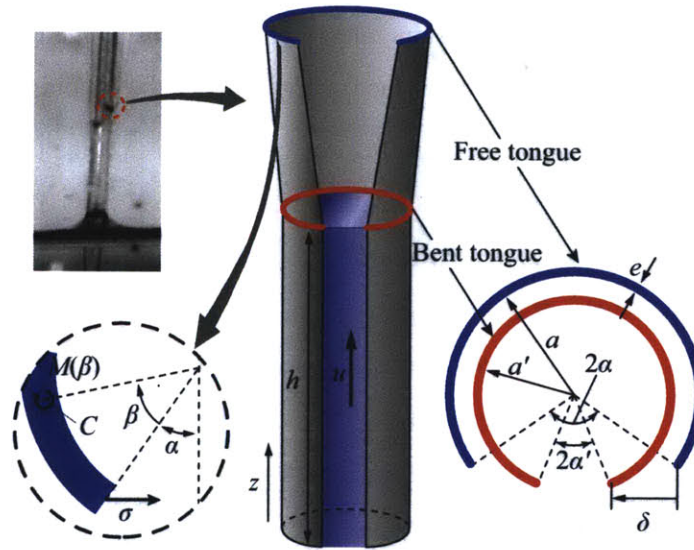


Figure 4-3: A schematic illustration of nectar rise along the flexible tongue of the hummingbird, which closes in response to the surface tension. For the sake of clarity, only one of the tongue's two grooves is illustrated.

and $\Omega = (1/4)[2(\pi - \alpha)(2 + \cos 2\alpha) + 3 \sin 2\alpha]$. The dimensionless deformation thus scales as $\delta/a \sim \Gamma$, where $\Gamma = a^2\sigma/B$ represents the control parameter of the system. By measuring $Y \sim 300$ kPa (see § 4.6), we estimate $\Gamma \sim 0.3$ and thus consider the regime of weak deformation, which is consistent with our direct observations of the tongue diameter contracting by approximately 10% near the advancing meniscus.

4.3 Elastocapillary suction

We define the Weber number $We = \rho au^2/\sigma$, the ratio of inertial to curvature pressures, and the reduced Reynolds number $Re = \rho ua^2/\mu l$, the ratio of inertial to viscous forces. We rely on the reported nectar viscosity [142], which strongly depends on sucrose concentrations, and $0.001 < \mu < 0.1$ for sucrose concentrations between 0 and 65%. For typical rise speeds $u \sim 0.1$ m/s (Figure 4-2b), we estimate $We \sim 0.02$ and $0.002 < Re < 0.2$. Therefore, inertial effects are negligible, and the nectar flow through the hummingbird's tongue is described by Stokes equation: $-\partial P/\partial z + \mu \nabla^2 u = 0$, where P is the pressure. The pressure gradient may thus be expressed by $\partial P/\partial z = (\partial E/\partial h)/V$, where V is the nectar volume

inside the tongue, and E the total system energy contained inside the tongue of height h (see Figure 4-3), specifically, the free surface energy E_s plus the bending energy E_b .

For nectar rise by an infinitesimal height Δh from h to $h + \Delta h$, the free surface energy associated with the inner surface of the tongue increases by $2(\pi - \alpha)(\gamma_{SL} - \gamma_{SV})a\Delta h$, where γ_{SL} and γ_{SV} are the interfacial energy per unit area between solid and liquid and solid and gas, respectively. Also, owing to the interfacial area between liquid and gas at the gap of both edges, the free surface energy increases by $2a' \sin \alpha' \sigma \Delta h$, where a' and α' are respectively the radius of the groove and the half opening angle after deformation (see Figure 4-3). Using Young's equation, $\gamma_{SV} - \gamma_{SL} = \sigma \cos \theta_c$, the increase of free surface energy ΔE_s can thus be expressed by $\Delta E_s = 2[-(\pi - \alpha)a \cos \theta_c + a' \sin \alpha']\sigma \Delta h$, where θ_c is the contact angle. The bending energy is principally associated with the change of the cross-sectional tongue shape. Since the strain energy per unit longitudinal length is $2\sigma\delta = 2\sigma a\Gamma\Omega$, the increase of the strain energy for deformation over a length Δh is given by $\Delta E_b = 2a\sigma\Gamma\Omega\Delta h$.

Substituting into Stokes equation yields:

$$\nabla^2 u = \frac{1}{\mu V} \frac{\partial}{\partial h} (E_s + E_b) = -\frac{2\sigma}{\mu Ah} \{(\pi - \alpha)a \cos \theta_c - a' \sin \alpha' - a\Gamma\Omega\}, \quad (4.2)$$

where $A = (\pi - \alpha' + \cos \alpha' \sin \alpha')a'^2$ denotes the cross-sectional area of the rising nectar. The no-shear and no-slip boundary conditions are applied at, respectively, the meniscus between the edges and the inner wall of the tongue (see Figure 4-3).

The solution of Stokes equation gives the velocity distribution of u over the cross-sectional area A . From the computation of the velocity field via the Finite Element Method (FEM), we estimate the average flow speed and the nectar rise $h(t)$ (see § 4.6). For a licking frequency f , the energy per volume of nectar c , and the time of contact with the nectar τ for each lick, the energy intake rate ε predicted by our model is $\varepsilon = fcAh(\tau)$.

We restrict our attention to a given f , τ , nectar properties (μ , σ , c), and lateral perimeter of the tongue. While the driving capillary pressure decreases with α , the cross-sectional area through which nectar flows increases with α , so one anticipates an optimal opening angle for which the hummingbird attains the fastest energy intake. In Figure 4-4, we plot

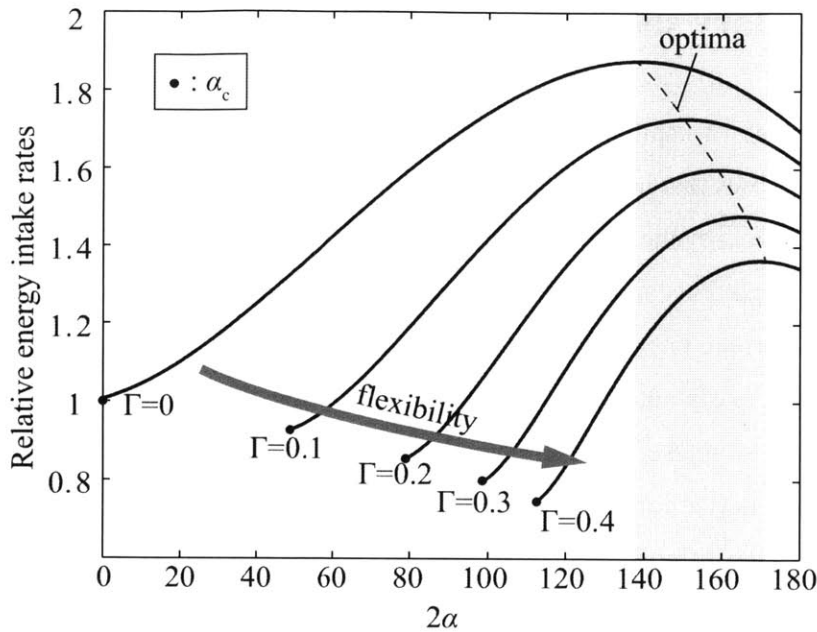


Figure 4-4: The dependence of the energy intake rates on the opening angle 2α for different $\Gamma = \sigma a^2/B$, where a is the undeformed radius and B is the bending stiffness per unit length. Here the energy intake rate is scaled by that for the tongue of $\alpha = 0$, $\Gamma = 0$, and $a = 150 \mu\text{m}$. The closed circles represent α_c , a limit below which the two lateral edges come into contact after bending. The tongue perimeter is the same for all cases. The optimal opening angles 2α that maximize energy intake rates are indicated by the dashed line and lie between 140° and 170° .

the energy intake rates for tongues that have the same perimeter but different Γ . The energy intake rates are normalized by that obtained for $\alpha = 0$, $\Gamma = 0$, and $a = 150 \mu\text{m}$, and α_c represents a limit below which the two lateral edges come into contact after bending. Although the optimal opening angle depends on Γ , the normalized energy intake rate is maximized at opening angles between 140° and 170° . For parameters relevant for the hummingbird, we conclude that opening angles $140^\circ < 2\alpha < 170^\circ$ optimize energy uptake because viscous resistance relative to curvature pressure is minimized for the optimal angles. Since the results presented in Figure 4-4 are independent of the frequency, we expect them to be valid even at higher licking frequencies, which can be as large as 17 Hz when the distance between the beak tip and the nectar is smaller [32].

4.4 Capillary suction vs. Fluid trapping

Recently, the role of capillary action in hummingbird feeding has been questioned: a new model proposes that instead of being taken up via capillary suction, fluid is captured through entrainment by the tongue following submergence, a mechanism called ‘fluid trapping’ [108]. Arguments against the role of capillary action include the observation that nectar intake rates are only weakly dependent on flower orientations (pendulous or erect). However, as previously noted, the value of $Bo \sim 0.2$ indicates that gravitational effects are negligible in nectar uptake. Another potential inconsistency of the capillary model is that it predicts optimal nectar concentrations (30-40%), specifically those that maximize energy uptake rate, that are different from preferred concentrations (45-60%), as deduced from the statistics of visit frequency to feeders with different nectar concentration [133, 110]. However, a bird’s preferred concentration may depend on factors such as gustatory preferences [83] or physiological state [19] and thus may not correspond to the optimal concentrations.

We note that fluid trapping does not inherently preclude capillary suction, so hummingbirds can use both mechanisms. In our experimental set-up, we can assess the importance of each mechanism. To permit visualization of the tongue outside of the bill and in a vertical orientation (Figure 4-2), we positioned the level of the sucrose solution (20% by mass) in the feeder sufficiently far from the opening of the feeder that the tongue must extend approximately 15 mm from the bill to be immersed by an amount $h_i \sim 2$ mm in the sucrose solution. We measured $a \sim 150 \mu\text{m}$, $\tau \sim 50$ ms, $\mu \sim 2$ mPa·s, so the length loaded via capillary suction in a time τ is given by $h_c \sim (\sigma a \tau / (2\mu))^{1/2} \sim 1$ cm (see § 4.6). We thus deduce $h_c/h_i \sim 5$, and so assess that capillary suction is the dominant nectar loading mechanism in this experimental setting.

Our experimental set-up likely resulted in a longer tongue extension and slower licking frequency than may occur in natural feeding bouts. The relative importance of capillary suction and fluid trapping in the wild will in general depend on the depth of the nectar reservoir of the visited flower as well as on the licking frequency of the hummingbird. Very little data exist for heights of nectar, and estimating this is challenging: nectar volume can vary temporally as well as within and among populations [9, 58, 70, 42, 5], and data

on corolla diameter are scarce [136]. Moreover, the diameter at the base of the corolla tube may be different from the distal corolla diameter.

We list corolla measurements of six species of flowers visited by ruby-throated hummingbirds (see Table S1). Using images obtained from the digital herbaria of the New York and Missouri Botanical Gardens as well as specimens from the Gray Herbarium (Harvard University Herbaria), we obtained a rough measurement of proximal corolla width, which we used to estimate a possible upper-bound value for nectar height (see Table A.1 and Fig. B-1-B-5). Due to the uncertainties associated with estimates of nectar volume as well as internal corolla shape, these calculations are approximations, yet it appears that some plants may have a small nectar height H compared to the tongue groove length of $l \sim 1$ cm in the ruby-throated hummingbird [44]. In addition, during a natural drinking bout, the volume of nectar in a flower will decrease progressively. Thus, partial immersion of the tongue ($h_i \sim H \sim 1$ mm) may commonly arise in the wild.

The capillary loading length h_c depends critically on μ and τ . The loading time τ may be bounded by the licking frequency f , which ranges from 6 Hz (our observations) to 17 Hz [32], and has been shown to depend on tongue's extrusion length and corolla shape [134]. In our observations (Figure 4-2), $\tau \sim 50$ ms is approximately 1/3 of the period of the full licking cycle $T = 1/f \sim 150$ ms. If we were to assume similar tongue kinematics of $\tau/T \sim 1/3$ for different licking frequencies, we would expect that $20 < \tau < 50$ ms for $6 < f < 17$ Hz. By using the empirical dependence of μ on sucrose concentration c [142], we deduce the dependence of h_c on c for different τ (see Figure 4-5). As the concentration of the hummingbird flowers is typically 20-25% [102], the model results presented in Figure 4-5 indicate that when a hummingbird drinks nectar from a flower with a shallow nectar reservoir of $H_1 = 1$ mm, the majority of its nectar is loaded via capillary suction for biologically relevant values of τ . Fluid trapping becomes appreciable when the hummingbird drinks from deeper nectar reservoirs (i.e. $H_3 = 10$ mm) or with high licking frequencies. While the relative importance of capillary suction and fluid trapping will thus in general depend on feeding rates, tongue and plant morphology, available estimates indicate that hummingbirds may benefit from capillary suction in many natural settings.

Previous laboratory experiments of the hummingbirds drinking [44, 133, 85, 111, 67]

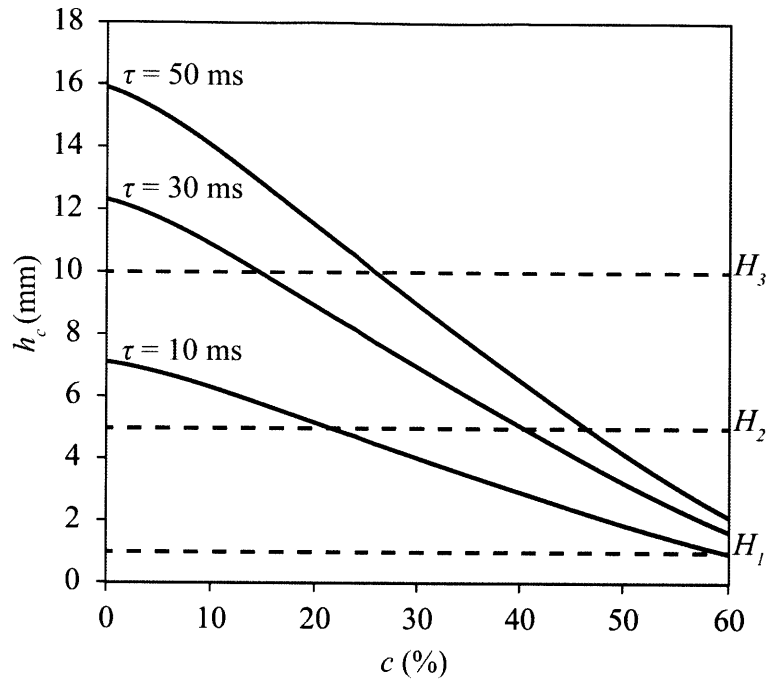


Figure 4-5: The dependence of the tongue length loaded by capillary suction, h_c , on sucrose concentrations c for a range of biologically relevant loading times τ . We represent three different nectar reservoir depths of $H_1 = 1$ mm, $H_2 = 5$ mm, and $H_3 = 10$ mm by dotted lines. Provided that the tongue immersion depth $h_i \sim H$, curved and dotted lines allow for a comparison between nectar volumes loaded via capillary suction and fluid trapping.

lend support to the capillary suction model [65]. These indicate that the observed dependence of nectar intake rates on nectar concentrations are satisfactorily rationalized by the capillary suction model [62]. Moreover, the fact that the average volumetric uptake rate decreases with nectar concentrations [67] is consistent with the capillary suction model, but inconsistent with the fluid trap model, which suggests that nectar uptake rates are independent of nectar concentration.

4.5 Discussion

We have presented *in vivo* observations of a hummingbird drinking that indicate both the elastocapillary deformation of the hummingbird's tongue and capillary suction along its length. The hummingbird's tongue may thus be best described as a self-assembling capil-

lary syphon. Our observations clearly indicate that fluid trapping and capillary suction are complementary rather than mutually exclusive mechanisms. While both are viable mechanisms for nectar uptake, we conclude that capillary suction is important in many natural settings. Nectar reservoirs are often shallow relative to the tongue's groove length, thus precluding tongue submergence, in which case capillary suction is predominantly used. Moreover, the dependence of nectar uptake rates on nectar concentrations reported in the biological literature [44, 133, 85, 111, 67] for the hummingbird are well rationalized by the capillary suction model [62].

Guided by our observations, we have developed a theoretical model for the elastocapillary suction of nectar. The model suggests that the hummingbird can maximize the energy uptake rate when the opening angle of its tongue is roughly 150° . Our model thus provides new rationale for the shape of the tongue: specifically, the fact that each of the two grooves of a hummingbird's tongue is nearly semicircular (Figure 4-1a). The results of our model (Figure 4-4) suggest that, for a given opening angle, a rigid tongue ($\Gamma = 0$) enables the hummingbird to maximize the energy uptake. Nevertheless, tongue flexibility $\Gamma \sim 0.3$ presumably evolved since it is advantageous for both accessing and unloading nectar.

Floral nectar is the primary energy source of hummingbirds, and their inter-flower movement serves to pollinate flowers. This mutual reliance can result in coevolution of bill shape and floral morphologies [135, 136, 106]. Thus, the detailed shape of the hummingbird's tongue may also be affected by the corolla morphology and nectar attributes of its target flowers. Nevertheless, flexible tongues with semicircular cross-sectional shapes are characteristic of many hummingbirds, as well as sunbirds and honeyeaters [94], which may rely on similar nectar uptake styles.

4.6 Methods

4.6.1 *In vivo* high-speed imaging

The images were taken at the Concord Field Station, in Concord, Massachusetts. We filmed four individuals (of the species *Archilochus colubris*), feeding during flight in a cage (Fig-

ure 4-1) or while held in the hand (Figure 4-2). The birds fed spontaneously. The feeders contain a sucrose solution of concentration 10% (Figure 4-1) or 20% (Figure 4-2) by mass, which is sufficiently far from the opening of the feeder for the birds to have to extend their tongues out of their bill in order to reach the liquid. We filmed the dynamics of the tongue and nectar with high-speed cameras (Phantom V5.2 running at frame rates of 1000 fps for Figure 4-1 and Photron Fastcam 1024 PCI running at frame rates of 2000 fps for Figure 4-2).

4.6.2 Tension stress experiment

We prepared a rectangular sample (1.0×0.2 mm) from the tongue tip of a deceased hummingbird (*Archilochus colubris*). We stuck the extremities of the samples on a plastic holder. By using a high-precision dynamometer, we recorded the force exerted on the sample while extending it. By measuring a deformation rate in the elastic regime, we calculated the Young's modulus. Although the thickness of the tongue is not uniform, we assumed a thickness of $25 \mu\text{m}$ in order to calculate a value of $Y \sim 300$ kPa.

4.6.3 Finite Element Method

The linearity of Stokes equation enables us to find the solution via numerical solution of

$$\nabla^2 u_n = -1, \quad (4.3)$$

with the boundary conditions:

$$\left. \begin{aligned} u_n(r, \theta) = 0 \quad \text{on} \quad r = 1 \quad \text{and} \quad \alpha' < \theta < 2\pi - \alpha' \\ \frac{1}{\cos \theta} \frac{\partial u_n}{\partial r} - \frac{1}{r \sin \theta} \frac{\partial u_n}{\partial \theta} = 0 \quad \text{on} \quad r = \frac{\cos \alpha'}{\cos \theta} \quad \text{and} \quad -\alpha' < \theta < \alpha'. \end{aligned} \right\} \quad (4.4)$$

By using the FreeFEM++ software (see <http://www.freefem.org>), the velocity distribution of u_n is found. The dimensionless volumetric flow rate Q_n through A_n , the cross-sectional area bounded by (4.4), depends only on α' . The volumetric flow rate Q for the tongue dimensions is then given by $Q = -(\partial P / \partial z) a'^4 Q_n(\alpha') / \mu$. Since Q is the product of the

cross-sectional area A and the rise speed dh/dt , one readily obtains the differential equation:

$$\frac{dh}{dt}A = -\frac{1}{\mu} \frac{\partial P}{\partial z} a'^4 Q_n(\alpha'), \quad (4.5)$$

which we solve with the initial condition $h(0) = 0$. For the prewetted tongue ($\theta_c = 0$), the solution of (4.5) yields the dependence of rise height on time:

$$h(t) = \frac{2a'^2}{A} \sqrt{\frac{\sigma Q_n(\alpha')}{\mu} [a(\pi - \alpha) - a' \sin \alpha' - a\Gamma\Omega] t}. \quad (4.6)$$

The lateral perimeter of the tongue groove does not change through bending, $(\pi - \alpha)a = (\pi - \alpha')a'$ and $\delta = a\Gamma\Omega \approx a\alpha - a'\alpha'$. Solving these equations for a' and α' yields: $a' = (1 - \Gamma\Omega/\pi)a$ and $\alpha' = [1 - (\pi - \alpha)/(\pi - \Gamma\Omega)]\pi$ in (4.6). For a rigid, circular tube ($\Gamma = 0$, $\alpha' = \alpha = 0$, $a = a'$), $Q_n(0) = \pi/8$ and $h(t) = (a\sigma t/(2\mu))^{1/2}$.

Animal Care

Animals used in these experiments have been captured under state and federal collection permits and have been maintained and filmed following protocols approved by Institutional Animal Care and Use Committee at Harvard University, Faculty of Arts and Science, to M. Baldwin and A. Biewener.

Chapter 5

Optimal Concentrations in Transport Networks

Transport networks are ubiquitous in nature and technology. Whether biological such as the vascular systems of plants and animals or engineered such as man-made pipes, roads, electrical grids, and the internet, they serve to move matter, energy, or information from one place to another. Due to the cost of constructing and maintaining redundant channels, it is advantageous for biological transport systems to distribute matter efficiently [69, 139]. Oxygen transport in vertebrates [90, 130], sugar transport in plants [54], and drinking strategies of many animals [60, 63] are known to be optimized for efficient transport of energy and material. Engineered systems must likewise be cost-effective and able to provide efficient transport under a variety of conditions; for example, considerable resources are spent annually to ease traffic congestion.

In our examination of transport networks, we consider material flow in four different natural systems: blood flow in vertebrates, sugar transport in vascular plants, and two modes of nectar drinking in birds and insects. A common feature of these and other transport networks is that the flow impedance depends on concentration. While the most concentrated solutions offer the greatest potential in terms of material transfer, the increase of impedance with concentration also makes them the most difficult to transport. Additionally, most transport networks are subject to a set of limiting constraints. For example, nectar feeders are typically constrained by a constant work rate, which in turn is a function of flow

impedance and hence concentration [98, 62, 63]. These transport networks may thus be characterized in terms of an optimization problem subject to appropriate constraints. This approach has been used to rationalize observed concentrations in a wide range of natural systems [98, 11, 62, 130]. For example, the observed volume fraction of erythrocytes (red blood cells), typical $\sim 40\% - 50\%$ in humans, has been shown to maximize oxygen transport [11, 130]. With the widespread use of bio-inspired design in the development of novel engineered systems, it seems likely that man-made transport networks such as roads or the electrical grid may benefit from improved understanding of natural transport systems.

We here develop a general framework for determining the concentration that maximizes material transfer in transport systems. By drawing on a number of natural examples – both new and derived from the biology literature – we show how these can be treated within a single framework that provides new insight into the efficiency of transport networks. We compare our model predictions to experimental data from more than 100 animal and plant species collected from the literature. Finally, we show that similar optimization criteria may be applied to engineered systems, and consider traffic flow in the context of our new framework.

5.1 General formulation

We consider systems in which the material transfer rate (material flow) J can be expressed as the product of a volumetric flow rate (volume flow) Q and a concentration of material c

$$J = Qc \tag{5.1}$$

We express the volume flow as $Q = Xf/\mu$ where X is a geometric factor, f quantifies the mechanism driving the flow, and μ characterizes the impedance. The material flow in Eq. (5.1) can be expressed as

$$J = \frac{Xf}{\mu}c \tag{5.2}$$

where X , f and μ can all depend on c . We now seek the optimal concentration $c = c_{\text{opt}}$ that maximizes J in Eq. (5.2) subject to a set of constraints, e.g. constant driving pressure or

constant work rate. As we observe later, these constraints imply that the product Xf will scale with impedance μ as $Xf \propto \mu^\gamma$, where in general $\gamma < 1$.

Although we may have limited knowledge of the exact functional form of the material flow $J(c)$ in Eq. (5.2), two general statements can be made. First, we expect the material flow to be a linear function of material concentration c at low concentrations and to approach zero with the concentration: $J(0) = 0$. Second, we are concerned with situations where the system impedance depends on concentration and J increases monotonically up to a maximum value $J(c_{\text{opt}})$ where $\partial J/\partial c = 0$ and $\partial^2 J/\partial c^2 < 0$. For such situations, we can approximate the normalized material flow $J^* = J(c)/J(c_{\text{opt}})$ by a simple function of the normalized concentration $c^* = c/c_{\text{opt}}$:

$$J^* = c^*(2 - c^*) \quad (5.3)$$

While Eq. (5.3) does not reveal the absolute value of the optimum concentration c_{opt} , it does contain information concerning the impedance at the optimum concentration $\mu(c_{\text{opt}})$. Assuming $Xf \propto \mu^\gamma$, we find from Eq. (5.2) that the normalized flux J^* can also be written as $J^* = c^*/(\mu^*)^{1-\gamma}$, so that the normalized impedance $\mu^* = \mu/\mu(c_{\text{opt}})$ may be expressed as

$$\mu^* = \left(\frac{1}{2 - c^*} \right)^{1/(1-\gamma)} \quad (5.4)$$

It follows that the impedance at the optimum concentration is

$$\mu(c_{\text{opt}}) = 2^\alpha \mu(0) \quad (5.5)$$

where the power $\alpha = 1/(1 - \gamma) = \log_2(\mu(c_{\text{opt}})/\mu(0))$ and $\mu(0)$ is the impedance at zero concentration.

Eqns. (5.3), (5.4), and (5.5) provide a general framework for analyzing optimization of concentration impeded material flow in biological and engineered systems. To test the quantitative predictions of the theory we proceed in Sec. 5.2 by considering a series of biological examples where the flux J can be optimized along the lines outlined above. In Sec. 5.3, we apply our model to traffic flow. Finally, in Sec. 5.4, we consider universal

properties of concentration impeded material transport systems.

5.2 Biological transport networks

5.2.1 Nectar drinking from a tube

Perhaps the simplest situation in which we may apply Eq. (5.2) is drinking from a cylindrical tube. Many insects and birds such as butterflies and hummingbirds [63] feed on floral nectar, an aqueous solution of sugars, through tubes formed from probosci or tongues. Quick energy ingestion is advantageous for nectar feeders owing to the threat of predation. While the sweetest nectar offers the greatest energetic rewards, the increase of viscosity with sugar concentration also makes the sweetest nectar the most difficult to transport [65]. An optimal concentration may thus be sought for maximizing energy uptake rate.

Two different suction mechanisms are typically used by nectar feeders: active suction and capillary suction [65, 98, 62, 63]. Active suction feeders such as butterflies use muscle contraction to suck nectar through their roughly cylindrical probosci. The nectar flow rate J_s can be expressed as

$$J_s = \rho \bar{c} \frac{\pi a^4}{8\eta l} \Delta p \quad (5.6)$$

where a is the radius and l the length of the proboscis, \bar{c} is the wt/wt sugar concentration, η the viscosity (see § 5.6.1), ρ the density of the nectar solution, and Δp the pressure difference generated by muscular contraction. The manner in which biological constraints determined the dependence of the pressure Δp on nectar viscosity has been treated elsewhere [98, 62]. Active suction feeders are typically constrained by constant work rate $W = Q\Delta p = \pi a^4/(8\eta l)\Delta p^2$, so the pressure $\Delta p = (8Wl/(\pi a^4))^{1/2}\eta^{1/2}$ depends on viscosity and hence concentration. Comparing the nectar flow rate in Eq. (5.6) to the general expression in (5.2), we find that the impedance corresponds to the viscosity of the sugar solution $\mu = \eta$, the concentration to $c = \rho \bar{c}$, the geometric factor to $X = \pi a^4/(8l)$, and the driving mechanism to the pressure, $f = \Delta p$. We can thus express the constraint as $f = (8Wl/(\pi a^4))^{1/2}\mu^{1/2}$ (see Table 5.1).

Capillary suction feeders such as hummingbirds use surface tension to draw nectar

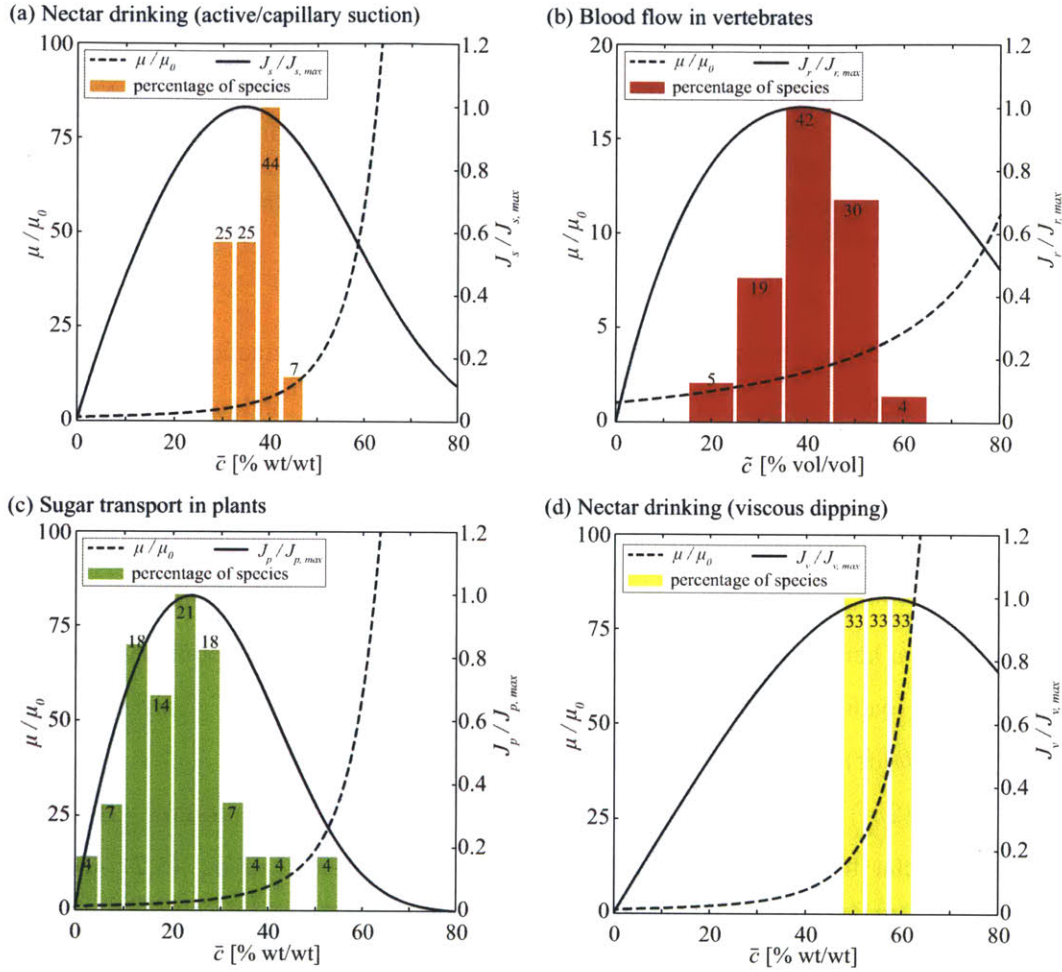


Figure 5-1: Optimal concentrations in biological transport networks. (a) Drinking from a tube. Histogram showing distribution of observed sugar concentrations that maximizes nectar uptake for 16 bird and insect species that use muscular contractions or surface tension to feed through cylindrical tubes [62, 91]. Normalized sugar mass flow $J_s/J_{s,max}$ (solid line, Eqns. (5.6) and (5.7)) and nectar viscosity μ/μ_0 (dashed line, data from [47]) are plotted as a function of nectar sugar concentration \bar{c} . Mass flow is predicted to be maximum when $\bar{c}_{opt} = 35\%$, in good agreement with the observed average nectar concentration (37%). (b) Blood flow. Histogram showing distribution of observed red blood cell concentrations (hematocrit) from 57 vertebrate species [130]. Normalized oxygen flow $J_r/J_{r,max}$ (solid line, Eq. (5.8)) and blood viscosity μ/μ_0 (dashed line, see § 5.6.2) are plotted as a function of hematocrit \bar{c} . Flow is predicted to be maximum when $\bar{c}_{opt} = 40\%$, in good agreement with the observed average hematocrit (40%). (c) Sugar transport in plants. Histogram showing distribution of observed sugar concentrations from 28 plant species that use active sugar loading [56]. Normalized sugar flow $J_p/J_{p,max}$ (solid line, Eq. (5.9)) and sap viscosity μ/μ_0 (dashed line, data from [47]) are plotted as a function of nectar sugar concentration \bar{c} . Mass flow is predicted to be at a maximum when $\bar{c}_{opt} = 24\%$, in good agreement with the observed average sugar concentration (22%).

Figure 5-1 (*continued*): (d) Nectar drinking by viscous dipping. Histogram showing distribution of observed sugar concentrations that maximizes nectar uptake for 6 insect species that use viscous dipping [62, 91]. Normalized sugar mass flow $J_v/J_{v,max}$ (solid line) and nectar viscosity μ/μ_0 (dashed line, data from [47]) are plotted as a function of nectar sugar concentration \bar{c} . Mass flow is predicted to be at a maximum when $\bar{c}_{opt} = 57\%$, in good agreement with the observed average nectar concentration (55%). In (a)-(d), the numbers given above the bins indicate the percentage of species in the bin.

along their tongue, during repeated cycles of tongue insertion and retraction [62, 63]. If the duration of a cyclic motion is the sum of the nectar loading time T and unloading time T_0 , the average nectar flow rate J_s can be expressed as

$$J_s = \rho \bar{c} \frac{\pi a^4}{8\eta l} \frac{T}{T + T_0} \Delta p \quad (5.7)$$

where the nectar height $l = l(t)$ is time-dependent and $\Delta p = 2\sigma/a$ is the capillary pressure. During nectar loading, the volumetric flow rate is given by $\pi a^2(dl/dt) = \pi a^4 \Delta p / (8\eta l)$, yielding $4\eta l(dl/dt) = a\sigma$. The solution with initial condition $l(0) = 0$ is given by $l(t) = (a\sigma t / (2\eta))^{1/2}$, which depends on viscosity and hence concentration. By comparing the nectar flow rate in Eq. (5.7) to the general expression in Eq. (5.2), we find that $X = \pi a^4 T / (8l(T + T_0))$, $f = 2\sigma/a$ and $\mu = \eta$. We express the constraint as $X = \pi [(a^7)/(32\sigma)]^{1/2} T^{1/2} / (T + T_0) \mu^{1/2}$, where $T^{1/2}/(T + T_0)$ is assumed to be independent of viscosity [44] (see Table 5.1).

For both active and capillary suction we find that $Xf \propto \mu^{1/2}$ (i.e. $\gamma = 1/2$) and the optimal concentration \bar{c}_{opt} can therefore be found by maximizing $c/\mu^{1/2}$. For nectar sugar solutions, we therefore predict that $\bar{c}_{opt} = 35\%$ wt/wt and $\mu(\bar{c}_{opt}) = 4\mu_0$ (i.e. $\alpha = 2$ in (5.5)). This is in good agreement with experimental data on 16 butterfly and hummingbird species (see Figure 5-1(a) and Table 5.2), where optimal concentrations in the range 30% – 45% are reported.

5.2.2 Blood flow in vertebrates

Another biological flow problem that can be analyzed within our framework is oxygen and nutrient transport within the cardiovascular system of vertebrate animals. Here, red

Table 5.1: Parameters describing the material flow $J = Qc = Xfc/\mu$ (see Eq. (5.2)) for each of the systems considered. See Appendices 5.6.1 and 5.6.2 for details on the viscosity η of blood, nectar and phloem sap.

System	Geometry X	Driving force f	Concentration c	Impedance μ	Constraint
Nectar drinking (Active suction)	$\pi a^4(8l)^{-1}$	Δp	$\rho\bar{c}$	η	Const. work rate $W = Q\Delta p$ $f = (W/X)^{1/2}\mu^{1/2}$
Nectar drinking (Capillary suction)	$\pi a^4 T [8l(T + T_0)]^{-1}$	$2\sigma a^{-1}$	$\rho\bar{c}$	η	Cyclic suction period $T + T_0$ $X = \pi [a^7 T / (32\sigma)]^{1/2} (T + T_0)^{-1} \mu^{1/2}$
Blood flow in vertebrates	$\pi a^4(8l)^{-1}$	Δp	\bar{c}	η	Const. pressure Δp $f = f_0 = \Delta p$
Sugar transport in plants	$\pi a^4(8l)^{-1}$	Δp	$\rho\bar{c}$	η	Const. pressure Δp $f = f_0 = \Delta p$
Nectar drinking (Viscous dipping)	$\pi a e^3$	$\eta u e^{-2}$	$\rho\bar{c}$	η	Const. work rate $W = \eta u^2 l$ $X f = 2\pi a^2 W^{5/6} l^{-5/6} \sigma^{-2/3} \mu^{5/6}$
Traffic flow (Greenberg)	N	\mathcal{C}	ρ/ρ_m	$\ln(c_0/c)^{-1}$	Const. optimum speed \mathcal{C} $f = f_0 = \mathcal{C}$
Traffic flow (Bando)	N	v_{max}	ρ/ρ_m	$\tanh(\frac{1-\rho L}{\rho s})^{-1}$	Const. speed limit v_{max} $f = f_0 = v_{max}$

blood cells transport oxygen between the lungs and distal parts of the organism. The cells are suspended in blood plasma, which primarily consists of water [112]. Red blood cells typically measure 10 μm in diameter [41], and the blood's bulk viscosity depends on the hematocrit \tilde{c} , the volume concentration of red blood cells. While blood with the highest hematocrit is the most oxygen rich, the increase of viscosity with the hematocrit also makes such blood the most difficult to transport. Accordingly, an optimal hematocrit may be sought for maximizing oxygen transport.

The red blood cell flow rate J_r can be expressed as

$$J_r = \tilde{c} \frac{\pi a^4}{8\eta l} \Delta p \quad (5.8)$$

where a and l are the radius and length of the blood vessel, η the blood viscosity (see § 5.6.2), and Δp the pressure difference generated by the heart. Blood pressure is on the order of 10 kPa for most animals [126], and the dependence of blood pressure on the hematocrit is negligible [130]. Although blood viscosity η generally depends on the shear rate, this dependence is weak for typical blood conditions, specifically high shear rates ($> 50 \text{ s}^{-1}$) [112]. Comparing the blood flow rate in Eq. (5.8) to the general expression in Eq. (5.2) we find that $c = \tilde{c}$, $\mu = \eta$, $X = \pi a^4 / (8l)$ and $f = \Delta p$. We express the constraint as that of constant pressure $f = f_0 = \Delta p$ (see Table 5.1).

For blood flow we thus find that $Xf \propto \mu^0$ (i.e. $\gamma = 0$) and the optimum concentration \tilde{c}_{opt} can be found by maximizing c/μ . We therefore predict that $\tilde{c}_{\text{opt}} = 40\% \text{ vol/vol}$ and $\mu(\tilde{c}_{\text{opt}}) = 2\mu_0$ (i.e. $\alpha = 1$, in (5.5)), in good agreement with experimental data from 57 species observed throughout the animal kingdom (see Figure 5-1(b) and Table 5.2). We note that for some diving mammals (e.g. Weddell seals and whales), oxygen storage in the blood may also be an important factor, resulting in a higher hematocrit (up to 63%) [130]. It is also likely that lack of thermoregulation may explain why poikilothermic animals (e.g. the rainbow trout) has a lower hematocrit value (23%) than the average, likely due to thermally induced variations in blood viscosity [31].

5.2.3 Sugar transport in plants

Plants, like animals, rely on vascular systems for distribution of energy and nutrients. Energy distribution in plants takes place in the phloem vascular system. Here, an aqueous solution of sugars, amino acids, proteins, ions, and signaling molecules flows through a series of narrow elongated cylindrical cells, known as sieve tube elements, that lie end-to-end forming a microfluidic network spanning the entire length of the plant. The flow is driven by differences in chemical potential between distal parts of the plant [55]. While phloem sap with high sugar concentration has the greatest potential for energy transfer, the increase of viscosity with sugar concentration makes it the most difficult to transport. Accordingly, an optimal concentration may again be sought for maximizing energy flow.

The phloem energy flow J_p can be expressed as

$$J_p = \rho \bar{c} \frac{\pi a^4}{8\eta l} \Delta p \quad (5.9)$$

where a is the radius of the phloem sieve tube ($a \simeq 10 \mu\text{m}$), l the length of the plant, \bar{c} the sugar concentration, η the phloem sap viscosity, and Δp the pressure difference driving the flow. By comparing the sugar flow rate (5.9) to the general expression in (5.2), we find that $\mu = \eta$, $c = \bar{c}\rho$, $X = \pi a^4/(8l)$ and $f = \Delta p$. We express the constraint as that of constant pressure $f = f_0 = \Delta p$ (see Table 5.1).

For sugar transport in plants we thus find that $Xf \propto \mu^0$ (i.e. $\gamma = 0$) and the optimum concentration \bar{c}_{opt} can therefore be found by maximizing c/μ . We find that $\bar{c}_{\text{opt}} = 24\%$ wt/wt and $\mu(\bar{c}_{\text{opt}}) = 2\mu_0$ (i.e. $\alpha = 1$, in (5.5)), in good agreement with experimental data (see Figure 5-1(c) and Table 5.2). While sugar concentrations observed in plants generally span a wide range, this analysis provides a rationale for the observation that plants that use active sugar loading (data shown in Figure 5-1(c)) typically have higher sugar concentration than plants that use passive loading [56]. Active loaders spend metabolic energy to increase the sugar concentration in the phloem [107], and thus enhance the transport of sugar into the vasculature when compared to passive loaders which rely solely on the concentration gradient generated by photosynthesis to drive the transport [56]. We also note that plants with the highest sugar concentrations are crop plants, for example potato (50%) and maize

(40 %) [56], suggesting that selection for high crop yield tends to lead to increased sugar concentration in the phloem sap.

5.2.4 Drinking by viscous dipping

So far, we have limited our attention to transport in closed channels. However, it is straightforward to extend the problem to situations where free surfaces are involved. Most bees whose tongues are solid rather than hollow use a drinking style termed “viscous dipping” in which the fluid is entrained by the tongue surface. The average nectar volume entrained can be expressed by $Q \sim 2\pi aeu$, where a is the tongue radius, e the thickness of the nectar layer on the tongue, and u the tongue extraction speed. Based on Landau-Levich-Derjaguin theory when the Reynolds number $Re \ll 1$ and Bond number $Bo \ll 1$, the nectar film thickness is given by $e \sim aCa^{2/3}$, where $Ca = \eta u/\sigma \ll 1$ is the ratio of viscous to capillary forces [29]. Since the fluid is entrained on the tongue by viscous forces, we define f as the viscous force per unit volume of liquid, so that $f = \eta u/e^2$ and $X = 2\pi a e^3$. The movement of the tongue in the fluid requires power $W \sim \eta u^2 l$ to overcome the viscous drag, where l is the immersed tongue length. Assuming a constant work rate W for a given creature leads to the constraint on velocity $u \sim (W/(\eta l))^{1/2}$ so $Xf = 2\pi a^2 W^{5/6} l^{-5/6} \sigma^{-2/3} \mu^{5/6}$ [62] (see Table 5.1).

For viscous dipping, we find that $Xf \propto \mu^{5/6}$ (i.e. $\gamma = 5/6$) and the optimum concentration \bar{c}_{opt} can therefore be found by maximizing $c/\mu^{1/6}$. We find that $c_{\text{opt}} = 57\%$ wt/wt and $\mu(c_{\text{opt}}) = 64\mu_0$ (i.e. $\alpha = 6$, c.f. Eq. (5.5)). This is in reasonable agreement with experimental data on 6 bees species (see Figure 5-1(d) and Table 5.2), where optimal concentrations in the range 50 % – 60 % are found. This may explain why the nectar concentration of flowers pollinated by bees is generally higher than that of those pollinated by tube feeding butterflies and hummingbirds [62].

5.3 Applications to engineered transport systems: Traffic flow

We have thus far seen many qualitative similarities between different biological flows. Although the detailed physiological and physical mechanisms are different, provided increased concentration leads to greater impedance, we can rationalize the optimal concentrations. An interesting question naturally arises. In which engineered systems might one expect to observe similar phenomena? It appears likely that most efficient communication and transport networks will exhibit similar features. Nevertheless, we limit our discussion to traffic congestion on highways.

A measure of the efficiency of a given section of road is the vehicle flow J_v , the number of vehicles passing a given point per unit time [119, 125, 51, 35]. Designers of road networks strive to maximize the vehicle flow which can be expressed as $J_v = \rho v$, where v is the speed of the individual vehicle and ρ the number of vehicles per unit length of roadway. Generally, the car speed $v = v(\rho)$ is a decreasing function of density ρ . At very low densities, where inter-vehicle interaction is negligible, however, the speed approaches the speed limit v_{\max} and the vehicle flow is proportional to density $J_v \simeq \rho v_{\max}$. At higher vehicle densities, interaction between adjacent cars leads to flow impedance and a significant reduction in the speed of the individual vehicles, causing congestion and a net decrease in J_v . One thus anticipates an optimal vehicle density ρ_{opt} that maximizes the vehicle flow rate.

To estimate ρ_{opt} , we require $v(\rho)$ which can be found either empirically, or deduced from vehicle interaction models. One of the simplest models that leads to a reasonable expression for $v(\rho)$ was proposed by Greenberg [40], who treated traffic flow as a one-dimensional flow of an ideal compressible gas. He assumed (i) that the local speed is a function of density only $v = v(\rho(x, t))$, (ii) that vehicles are conserved $\partial\rho/\partial t + \partial J_v/\partial x = 0$, (iii) that vehicle flow satisfies the Euler equation $Dv/Dt = -(1/\rho)\partial p/\partial x$, and (iv) that traffic “pressure” is proportional to density $p = \mathcal{C}^2\rho$. This leads to the relation $v(\rho) = \mathcal{C} \ln(\rho_{\max}/\rho)$ where ρ_{\max} is the density at which traffic stops due to congestion. The vehicle flow rate $J_v = \mathcal{C}\rho \ln(\rho_{\max}/\rho)$ is at a maximum when $\rho = \rho_{\text{opt}} = \rho_{\max}/e$, and the constant

$C = v(\rho_{\text{opt}})$ is the vehicle speed at the optimal concentration. Since vehicles typically occupy 7.5 m in a totally congested flow [119], we estimate that $\rho_{\text{max}} \simeq 133$ vehicles/km. Greenberg's model overestimates the optimal density, predicting $\rho_{\text{opt}} = \rho_{\text{max}}/e \sim 50$ vehicles/km, while the true value is known to be ~ 20 vehicles/km. Nevertheless, the vehicle flow rate J_v is qualitatively consistent with empirical traffic data, see Figure 5-2. The data is plotted as a function of vehicle concentration $c = \rho/\rho_{\text{max}}$ in Figure 5-2 along with Greenberg's flow rate J_v , deduced using $\rho_{\text{max}} = 133$ vehicles/km.

A shortcoming of Greenberg's theoretical model is that the vehicle speed v diverges when the car density is very low. To ensure that $v(\rho/\rho_{\text{max}} \rightarrow 0) = v_{\text{max}}$ and to account for other aspects of traffic flows, numerous other models have been proposed [3, 119, 125, 51, 35]. For example, Bando and Hasebe [3] suggested a traffic model in which the vehicle speed depends on the distance from the car in front, Δx . This leads to $v = v_{\text{max}} \tanh(\Delta x/s)$, where s is a fixed length scale determined by the road conditions. With a minimum vehicle distance $L = 7.5$ m, we can express the density in terms of Δx as $\rho = 1/(L + \Delta x)$. This leads to $v(\rho) = v_{\text{max}} \tanh[(1/\rho - L)/s]$, in which case the flow rate $J_v = v\rho$ is optimized when $\rho = 0.21\rho_{\text{max}} = 28$ vehicles/km. With $v_{\text{max}} = 120$ km/h and $s = 60$ m, the Bando-Hasebe model provides a better quantitative fit to the empirical data than Greenberg's model (see Figure 5-2).

Comparing the Greenberg and Bando-Hasebe models of traffic flow to the formulation introduced in Eq. (5.2), we see that traffic flow can be treated in the same general framework where

$$X = N, \quad f = C = v(\rho_{\text{opt}}), \quad \mu = (\ln \rho_{\text{max}}/\rho)^{-1} \quad (5.10)$$

for Greenberg's model, and

$$X = N, \quad f = v_{\text{max}}, \quad \mu = \tanh\left(\frac{1 - \rho L}{\rho s}\right)^{-1} \quad (5.11)$$

for the Bando-Hasebe model. In both cases, N is the number of lanes.

Comparing traffic flow to the biological transport problems considered above, we find that the normalized flux and impedance curves follow the same pattern (see Figure 5-2). While traffic flow can be treated in the same framework as biological flows, it is important

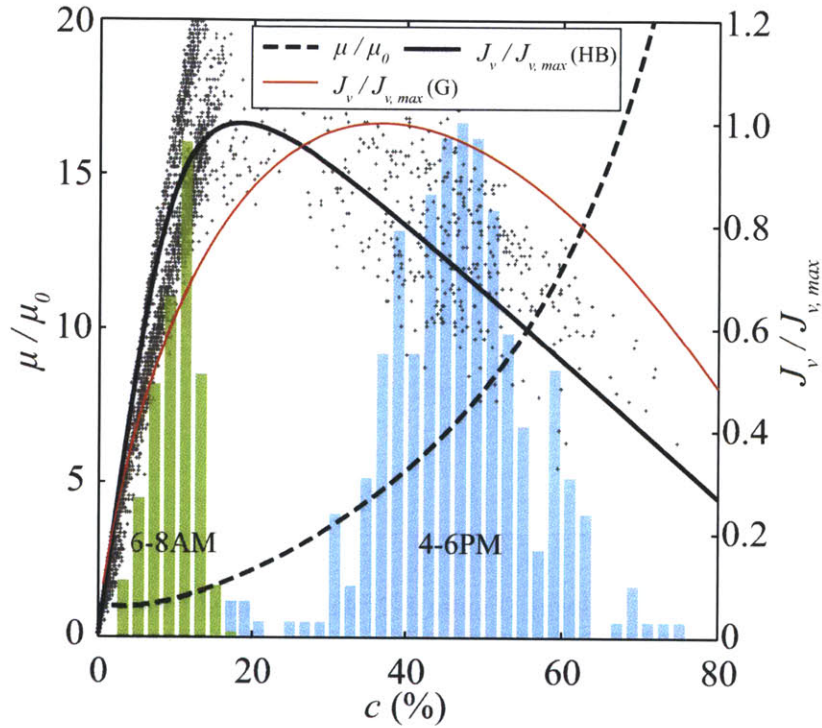


Figure 5-2: Optimal vehicle concentration for maximizing traffic flow. Grey dots show measured vehicle flow rate J_v plotted as a function of vehicle concentration $c = \rho/\rho_{\text{opt}}$ where $\rho_{\text{opt}} = 133$ vehicles/km. The flow rate is normalized by 1483 vehicles/hour which corresponds to $J_v(\rho_{\text{opt}}) = J_{v,\text{max}}$ in Bando & Hasebe's model [3]. Histograms show the states occupied by the system in the morning (green, 6-8AM) and evening (blue, 4-6PM) rush-hour traffic. The data were collected by the Minnesota Department of Transportation from a sensor on the westbound direction of I-94 (Minneapolis, MN, USA) on Fridays (7, 14, 21, 28) in September 2012 [84]. The predicted vehicle transport rate $J_v/J_{v,\text{max}}$ (thick solid black line: Bando & Hasebe's model; thin solid red line: Greenberg's model) and traffic impedance μ/μ_0 (dashed line: Bando & Hasebe's model) are plotted as a function of vehicle concentration c .

Table 5.2: Comparison between theoretical predictions (T) and experimental observations (E) of the optimum concentration c_{opt} , the optimum viscosity μ_{opt} and the exponent α . Concentration units are % wt/wt for nectar drinking and sugar transport in plants, % vol/vol for blood flow, and % vehicle density/max vehicle density for traffic flow.

System	c_{opt}		μ_{opt}/μ_0		α	
	T	E	T	E	T	E
Nectar drinking (Suction)	35	36.9 ± 5.3	4	$3.5 - 7.4$	2	$1.8 - 2.9$
Blood flow in vertebrates	40	40.2 ± 8.6	2	$2.2 - 3.4$	1	$1.1 - 1.8$
Sugar transport in plants	24	21.8 ± 10.3	2	$1.4 - 3.6$	1	$0.5 - 1.8$
Nectar drinking (Viscous dipping)	57	55.0 ± 4.1	64	$17.5 - 49.4$	6	$4.1 - 5.6$
Traffic flow (Greenberg)	37	18	-	-	-	-
Traffic flow (Bando)	21	18	2	1.9	1	0.9

to note that the congested highway (Figure 5-2, data recorded from 4-6 PM) is very far from being optimized. This is presumably due to two main effects. First, the individual vehicle operator attempts to minimize his or her own travel time which does not necessarily optimize the overall vehicle flow J_v . Second, traffic flows are intrinsically time dependent which leads to the formation of traveling density waves and shocks [119, 125, 51, 35].

5.4 Universal properties of transport networks

To compare characteristics of the particular biological and man-made transport networks considered in Sec. 5.2 and 5.3 to the general formulation in Eqns. (5.3) and (5.4), normalized material flow and impedance curves are plotted in Figure 5-3. Despite the complex dependence of impedance on concentration (see Appendices 5.6.1 and 5.6.2), both the material flow J^* and impedance μ^* are adequately approximated by the simple forms given in Eqns. (5.3) and (5.4). From (5.4), it follows that the impedance at the optimum concentration is $\mu_{\text{opt}} = 2^\alpha \mu_0$, where μ_0 is the impedance of the pure carrier medium (with $c = 0$)

and the power α is determined by the flow constraints. In the cases of vascular transport in plants and animals, the power $\alpha = 1$, since there is no coupling between the constant driving pressure (f) or the vascular geometry (X) and the impedance (μ). This suggests that the optimum in material flow should occur when the blood or phloem sap is twice as viscous as water, i.e. $\eta_{\text{opt}} = 2\eta_0$, in good agreement with observed values (see Table 5.2).

In transport systems that are constrained, for example by constant work rate, α will generally be greater than unity, because of the coupling between flow and impedance. The impedance at the optimum concentration $\mu_{\text{opt}} = 2^\alpha \mu_0$, can therefore be significantly greater than that of the carrier medium. This is most clearly seen in the case of viscous dipping (Sec. 5.2.4), where the observed nectar viscosity is up to 50 greater than that of water, roughly consistent with the value ($2^6 = 64$) predicted by our simple model (see Table 5.2).

These observations suggest that this general framework may also provide rationale for the viscosities found in other biological transport systems where efficient transport is favored. Examples of systems with constant forcing include mammals that drink whole milk (observed viscosity: $\eta \sim 2\eta_0$ [80]), and in the macro-alga *Chara* where streaming distributes the content of the cell cytosol (observed viscosity: $\sim 3\eta_0$ [122]). Although detailed studies of these systems are left for future consideration, we note that both are roughly consistent with the predictions of our general theory with $\alpha = 1$.

Comparing traffic flow to the biological transport problems considered, we find that the normalized flux and impedance curves follow the same pattern (see Figure 5-3 and Table 5.2). Since the speed limit v_{max} , which is fixed on a given road section, corresponds to the flow driving mechanism in the Bando-Hasebe model, traffic flow is analogous to vascular transport in animals and plants that operate at constant pressure. Our model thus indicates that the flow constraint does not couple to impedance, $Xf \propto \mu^0$ ($\gamma = 0$, $\alpha = 1$), and hence that the optimal impedance is $\mu_{\text{opt}} = 2\mu_0$. This is in rough accord with Bando-Hasebe's model which yields $\mu_{\text{opt}} = 1.9\mu_0$.

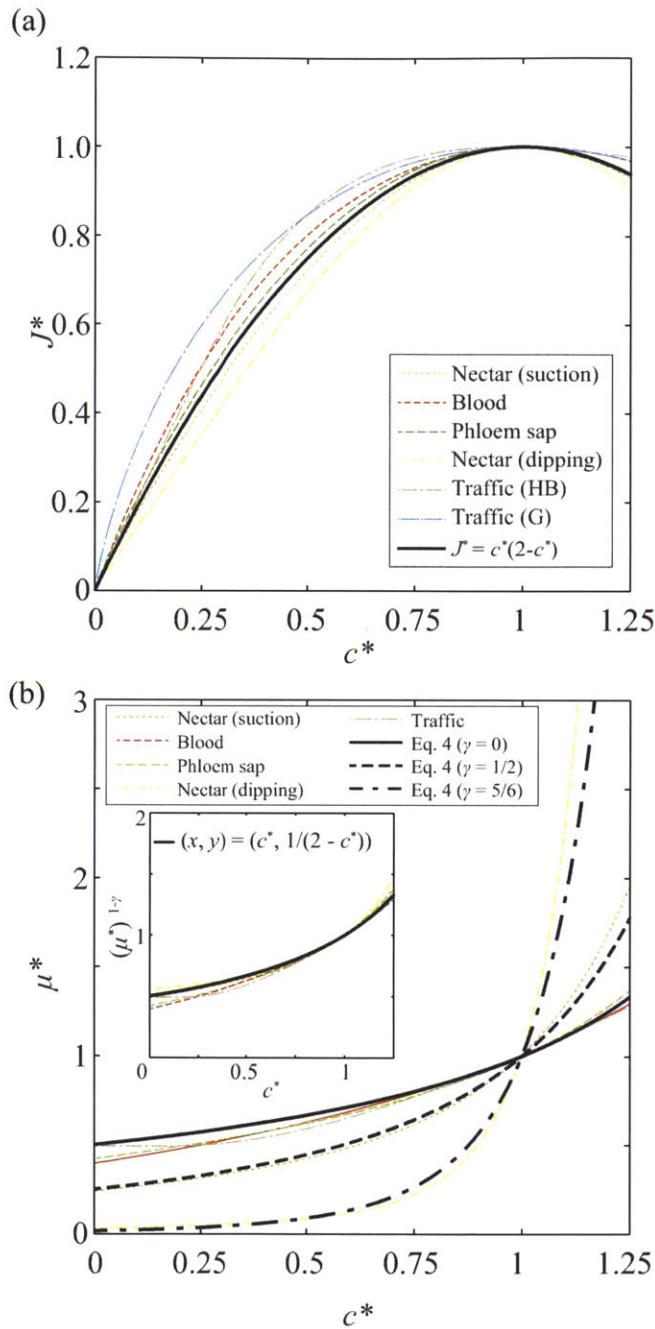


Figure 5-3: Universal properties of biological and engineered flows. (a) Normalized flow rate $J^* = J(c)/J(c_{\text{opt}})$ plotted as a function of normalized concentration $c^* = c/c_{\text{opt}}$. The solid thick black line shows the prediction of Eq. (5.3). (b) Normalized impedance $\mu^* = \mu(c)/\mu(c_{\text{opt}})$ plotted as a function of normalized concentration c^* . The solid and dashed thick black lines show the predictions of Eq. (5.4). The inset indicates the dependence of $(\mu^*)^{1-\gamma}$ on c^* .

5.5 Discussion

We have seen many qualitative and quantitative similarities between different natural and engineered transport networks. Although the detailed mechanisms are different, key common features have allowed us to develop a general framework. Provided impedance increases with concentration, our model provides means of rationalizing the optimal concentrations. Collecting data from more than 100 plant and animal species, we have observed that optimization of material flow appears to be a universal feature of biological transport systems. This deduction provides rational for the observation that the simple model introduced in Sec. 5.1 collapses flow and impedance curves for all the systems considered (Figure 5-3), suggesting a universal component to all natural transport networks.

Finally, we have shown that an interesting analogy can be made between biological systems and self-driven systems such as traffic flows. Here we find that the impedance analogy is still valid, but that the system is far from optimized due to conflicting interests between individuals and the collective. The consideration of other man-made transport systems, such as the electrical grid or the internet, is left for future consideration.

5.6 Methods

5.6.1 Viscosity and density of nectar and phloem sap

Phloem sap and flower nectar consist of an aqueous solution of sugars, amino acids, proteins, and other nutrients. Sugars, of which sucrose, fructose and glucose are the most abundant types, constitute about 90 % of the total solute mass [93]. To approximate the viscosity η and density ρ of phloem sap and nectar, we therefore used data from sucrose solutions of concentration \bar{c} obtained from [47]. Least square fits to sucrose data yields the approximate expressions for viscosity $\eta = \eta_0 g_n(\bar{c}) = \eta_0 \exp [0.032 \bar{c} - (0.012 \bar{c})^2 + (0.023 \bar{c})^3]$ and density $\rho = \rho_0 (1 + 0.0038\bar{c} + (0.0037 \bar{c})^2 + (0.0033 \bar{c})^3)$. We note that viscosity and density data from other sugar types (glucose and fructose) are well approximated by the fit, suggesting that the major determinant of viscosity is the mass fraction \bar{c} , and not the type of solute.

5.6.2 Viscosity of blood

Vertebrate blood is composed of blood cells suspended in blood plasma, a liquid which consists mostly of water. The viscosity of blood η depends primarily on the volume concentration \tilde{c} (hematocrit) of red blood cells, and on temperature [31, 130]. As demonstrated by Saito [118] and Stark [130], blood viscosity is well described by the function $\eta/\eta_0 = 1 + 2.5\tilde{c}/(1 - \tilde{c})$, which for blood vessels with diameters larger than 1 mm is consistent with empirical data with less than 5% error for $0 < \tilde{c} < 70\%$ [100, 39].

Chapter 6

Conclusions

We have explored a variety of natural designs for fluid transport and presented physical pictures of many such systems. We have rationalized a number of nature's strategies for fluid uptake and demonstrated that many such strategies are optimized for efficient transport. By identifying qualitative similarities between a number of transport systems, we have developed a general framework for determining optimal concentrations in concentration-impeded flows.

Nature's myriad drinking techniques make clear that the optimal fluid transport mechanism for a given creature depends on both its geometry and scale. We have identified the dominant forces and suggested physical pictures for each drinking style, thereby classifying the natural drinking styles of terrestrial creatures according to mechanism. Simple scaling arguments have been validated by comparison with existing data. Suction is the most common drinking strategy, the suction pressure being applied to overcome either viscous forces for small creatures ($Re < 1$) or inertial forces for large creatures ($Re > 1$). In suction drinking, gravitational effects are negligible for all but the largest creatures. Scaling arguments indicate that the pressure generated by muscular contraction is comparable for all creatures, and larger for large creatures than the characteristic capillary pressure. Conversely, capillary pressure is employed by many small creatures and others for which morphological constraints preclude active suction. Creatures for which suction is impossible have developed various drinking styles. Inertial forces facilitate lapping or ladling for large creatures ($Bo > 1$), while interfacial and viscous forces facilitate licking and viscous

dipping for small creatures. A few such small creatures have developed ingenious drinking techniques that rely critically on contact angle hysteresis. The critical importance of wetting properties in the drinking strategies of these creatures makes immediately clear their vulnerability to surface-active pollutants such as petroleum or detergent.

Guided by the presupposition that evolution leads to optimal design, it is natural for applied mathematicians to attempt to rationalize natural systems through consideration of constrained optimization problems. However, it is rarely clear what, precisely, is being optimized and what are the relevant constraints. For example, attempting to rationalize the shapes of bird beaks or insect probosci exclusively in terms of their drinking efficiency would mistakenly neglect their importance in many other tasks, for example, foraging and combat. Nevertheless, we have considered a number of instances where it is fruitful to consider the role of optimization in natural drinking strategies. In particular, we have demonstrated that the optimal sugar concentrations for nectar-feeding via viscous dipping or active suction can be rationalized as those that maximize energy flux subject to the constraint of constant work rate [62]. In addition, we have suggested new rationale for the shape of the hummingbird's tongue: specifically, the fact that each of the tongue's two grooves is nearly semicircular.

We have identified many qualitative and quantitative similarities between different natural and engineered material flows. Although the detailed mechanisms are different, key common features have allowed us to develop a general framework for transport networks. Provided an increase in concentration leads to greater impedance, our framework allows us to rationalize the optimal concentrations. Collecting data from more than 100 plant and animal species, we have observed that optimization of material flow appears to be an universal feature of biological transport systems. Finally, our general framework was applied to assess the efficiency of an engineered system, traffic flow.

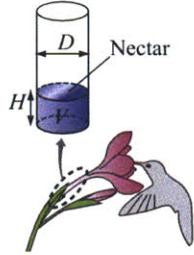
Nature has been optimizing transport strategies on small scales for millions of years while man has only recently become interested in transporting fluid on the nanoliter scale, for applications ranging from drug delivery to the handling of biomolecules [132]. Although biomimicry is now a central methodology in the engineering sciences, nature's myriad mechanisms for fluid transport on the scale of interest to microfluidics remain rel-

atively unexplored. It is expected that continued exploration of this class of problems will prompt further biomimetic technological advance.

Appendix A

Supplementary Tables

Table A.1: . Estimation of the nectar depth for six flowers visited by *A. colubris*.

Plant	V (μl)	D^a (mm)	H^b (mm)	Schematic
<i>Campsis radicans</i>	40 [9]	4.2	2.9	
<i>Ipomoea coccinea</i>	1.6 [79]	2.0	0.5	
<i>Ipomopsis rubra</i>	0.8 [5]	2.0	0.2	
<i>Lobelia cardinalis</i>	18.8 [24]	5.8	0.7	
<i>Aquilegia canadensis</i>	3.0 [42]	0.9	5.2 ^c	
<i>Impatiens hiflora</i>	-	-	11.7 ^d	

^aCorolla diameter at base (see Figure B-1–B-5).

^bNectar height H is estimated as $H = 4V/(\pi D^2)$.

^cNectar bulb at corolla base is omitted to estimate an upper limit for H (see Figure B-5).

^dDirect measurements have been reported for *Impatiens biflora* whose spur is transparent [72].

Table A.2: . Corolla measurement (diameter at base of corolla tube).

Plant	Numbers of flowers	Average diameter ^a (S.D.) [mm]	Collection [Source]
<i>Campsis radicans</i>	9	4.2 (0.3)	MO ^b [1,2]
<i>Ipomoea coccinea</i>	6	2.0 (0.1)	MO ^b [3] & NY ^c [4]
<i>Ipomopsis rubra</i>	12	2.0 (0.2)	GH ^d [5,6]
<i>Lobelia cardinalis</i>	10	5.8 (0.3)	MO ^b [7] & NY ^c [8]
<i>Aquilegia canadensis</i>	6	0.9 (0.1)	MO ^b [9] & NY ^c [10]

^aWe measured corolla diameters at the base from two specimens in the program ImageJ took the average value.

^bMO=Missouri Botanical Gardens (images obtained from Tropicos, the botanical information system at the Missouri Botanical Garden - www.tropicos.org).

^cNY=New York Botanical Garden, C.V. Starr Virtual Herbarium.

^dGH= Gray Herbarium, Harvard University Herbaria.

Source

- [1] <http://www.tropicos.org/Image/100137855>
- [2] <http://www.tropicos.org/Image/100002820>
- [3] <http://www.tropicos.org/Image/100004180>
- [4] <http://sweetgum.nybg.org/vh/specimen.php?irn=1139533>
- [5] A. Arthur Heller 1869
- [6] J. M. Tracy No.8311
- [7] <http://www.tropicos.org/Image/100015764>
- [8] <http://sweetgum.nybg.org/vh/specimen.php?irn=634937>
- [9] <http://www.tropicos.org/Image/100105516>
- [10] <http://sweetgum.nybg.org/vh/specimen.php?irn=1495657>

Appendix B

Supplementary Figures

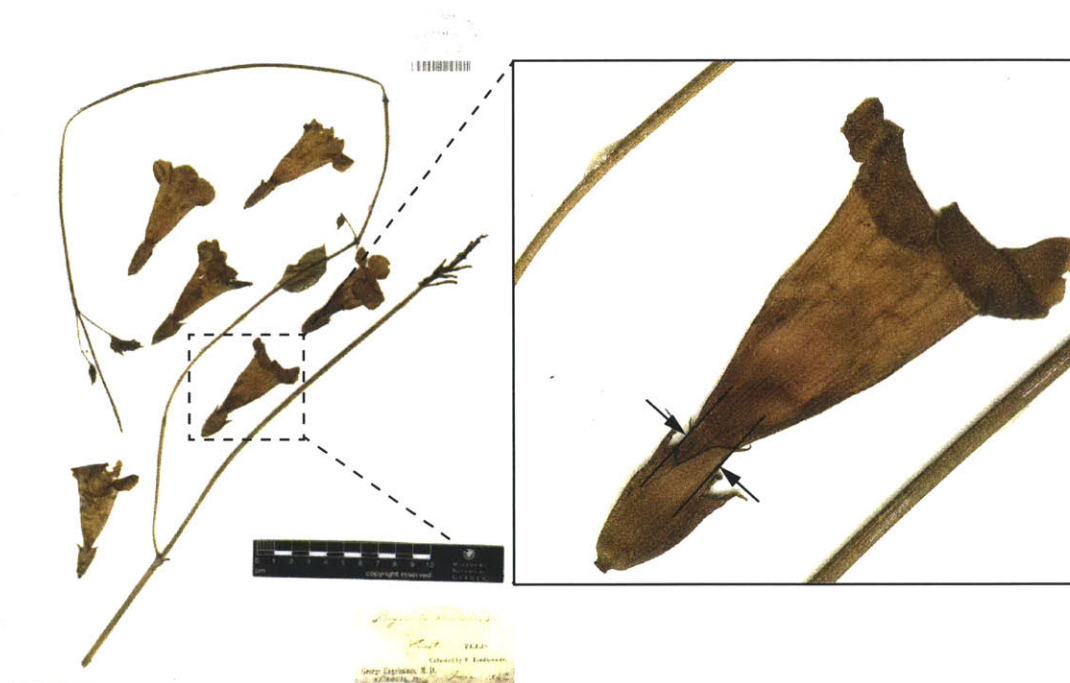


Figure B-1: *Campsis radicans*. The arrows indicate the basal corolla diameters used in our estimation of nectar height. (<http://www.tropicos.org/Image/100002820>)



Figure B-2: *Ipomoea coccinea*. The arrows indicate the inferred basal corolla diameters. (<http://www.tropicos.org/Image/100004180>)



Figure B-3: *Ipomopsis rubra*. The arrows indicate the inferred basal corolla diameters. (Gray Herbarium, Harvard University Herbaria, *Ipomopsis rubra* J.M. Tracy No.8311)



Figure B-4: *Lobelia cardinalis*. The arrows indicate the inferred basal corolla diameters. (<http://www.tropicos.org/Image/100015764>)



Figure B-5: *Aquilegia canadensis*. The arrows indicate the inferred basal corolla diameters. (<http://www.tropicos.org/Image/100105516>)

Bibliography

- [1] E. F. Adolph. Measurements of water drinking in dogs. *Am. J. Physiol.*, 125:75–86, 1939.
- [2] M. Andersson, J. Schaar, and H. Wiktorsson. Effects of drinking water flow rates and social rank on performance and drinking behaviour of tied-up dairy cows. *Livest. Prod. Sci.*, 11:599–610, 1984.
- [3] M Bando, K Hasebe, and A Nakayama. Dynamical model of traffic congestion and numerical simulation. *Physical Review E*, 51(2):1035–1042, 1995.
- [4] V. L. Bels, J. Davenport, and S. Renous. Drinking and water expulsion in the diamondback turtle *Malaclemys terrapin*. *J. Zool.*, 236:483–497, 1995.
- [5] R. B. Benjamin and F. R. Hainsworth. Sex change with inbreeding: experiments on separate versus combined sexes. *Evolution*, 40:843–855, 1986.
- [6] H. C. Bennet-Clark. Negative pressures produced in the pharyngeal pump of the blood sucking bug, *Rhodnius prolixus*. *J. Exp. Biol.*, 40:223–229, 1963.
- [7] P. J. Bentley, W. L. Bretz, and K. Schmidt-Nielsen. Osmoregulation in the diamondback terrapin, *Malaclemys terrapin centrata*. *J. Exp. Biol.*, 46:161–167, 1967.
- [8] G. Berkhoudt, K. V. Kardong, and G. A. Zweers. Mechanics of drinking in the brown tree snake, *Boiga irregularis*. *Zoology*, 98:92–103, 1995.
- [9] R. I. Bertin. Floral biology, hummingbird pollination and fruit production of trumpet creeper (*Campsis radicans*, Bignoniaceae). *Am. J. Bot.*, 69:122–134, 1982.
- [10] J. Bico, B. Roman, L. Moulin, and A. Boudaoud. Adhesion: Elastocapillary coalescence in wet hair. *Nature*, 432:690, 2004.
- [11] G. F. Birchard. Optimal Hematocrit: Theory, Regulation and Implications. *Integrative and Comparative Biology*, 37(1):65–72, 1997.
- [12] C. L. Boggs. Rates of nectar feeding in butterflies: effects of sex, size, age and nectar concentration. *Funct. Ecol.*, 2:289–295, 1988.
- [13] B. J. Borrell. Suction feeding in orchid bees (Apidae: Euglossini). *Proc. R. Soc. London Ser. B*, 271:S164–S166, 2004.

- [14] B. J. Borrell. Mechanics of nectar feeding in the orchid bee *Euglossa imperialis*: pressure, viscosity and flow. *J. Exp. Biol.*, 209:4901–4907, 2006.
- [15] B. J. Borrell. Scaling of nectar foraging in orchid bees. *Am. Nat.*, 169:569–580, 2007.
- [16] E. Bott, D. A. Denton, and S. Weller. Water drinking in sheep with oesophageal fistulae. *J. Physiol.*, 76:323–336, 1965.
- [17] J. W. M. Bush and D. L. Hu. Walking on water: Biocomotion at the interface. *Annu. Rev. Fluid Mech.*, 38:339–369, 2006.
- [18] J. W. M. Bush, D. L. Hu, and M. Prakash. The integument of water-walking arthropods: form and function. *Adv. Insect Physiol.*, 34:117–192, 2008.
- [19] W. A. Calder. On the temperature-dependency of optimal nectar concentrations for birds. *J. Theor. Biol.*, 78:185–196, 1979.
- [20] W. A. Calder. Scaling of physiological processes in homeothermic animals. *Ann. Rev. Physiol.*, 1981.
- [21] P. W. Carpenter, K. Berkouk, and A. D. Lucey. Pressure wave propagation in fluid-filled co-axial elastic tubes. Part 2: Mechanisms for the pathogenesis of syringomyelia. *ASME J. Biomech. Eng.*, 125:857–863, 2003.
- [22] A. Carré and K. L. Mittal. *Superhydrophobic surfaces*. VSP/Brill, Leiden, 2009.
- [23] A. W. Crompton and C. Musinsky. How dogs lap: ingestion and intraoral transport in *Canis familiaris*. *Biol. Lett.*, 7:882–884, 2011.
- [24] R. W. Cruden, S. M. Hermann, and S. Peterson. Patterns of nectar production and plant-pollinator coevolution. In B. Bentley and T. Elias, editors, *The biology of nectaries*, pages 80–125. Columbia Univ. Press, New York, 1983.
- [25] D. Cundall. Drinking in snakes: kinematic cycling and water transport. *J. Exp. Biol.*, 203:2171–2185, 2000.
- [26] T. L. Daniel and J. G. Kingsolver. Feeding strategy and the mechanics of blood sucking in insects. *J. Theor. Biol.*, 105:661–672, 1983.
- [27] T. L. Daniel, J. G. Kingsolver, and E. Meyhofer. Mechanical determinants of nectar-feeding energetics in butterflies: muscle mechanics, feeding geometry, and functional equivalence. *Oecologia*, 79:66–75, 1989.
- [28] J. Davenport and E.-A. Macedo. Behavioural osmotic control in the euryhaline diamondback terrapin *Malaclemys terrapin*: responses to low salinity and rainfall. *J. Zool.*, 220:487–496, 1990.
- [29] P.-G. de Gennes, F. Brochard-Wyart, and D. Quere. *Capillarity and Wetting Phenomena: Drops, Bubbles, Pearls, Waves (Google eBook)*. Springer, New York, 2003.

- [30] R. H. Dettre and R. E. Johnson. Contact angle hysteresis II. Contact angle measurements on rough surfaces. In F. M. Fowkes, editor, *Contact Angle, Wettability, and Adhesion*, volume 43 of *Advances in Chemistry Series*, pages 136–144. American Chemical Society, Washington, DC, 1964.
- [31] D. M. Eckmann, S. Bowers, M. Stecker, and A. T. Cheung. Hematocrit, volume expander, temperature, and shear rate effects on blood viscosity. *Anesthesia & Analgesia*, 91(3):539–545, 2000.
- [32] P. W. Ewald and W. A. Williams. Function of the bill and tongue in nectar uptake by hummingbirds. *The Auk*, 99:573–576, 1982.
- [33] L. Feng, S. Li, Y. Li, H. Li, L. Zhang, J. Zhai, Y. Song, B. Liu, L. Jiang, and D. Zhu. Super-hydrophobic surfaces: From natural to artificial. *Advanced Materials*, 24:1857–1860, 2002.
- [34] X.-Q. Feng and L. Jiang. Design and creation of superwetting/antiwetting surfaces. *Adv. Mater.*, 18:2063–3078, 2006.
- [35] M. R. Flynn, A. R. Kasimov, J.-C. Nave, R. R. Rosales, and B. Seibold. Self-sustained nonlinear waves in traffic flow. *Phys. Rev. E*, 79:056113, May 2009.
- [36] H. Gadow. On the suctorial apparatus of the Tenuirostres. *Proc. Zool. Soc. London*, pages 62–69, 1883.
- [37] R. P. Garrod, L. G. Harris, W. C. E. Schofield, J. McGettrick, L. J. Ward, D. O. H. Teare, and J. P. S. Badyal. Mimicking a *Stenocara* beetle’s back for microcondensation using plasmachemical patterned superhydrophobic-superhydrophilic surfaces. *Langmuir*, 23:689–693, 2007.
- [38] G. B. Gillis and G. V. Lauder. Aquatic prey transport and the comparative kinematics of *Ambystoma tigrinum* feeding behaviors. *J. Exp. Biol.*, 187:159–179, 1994.
- [39] H. D. Green. Circulatory system: physical principles. *Medical physics*, 2(228), 1950.
- [40] H. Greenberg. An analysis of traffic flow. *Operations Research*, 7(1):79–85, 1959.
- [41] T. R. Gregory. Nucleotypic effects without nuclei: genome size and erythrocyte size in mammals. *Genome*, 901:895–901, 2000.
- [42] S. R. Griffin, K. Mavraganis, and C. G. Eckert. Experimental analysis of protogyny in *Aquilegia canadensis* (Ranunculaceae). *Am. J. Bot.*, 87:1246–1256, 2000.
- [43] J. B. Grotberg. Pulmonary flow and transport phenomena. *Annu. Rev. Fluid Mech.*, 26:529–571, 1994.
- [44] F. R. Hainsworth. On the tongue of a hummingbird: its role in the rate and energetics of feeding. *Comparative Biochemistry and Physiology*, 46:65–78, 1973.

- [45] F. R. Hainsworth, E. Precup, and T. Hamill. Feeding, energy processing rates and egg production in painted lady butterflies. *J. Exp. Biol.*, 156:249–265, 1991.
- [46] L. D. Harder. Effects of nectar concentration and flower depth on flower handling efficiency of bumble bees. *Oecologia*, 69:309–315, 1986.
- [47] W. M. Haynes, editor. *CRC Handbook of Chemistry and Physics*. CRC Press, Boca Raton, FL, 93 edition, 2012.
- [48] J. Heidweiller, J. A. van Loon, and G. A. Zweers. Flexibility of the drinking mechanism in adult chickens (*Gallus gallus*) (Aves). *Zoomorphology*, 111:141–159, 1992.
- [49] J. Heidweiller and G. A. Zweers. Drinking mechanisms in the zebra finch and the bengalese finch. *The Condor*, 92:1–28, 1990.
- [50] B. Heinrich and P. H. Raven. Energetics and pollination ecology. *Science*, 176:579–602, 1972.
- [51] D. Helbing. Traffic and related self-driven many-particle systems. *Reviews of modern physics*, 73(4):1067–1141, 2001.
- [52] A. J. Heyneman. Optimal sugar concentrations of floral nectars - dependence on sugar intake efficiency and foraging costs. *Oecologia*, 60:198–213, 1983.
- [53] A. H. Hurlbert, S. A. Hosoi, E. J. Temeles, and P. W. Ewald. Mobility of *Impatiens capensis* flowers: effect on pollen deposition and hummingbird foraging. *Oecologia*, 105:243–246, 1996.
- [54] K. H. Jensen, J. Lee, T. Bohr, H. Bruus, N. M. Holbrook, and M. A. Zwieniecki. Optimality of the Münch mechanism for translocation of sugars in plants. *Journal of the Royal Society Interface*, 8(61):1155–1165, August 2011.
- [55] K. H. Jensen, J. Liesche, T. Bohr, and A. Schulz. Universality of phloem transport in seed plants. *Plant, Cell and Environment*, 35(6):1065–1076, June 2012.
- [56] K. H. Jensen, J. A. Savage, and N. M. Holbrook. Optimal concentration for sugar transport in plants. *Submitted to Journal of the Royal Society Interface*, 2013.
- [57] R. B. Josens and W. M. Farina. Nectar feeding by the hovering hawk moth *Macroglossum stellatarum*: intake rate as a function of viscosity and concentration of sucrose solutions. *J. Comp. Physiol.*, 187:661–665, 2001.
- [58] D. Kessler, C. Diezel, and I. T. Baldwin. Changing pollinators as a means of escaping herbivores. *Curr. Biol.*, 20:237–242, 2010.
- [59] H.-Y. Kim and L. Mahadevan. Capillary rise between elastic sheets. *J. Fluid Mech.*, 548:141–150, 2006.
- [60] W. Kim and J.W.M. Bush. Natural drinking strategies. *Journal of Fluid Mechanics*, 705:7–25, 2012.

- [61] W. Kim, T. Gilet, and J. W. M. Bush. Reply to Rico-Guevara and Rubega: Nectar loading in hummingbirds. *Proc. Natl. Acad. Sci.*, 109:E868, 2012.
- [62] W. Kim, T. Gilet, and J.W.M Bush. Optimal concentrations in nectar feeding. *Proc. Natl. Acad. Sci.*, 108:16618–16621, 2011.
- [63] W. Kim, F. Peaudecerf, M.W. Baldwin, and J.W.M. Bush. The hummingbird’s tongue: a self-assembling capillary syphon. *Proceedings of the Royal Society B: Biological Sciences*, 279(1749):4990–4996, 2012.
- [64] J. G. Kingsolver and T. L. Daniel. On the mechanics and energetics of nectar feeding in butterflies. *J. Theor. Biol.*, 76:167–179, 1979.
- [65] J. G. Kingsolver and T. L. Daniel. Mechanical determinants of nectar feeding strategy in hummingbirds: energetics, tongue morphology, and licking behavior. *Oecologia*, 60:214–226, 1983.
- [66] J. G. Kingsolver and T. L. Daniel. Mechanics of food handling by fluid-feeding insects. In R. F. Chapman and G. de Boer, editors, *Regulatory mechanisms in insect feeding insects*, pages 32–53. Chapman and Hall, New York, 1995.
- [67] A. Köhler, C. D. C. Leseigneur, L. Verburt, and S. W. Nicolson. Dilute bird nectars: viscosity constrains food intake by licking in a sunbird. *Am. J. Physiol. Regul. Integr. Comp. Physiol.*, 299:R1068–R1074, 2010.
- [68] J. G. M. Kooloos and G. A. Zweers. Mechanics of drinking in the mallard (*Anas platyrhynchos*, Anatidae). *J. Morphol.*, 199:327–347, 1989.
- [69] M. LaBarbera. Principles of design of fluid transport systems in zoology. *Science*, 249(4972):992–1000, 1990.
- [70] J. Lanza, G. C. Smith, S. Sack, and A. Cash. Variation in nectar volume and composition of *Impatiens capensis* at the individual, plant, and population levels. *Oecologia*, 102:113–119, 1995.
- [71] E. Lauga and T. R. Powers. The hydrodynamics of swimming microorganisms. *Rep. Prog. Phys.*, 72:096601, 2009.
- [72] T. M. Laverty and R. C. Plowright. Competition between hummingbirds and bumble bees for nectar in flowers of *Impatiens biflora*. *Oecologia*, 66:25–32, 1985.
- [73] S. J. Lee, B. H. Kim, and J. Y. Lee. Experimental study on the fluid mechanics of blood sucking in the proboscis of a female mosquito. *J. Biomech.*, 42:857–864, 2009.
- [74] M. J. Lighthill. *Mathematical biofluidynamics*. SIAM, Philadelphia, 1975.
- [75] F. A. Lucas. On the structure of the tongue in hummingbirds. *Proc. U. S. Nat. Mus.*, 14:167–172, 1891.

- [76] S. Maddison, R. J. Wod, E. T. Rolls, B. J. Rolls, and J. Gibbs. Drinking in the rhesus monkeys: Peripheral factors. *J. Comp. Physiol. Psychol.*, 94:365–374, 1980.
- [77] W. C. L. Martin. *A General History of Humming-birds, or the Trochilidae*. H.G. Bohn, London, 1852.
- [78] P. G. May. Nectar uptake rates and optimal nectar concentrations of two butterfly species. *Oecologia*, 66:381–386, 1985.
- [79] P. G. May. Flower selection and the dynamics of lipid reserves in two nectarivorous butterflies. *Ecology*, 73:2181–2191, 1992.
- [80] O.J. McCarthy and H. Singh. Physico-chemical properties of milk. In Paul McSweeney and Patrick F. Fox, editors, *Advanced Dairy Chemistry*, pages 691–758. Springer New York, 2009.
- [81] J. R. McClung and S. J. Goldberg. Functional anatomy of the hypoglossal innervated muscles of the rat tongue: A model for elongation and protrusion of the mammalian tongue. *Anat. Rec.*, 260:378–386, 2000.
- [82] T. A. McMahon and J. T. Bonner. *On Size and Life*. Scientific American Library, New York, 1983.
- [83] N. Medina-Tapia, J. Ayala-Berdon, L. Morales-Pérez, L. M. Melo, and J. E. Schondube. Do hummingbirds have a sweet-tooth? Gustatory sugar thresholds and sugar selection in the broad-billed hummingbird *Cyananthus latirostris*. *Comp. Biochem. Physiol. A Mol. Integr. Physiol.*, 161:307–314, 2012.
- [84] Minnesota Department of Transportation, Mn/DOT Traffic Data. Website. <http://data.dot.state.mn.us/datatools>.
- [85] R. J. Mitchell and D. C. Paton. Effects of nectar volume and concentration on sugar intake rates of Australian honeyeaters (Meliphagidae). *Oecologia*, 83:238–246, 1990.
- [86] W. Moller. Über die Schnabel- und Zungenmechanik blütenbesuchender Vögel. 1. *Biologia Generalis*, 6:651–727, 1930.
- [87] W. Moller. Bemerkungen zu Scharke’s Mitteilung “Die Nektaraufnahme mit der Kolibrizunge”. *Ornith. Monatsber.*, 39:135–138, 1931.
- [88] W. Moller. Die Zungen der kostarizensischen Zuckervögel. *Zeitschrift für mikr-anat. Forschung*, 28:363–417, 1932.
- [89] N. J. Morrison, J. Richardson, L. Dunn, and R. L. Pardy. Respiratory muscle performance in normal elderly subjects and patients with copd. *Chest*, 95:90–94, 1989.
- [90] C. D. Murray. The physiological principle of minimum work: I. The vascular system and the cost of blood volume. *Proceedings of the National Academy of Sciences of the United States of America*, 12(3):207–214, March 1926.

- [91] S. W. Nicolson. Nectar consumers. In S. W. Nicolson, M. Nep, and E. Pacinir, editors, *Nectaries and nectar*, pages 289–342. Springer-Verlag, Dordrecht, 2007.
- [92] A. R. Parker and C. R. Lawrence. Water capture by a desert beetle. *Nature*, 414:33–34, 2001.
- [93] J. S. Pate. Nutrients and metabolites of fluids recovered from xylem and phloem: significance in relation to long-distance transport in plants. In I. F. Wardlaw and J. B. Passioura, editors, *Transport and transfer processes in plants*, pages 253–281. Academic Press, New York, 1976.
- [94] D. C. Paton and B. G. Collins. Bills and tongues of nectar-feeding birds: a review of morphology, function and performance, with intercontinental comparisons. *Austr. J. Ecol.*, 14:473–506, 1989.
- [95] J. Paul and F. Roces. Fluid intake rates in ants correlate with their feeding habits. *J. Insect Physiol.*, 49:347–357, 2003.
- [96] T. J. Pedley. Pulmonary fluid dynamics. *Annu. Rev. Fluid Mech.*, 9:229–274, 1977.
- [97] T. J. Pedley and J. O. Kessler. Hydrodynamic phenomena in suspensions of swimming microorganisms. *Annu. Rev. Fluid Mech.*, 24:313–358, 1992.
- [98] K. A. Pivnick and J. N. McNeil. Effects of nectar concentration on butterfly feeding: measured feeding rates for *Thymelicus lineola* (Lepidoptera: Hesperidae) and a general feeding model for adult. *Oecologia*, 66:226–237, 1985.
- [99] M. Prakash, D. Quéré, and J. W. M. Bush. Surface tension transport of prey by feeding shorebirds: the capillary ratchet. *Science*, 320:931–934, 2008.
- [100] A. R. Pries, D. Neuhaus, and P. Gaehtgens. Blood viscosity in tube flow: dependence on diameter and hematocrit. *American Journal of Physiology*, 263:1770–1778, 1992.
- [101] C. Py, P. Reverdy, L. Doppler, J. Bico, B. Roman, and C. N. Baroud. Capillary origami: spontaneous wrapping of a droplet with an elastic sheet. *Phys. Rev. Lett.*, 98:156103, 2007.
- [102] G. H. Pyke and N. M. Waser. The production of dilute nectars by hummingbird and honeyeater flowers. *Biotropica*, 13:260–270, 1981.
- [103] D. Quéré. Fluid coating on a fiber. *Annu. Rev. Fluid Mech.*, 31:347–384, 1999.
- [104] T. Rabinowitz and B. Tandler. Papillary morphology of the tongue of the American chameleon: *Anolis carolinensis*. *Anat. Rec.*, 216:483–489, 1986.
- [105] P. M. Reis, S. Jung, J. M. Aristoff, and R. Stocker. How cats lap: water uptake by *Felis catus*. *Science*, 330(6008):1231–4, November 2010.

- [106] C. Rengifo, L. Cornejo, and I. Akirov. One size fits all: corolla compression in *Aphelandra runcinata* (Acanthaceae), an adaptation to short-billed hummingbirds. *J. Trop. Ecol.*, 22:613–619, 2006.
- [107] Emilie A Rennie and Robert Turgeon. A comprehensive picture of phloem loading strategies. *Proceedings of the National Academy of Sciences of the United States of America*, 106(33):14162–14167, August 2009.
- [108] A. Rico-Guevara and M. A. Rubega. The hummingbird tongue is a fluid trap, not a capillary tube. *Proc. Natl. Acad. Sci.*, 108:9356–9360, 2011.
- [109] A. Rico-Guevara and M. A. Rubega. Hummingbird feeding mechanics: Comments on the capillary model. *Proc. Natl. Acad. Sci.*, 109:E867, 2012.
- [110] M. W. Roberts. Hummingbirds’ nectar concentration preferences at low volume: the importance of time scale. *Anim. Behav.*, 52:361–370, 1996.
- [111] W. M. Roberts. Hummingbird licking behavior and the energetics of nectar feeding. *The Auk*, 112:456–463, 1995.
- [112] A. M Robertson, A. Sequeira, and M. V Kameneva. *Hemodynamical Flows*, volume 37 of *Oberwolfach Seminars*. Birkhäuser Basel, Basel, 2008.
- [113] F. Roces, Y. Winter, and O. von Helversen. Nectar concentration preference and water balance in a flower visiting bat, *Glossophaga soricina antillarum*. In W. Barthlott, editor, *Animal-plant Interactions in Tropical Environments*, pages 159–165. Museum Koenig, Bonn, 1993.
- [114] B. Roman and J. Bico. Elasto-capillarity: deforming an elastic structure with a liquid droplet. *J. Phys. Condens. Matter*, 22:493101, 2010.
- [115] R. S. Rosenson, A. McCormick, and E. F. Uretz. Distribution of blood viscosity values and biochemical correlates in healthy adults. *Clin. Chem.*, 42:1189–1195, 1996.
- [116] D. W. Roubik and S. L. Buchmann. Nectar selection by melipona and *Apis mellifera* (Hymenoptera: Apidae) and the ecology of nectar intake by bee colonies in a tropical forest. *Oecologia*, 61:1–10, 1984.
- [117] M. A. Rubega and B. S. Obst. Surface-tension feeding in phalaropes: discovery of a novel feeding mechanism. *The Auk*, 110:169–178, 1993.
- [118] N. Saitô. Concentration dependence of the viscosity of high polymer solutions. I. *Journal of the Physical Society of Japan*, 5(1):4–8, 1950.
- [119] A. Schadschneider. Traffic flow: a statistical physics point of view. *Physica A: Statistical Mechanics and its Applications*, 313:153–187, 2002.
- [120] H. Scharnke. Beiträge zur Morphologie und Entwicklungsgeschichte der Zunge der Trochilidae, Meliphagidae, und Picidae. *Journal für Ornithol.*, 79:425–491, 1931.

- [121] H. Scharnke. Die Nektaraufnahme mit der Kolibrizunge. *Ornith. Monatsber.*, 39:22–23, 1931.
- [122] P. Scherp and K. H. Hasenstein. Anisotropic viscosity of the chara (characeae) rhizoid cytoplasm. *American Journal of Botany*, 94(12):1930–1934, 2007.
- [123] R. Schlamowitz, F. R. Hainsworth, and L. L. Wolf. On the tongues of sunbirds. *The Condor*, 78:104–107, 1976.
- [124] B. Schmidt-Nielsen, K. Schmidt-Nielsen, T. R. Houpt, and S. A. Jarnum. Water balance of the camel. *Am. J. Physiol.*, 185:185–194, 1956.
- [125] B. Seibold, M. R. Flynn, A. R. Kasimov, and R. R. Rosales. Constructing set-valued fundamental diagrams from jamiton solutions in second order traffic models. *arXiv preprint*, page 1204.5510, April 2012.
- [126] R.S. Seymour and A.J. Blaylock. The principle of laplace and scaling of ventricular wall stress and blood pressure in mammals and birds. *Physiological and Biochemical Zoology*, 73(4):389–405, 2000.
- [127] W. C. Sherbrooke. Integumental water movement and rate of water ingestion during rain harvesting in the Texas horned lizard, *Phrynosoma cornutum*. *Amphibia-Reptilia*, 25:29–39, 2004.
- [128] W. C. Sherbrooke, A. J. Scardino, R. de Nys, and L. Schwarzkopf. Functional morphology of scale hinges used to transport water: convergent drinking adaptations in desert lizards (*Moloch horridus* and *Phrynosoma cornutum*). *Zoomorphology*, 126:89–102, 2007.
- [129] T. Squires and S. R. Quake. Microfluidics: fluid physics at the nanoliter scale. *Rev. Mod. Phys.*, 77:977, 2005.
- [130] H. Stark and S. Schuster. Comparison of various approaches to calculating the optimal hematocrit in vertebrates. *Journal of Applied Physiology*, 113(3):355–67, August 2012.
- [131] R. D. Stevenson. Feeding rates of the tobacco hawkmoth *Manduca sexta* at artificial flowers. *Am. Zool.*, 31:302, 1991.
- [132] H. A. Stone, A. D. Stroock, and A. Ajdari. Engineering flows in small devices: microfluidics toward a lab-on-a-chip. *Annu. Rev. Fluid Mech.*, 36:381–411, 2004.
- [133] S. Tamm and C. L. Gass. Energy intake rates and nectar concentration preferences by hummingbirds. *Oecologia*, 70:20–23, 1986.
- [134] E. J. Temeles. A new dimension to hummingbird-flower relationships. *Oecologia*, 105:517–523, 1996.
- [135] E. J. Temeles and W. J. Kress. Adaptation in a plant-hummingbird association. *Science*, 300:630–633, 2003.

- [136] E. J. Temeles, Y. B. Linhart, M. Masonjones, and H. D. Masonjones. The role of flower width in hummingbird bill length-flower length relationships. *Biotropica*, 34:68–80, 2002.
- [137] S. P. Timoshenko and J. N. Goodier. *Theory of Elasticity*. McGraw-Hill, New York, 1970.
- [138] M. S. Triantafyllou, G. S. Triantafyllou, and D. K. P. Yue. Hydrodynamics of fishlike swimming. *Annu. Rev. Fluid Mech.*, 32:33–53, 2000.
- [139] S. Vogel. Living in a physical world. *Journal of Biosciences*, 29(4):391–397, 2004.
- [140] F. Wagemans, M. Chardon, J. P. Gasc, S. Renous, and V. L. Bels. Drinking behaviour in *Anolis carolinensis* (Voigt, 1837) and *Oplurus cuvieri* (Gray, 1831) (Reptilia: Iguania: Iguanidae). *Can. J. Zool.*, 77:1136–1146, 1999.
- [141] G. R. Wang. Laser induced fluorescence photobleaching anemometer for microfluidic devices. *Lab on a chip*, 5(4):450–6, April 2005.
- [142] R. C. Weast. *Handbook of Chemistry and Physics*. CRC Press, Cleveland, Ohio, 1974.
- [143] J. A. Weijnen. Licking behavior in the rat: Measurement and situational control of licking frequency. *Neurosci. Biobehav. Rev.*, 22:751–760, 1998.
- [144] J. B. West. Snorkel breathing in the elephant explains the unique anatomy of its pleura. *Respir. Physiol.*, 126:1–8, 2001.
- [145] R. D. Weymouth, R. C. Lasiewski, and A. J. Berger. The tongue apparatus in hummingbirds. *Acta Anat.*, 58:252–270, 1964.
- [146] P. G. Willmer and G. N. Stone. Behavioral, ecological, and physiological determinants of the activity patterns of bees. *Adv. Stud. Behav.*, 34:347–466, 2004.
- [147] J. F. Wilson, U. Mahajan, S. A. Wainwright, and L. J. Croner. A continuum model of elephant trunks. *J. Biomech. Eng.*, 113:79–84, 1991.
- [148] Y. Winter and O. von Helversen. Operational tongue length in phyllostomid nectar-feeding bats. *J. Mammal.*, 84:886–896, 2003.
- [149] T. Y. Wu. Fish swimming and bird/insect flight. *Annu. Rev. Fluid Mech.*, 43:25–58, 2011.
- [150] L. Zhai, M. C. Berg, F. C. Cebeci, Y. Kim, J. M. Milwid, M. F. Rubner, and R. E. Cohen. Patterned superhydrophobic surfaces: toward a synthetic mimic of the Namib desert beetle. *Nano Letters*, 6:1213–1217, 2006.
- [151] G. Zweers. Drinking of the pigeon (*Columba livia* L.). *Behaviour*, 80:274–317, 1982.
- [152] G. Zweers, F. de Jong, H. Berkhoudt, and J. C. V. Berge. Filter feeding in flamingos (*Phoenicopterus ruber*). *The Condor*, 97:297–324, 1995.